A STUDY OF THE BEHAVIOR AND LOCALIZATION OF PT(II) AZIDE AND ALKYNE-MODIFIED DERIVATIVES IN CELLS USING BIOORTHOGONAL CHEMISTRY AND FLUORESCENCE MICROSCOPY

by

ALAN D. MOGHADDAM

A DISSERTATION

Presented to the Department of Chemistry and Biochemistry
and the Graduate School of the University of Oregon
in partial fulfillment of the requirements
for the degree of
Doctor of Philosophy

September 2016

DISSERTATION APPROVAL PAGE

Student: Alan D. Moghaddam

Title: A Study of the Behavior and Localization of Pt(II) Azide and Alkyne-Modified Derivatives in Cells using Bioorthogonal Chemistry and Fluorescence Microscopy

This dissertation has been accepted and approved in partial fulfillment of the requirements for the Doctor of Philosophy degree in the Department of Chemistry and Biochemistry by:

Michael M. Haley	Chairperson
Victoria J. DeRose	Advisor
Michael D. Pluth	Core Member
Bruce P. Branchaud	Core Member
Raghuveer Parthasarathy	Institutional Representative

and

Scott L. Pratt	Dean of the Graduate School

Original approval signatures are on file with the University of Oregon Graduate School.

Degree awarded September 2016.

DISSERTATION ABSTRACT

Alan D. Moghaddam

Doctor of Philosophy

Department of Chemistry

September 2016

Title: A Study of the Behavior and Localization of Pt(II) Azide and Alkyne-Modified Derivatives in Cells Using Bioorthogonal Chemistry and Fluorescence Microscopy

Despite their ubiquitous use, Pt(II) anti-cancer drugs still suffer from many issues such as off-drug target effects, renal and nephrotoxicity as well as acquired and intrinsic drug resistance. To obtain a better understanding of how to mitigate these deleterious effects can be mitigated we first must know all the targets of these drugs. Highlighted in this dissertation is previous work performed by groups exploring the localization of Pt in cells using fluorescence microscopy. While Pt drugs such as cisplatin contain no native fluorescence, a great deal of work has been done to covalently modify complexes with fluorescent tags. From studies using this technique, it been reported that Pt can target a number of compartments within the cell ranging from the nucleus to the cytoplasm. With each different derivative being observed in varied cell lines it becomes difficult to deconvolute a universal pattern to where Pt localizes, furthermore, the connected fluorophore could also bias Pt localization.

To add general functionality and eliminate the bias of a pre-tethered fluorophore our lab has developed a number of different azide and alkyne-modified complexes that append a “reactive handle” to Pt compounds. This modification allows for use of the bioorthogonal azide-alkyne click reaction we are able to observe Pt localization after treatment. The focus of this work includes method development to conjugate a fluorophore

to our Pt complexes *in vitro* and in cell cultures. We examined a number of different cell lines and observed frequent localization in the nucleolus of the cell. Also in this work is the development of methods to append multiple fluorophores to each Pt site to increase our ability to visualize these complexes in cells. Finally, we have also constructed a new Pt-azide that exhibits slower exchange kinetics due to a chelating exchangeable group. The use of this new complex will enable studies to determine whether changing the leaving group results in differential localization of Pt drugs in cells.

The work presented here has both published and unpublished co-authored material. Chapter II has contributions from Dr. Jonathan D. White, Rachael M. Cunningham, Andrea N. Loes, Prof. Michael M. Haley and Prof. Victoria J. DeRose. Chapter III contains contributions from Regina M. Wirth, Dr. Jonathan D. White, Aurora L. Ginsberg, Prof. Michael M. Haley and Prof. Victoria J. DeRose. Chapter IV contains contributions from Regina M. Wirth, Dr. Jonathan D. White, Alison Wallum, Prof. Michael M. Haley and Prof. Victoria J. DeRose. Chapter V contains contributions from Regina M. Wirth, Emily Reister-Morris, Alison Wallum, Michael M. Haley and Prof. Victoria J. DeRose. Chapter VI contains contributions from Matthew M. Cerda, Rachael M. Cunningham, Michael M. Haley and Prof. Victoria J. DeRose.

CURRICULUM VITAE

NAME OF AUTHOR: Alan D. Moghaddam

GRADUATE AND UNDERGRADUATE SCHOOLS ATTENDED:

University of Oregon, Eugene, OR
The University of Arizona, Tucson, AZ

DEGREES AWARDED:

Doctor of Philosophy, Chemistry, 2016, University of Oregon
Bachelor of Science, Biochemistry, 2011, University of Arizona

AREAS OF SPECIAL INTEREST:

Chemical Biology
Analytical Chemistry
Transitional-metal chemistry

PROFESSIONAL EXPERIENCE:

Alan Alda Communicating Science Workshop Participant, University of Oregon, 2015
American Chemical Society Member, 2011-present

GRANTS, AWARDS, AND HONORS:

Award for Academic Distinction, University of Arizona, 2011
Dean's List Honorable Mention, University of Arizona, 2009
NSF Bridge REU, University of Arizona, 2007
Red and Blue Scholarship, University of Arizona, 2004

PUBLICATIONS:

Wirth, R;* White, J. D.;* **Moghaddam, A. D,;*** Ginzburg, A. L.; Zakharov, L. N.; Haley, M. M.; DeRose, V. J.; Azide vs Alkyne Functionalization in Pt(II) Complexes for Post-treatment Click Modification: Solid-State Structure, Fluorescent Labeling, and Cellular Fate; *J. Am. Chem. Soc.*, **2015**, 137(48), 15169-15175

Hammers, M. H.; Singh, L.; Montoya, L. A.; **Moghaddam, A. D.;** Pluth, M. D.; Synthesis of Amino-ADT Provides Access to Hydrolytically Stable Amide-Coupled Hydrogen Sulfide Releasing Drug Targets; *Synlett,* **2016**, 27, A–E

Moghaddam, A. D.;* White, J. D.;* Cunningham, R. C.; Loes, A. N.; Haley. M. M., DeRose, V. J; Convenient Detection of Metal-DNA, Metal-RNA, and Metal-Protein Adducts With a Click-Modified Pt(II) Complex; *Dalton Trans.*, **2015**, 44, 3536-3539

White, J. D.;* Osborn, M. F.;* **Moghaddam, A. D.**; Guzman, L. E.; Haley, M. M.; DeRose, V. J.; Picazoplatin, an Azide-Containing Platinum(II) Derivative for Target Analysis by Click Chemistry; *J. Am. Chem. Soc.,* **2013**, 135 (32): 11680–11683.

Johnson, G.M.; Chozinski, T.J.; Salmon, D.J.; **Moghaddam, A.D.;** Chen, H.C., Miranda, K.M.; Quantitative Detection of Nitroxyl Upon Trapping with Glutathione and Labeling with a Specific Fluorogenic Reagent; *Free Rad. Bio. Med.,* **2013,** 63, pp 476–484

*Co-first authors

ACKNOWLEDGMENTS

I wish to thank and show my deepest appreciation to Professor Victoria J. DeRose for her guidance and assistance in preparation of this manuscript. In that same context, both Vickie and Professor Michael Haley have been a pillar of support to both my scientific and professional development. I would like to thank the National Science Foundation (CHE-1413677 to V.J.D.) for funding. I would like to thank all previous and current members of the DeRose lab, namely, Dr. Jonathan D. White, Dr. Maire F. Osborne, Kory Plakos, Rachael Cunningham, Regina Wirth, and Emily Reister-Morris. Kory, you helped keep me on task and on point so many times during my tenure in graduate school. Rachael, you have been a sounding board for me, letting me express all my ideas good and bad. Jon and Maire, you were the original members of team Captains of Click, and I would have not accomplished anything in graduate school without you. I would also like to thank the Professor Michael Pluth and the Pluth lab. Spencer Bailey and Matt Hammers were not only close friends but amazing colleagues. The David Tyler lab has also been my lab away from lab, Alex Kendall and Justin Barry have been great friends and mentors to me. Oggie Golub has also been immensely helpful in answering any and every question I have had in respect to cellular imaging. I would also like to thank my committee members, Professor Bruce Branchaud and Professor Raghuveer Parthasarathy, for their input and guidance on my project.

I would also like to thank my academic family back in Arizona. Dr. Tony Pitucco taught me to question everything. Dr. Katrina Miranda took a chance on me when no one else would. My academic advisor, Deb Kruse, gave me tough love and encouragement, and her recent passing has been very heavy on my heart. Olivia Mendoza has done all she

can to make me feel like home is not so far away.

I also need to thank all the people who helped me make Oregon a second home. The Specific Heat soccer team has been an amazing experience, and through it I have met some of the best friends I have ever had in Connor Balzer, Brittany Nelson, Joseph Harmon, Will Campodonico, Seancy O'Cleary, and Edward McGlone.

Finally, I would like to thank my family and my partner Jennie. My mom and dad are the two most important people to me. My best friend/brother, Alexander Danehy, has been my partner in crime for so many years now. Jeff Matthews has been a close friend for quite some time now and has always been there to give me guidance and direction. Jennie, Grissom, and Olive are my family here in Oregon. You keep me grounded and you gave me strength when I was weak. I thank all of you.

If I missed anyone, I owe you the first round.

This work is dedicated to all organ donors. You give the gift of life.

TABLE OF CONTENTS

LIST OF FIGURES

Figure Page

Figure Page

Figure Page

LIST OF TABLES

Table Page

CHAPTER I

INTRODUCTION

Dubbed the "penicillin of cancer",[1] cisplatin is one of the most widely used anti-cancer drugs today and is prescribed in 50-70% of treatment regimes.[2] Since its FDA approval in 1978, cisplatin and other Pt-based anti-cancer drugs have been the vanguard of small molecule crosslinking agents in cancer treatment (Fig 1.1).

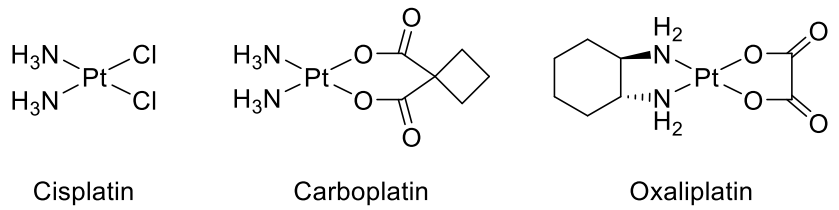

Figure 1.1. FDA approved Pt-based anticancer drugs: cisplatin, carboplatin and oxaliplatin.

Despite their widespread adoption, Pt-based anti-cancer drugs suffer from a myriad of issues. A primary issue of Pt drugs is the off-target drug effects such as renal toxicity, peripheral neuropathy, ototoxicity, and myelotoxicity. Furthermore, patients can develop intrinsic and acquired cellular resistance in prolonged treatment courses.[5] Ultimately, being able to understand the behavior and targeting of these drugs will afford us even better treatment regimens while minimizing undesirable side effects. This can only be done by being able to identify Pt targets with greater certainty and understand what factors direct Pt to these targets.

The general reactivity of these complexes stems from two exchangeable groups and two non-exchangeable groups coordinated to the Pt(II) center. The amine linkages on Pt are considered to be exchange-inert, but the chloride ligands (in the case of cisplatin) or

the carboxylic acid ligands (in the cases of carboplatin and oxaliplatin) can exchange with water, or with biomolecules within a cell. Once Pt-biomolecule adducts are formed they lead to cell cycle arrest and can ultimately cause cell death if not repaired. The ability of serum albumins to transport Pt within cells, as well as cell influx and efflux, is not fully elucidated. Understanding these mechanisms could also aide in understanding targeting as well.

Because of their intrinsic simplicity, Pt-based drugs are rather hard to study via spectroscopic methods. Unlike carbon-containing drugs, Pt therapeutics are much more difficult to track through methods relying on isotopically labelled nuclei. Inherently insensitive ^{195}Pt and ^{15}N nuclei and exchangeable amine protons preclude NMR as an easily accessible technique for studying these drug interactions within living cells. On a bulk level, a number of groups have explored utilizing mass spectrometry to identify Pt targets, but these methods rely on fractionating cells with greater accuracy and give very little detail on the specific Pt targets. These complexes also lack native fluorescence, further increasing the difficulty to study them *in vivo* through imaging based techniques.

A number of groups have explored functionalizing Pt drugs with a fluorophore to track Pt localization. Furthermore, our group as well as others have explored post-treatment fluorophore conjugation to gain insight on Pt localization. Herein we will discuss the outcomes, advantages and disadvantages of pre and post-treatment fluorophore-Pt conjugation.

Pt-fluorophore conjugation and imaging

One of the first reported Pt-tethered fluorophore complexes was made by Reedijk and co-workers (**1**) and was used to track the distribution of Pt within osteosarcoma cells

(U2-OS)[3]. Utilizing the carboxy-fluorescein moiety they witnessed broad fluorescence across the cell in the first hours, followed by localization primarily in the nucleus (Fig 1.3). After 24 h, there was sparse localization outside of the nucleus (less than 1% of the carboxy-fluorescence in the early hour marks) shown to be localization within the Golgi (by co-localization, Fig 1.4). As a control, the group also compared the distribution of the Boc protected diamine tethered to fluorescein (**3**) in cells.

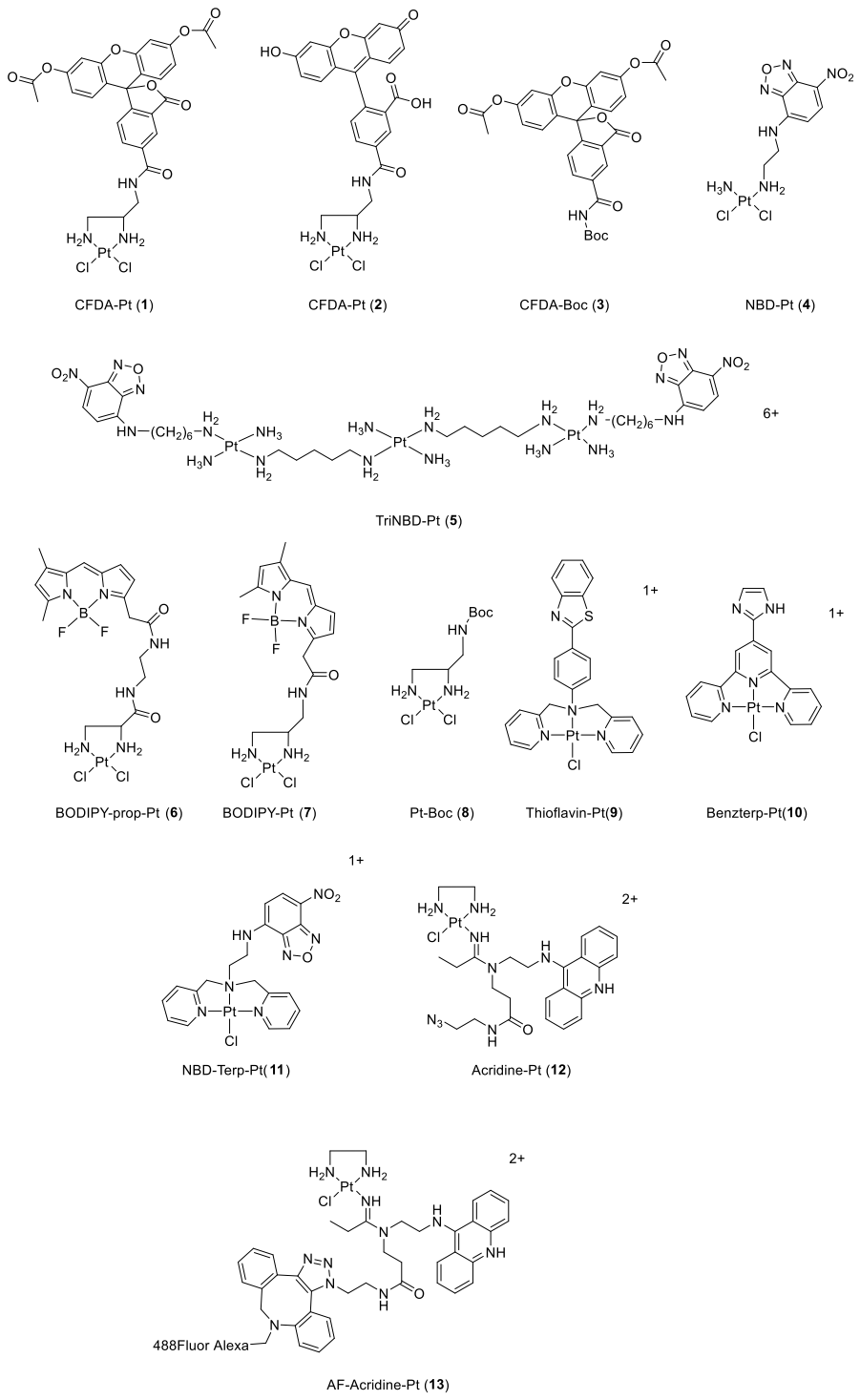

Figure 1.2. Cisplatin derivatives functionalized with a tethered fluorophore or an azide (for post treatment functionalization).[1-12]

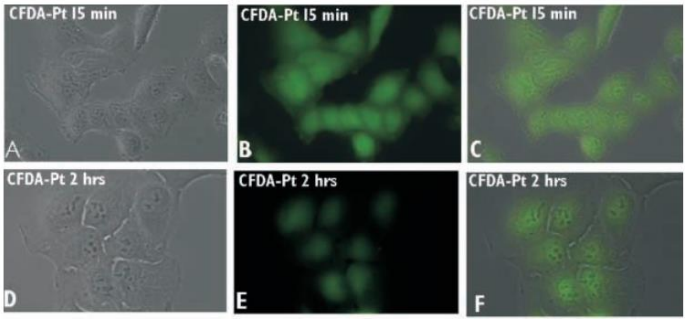

Figure 1.3. Brightfield and fluorescent images of U2-OS cells treated with **1**. In the first hours a broad fluorescent intensity is seen across the cell. Panels A and D show bright field images of the cells, panels B and E show the fluorescent channel, and panels C and F show the overlays of A/B and D/E respectively.[3]

The distribution of **3** in the first hours was quite similar to that of **1,** showing that the fluorescein unit could be directing the Pt complex. Howell and co-workers later showed that **1** is primarily localizing within vesicles of ovarian carcinoma 2008 cells, extensively mapping its trafficking into the Golgi and lysosomes as well as vesicles belonging to secretory pathways[4]. After 24 h, there was little to no intracellular signal for **3**, which is in contrast to the apparent Golgi localization of **1** (Fig 1.5).

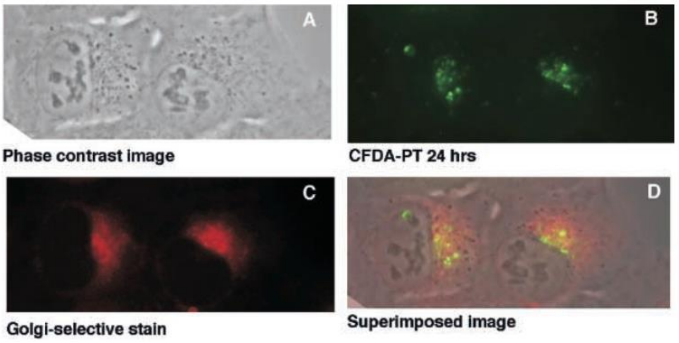

Figure 1.4. Brightfield (A) and fluorescent imaging (B and C) of U2-OS cells treated with **1** for 24 h. Co-localization analysis of **1** with a Golgi-selective stain shows a high correlation between the two as shown in the merged image (D).[3]

They also witnessed that **1** is less cytotoxic than cisplatin, but this difference is not dramatic. It should be noted that amine chelators of Pt complexes have been previously shown to be better tolerated by cells[5].

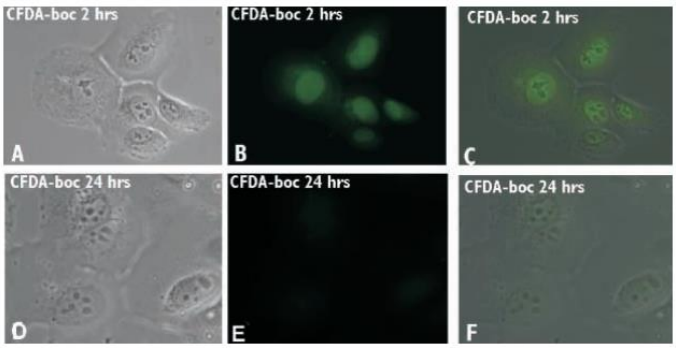

Figure 1.5. Treatment of U2-OS cells with **3** for 2 and 24 h. Early treatment shows broad localization of **3**, but after 24 h the fluorescent response not present. Panels A and D show bright field images of the cells, panels B and E show the fluorescent channel, and panels C and F show the overlays of A/B and D/E respectively.[3]

Farrell and co-workers investigated the synthesis and localization of **4** and **5**. Unlike previous complexes, **4** utilizes an NBD fluorophore and does not use an amine chelate[6]. Treatment of A2780 ovarian carcinoma cells with **4** and **5** in the presence and absence of human serum albumin (HSA) resulted in differences in localization. It was shown that **4** localized within the nucleus and cytoplasm in the absence of HSA, but in the presence of HSA was limited to the lysosomal and cytosolic areas (Fig 1.6A). Complex **5** showed nuclear/nucleolar localization in the presence and absence of HSA (Fig 1.6B). More importantly, these studies had shown that the presence of albumins can affect uptake and reinforced the localization pattern previously witnessed.

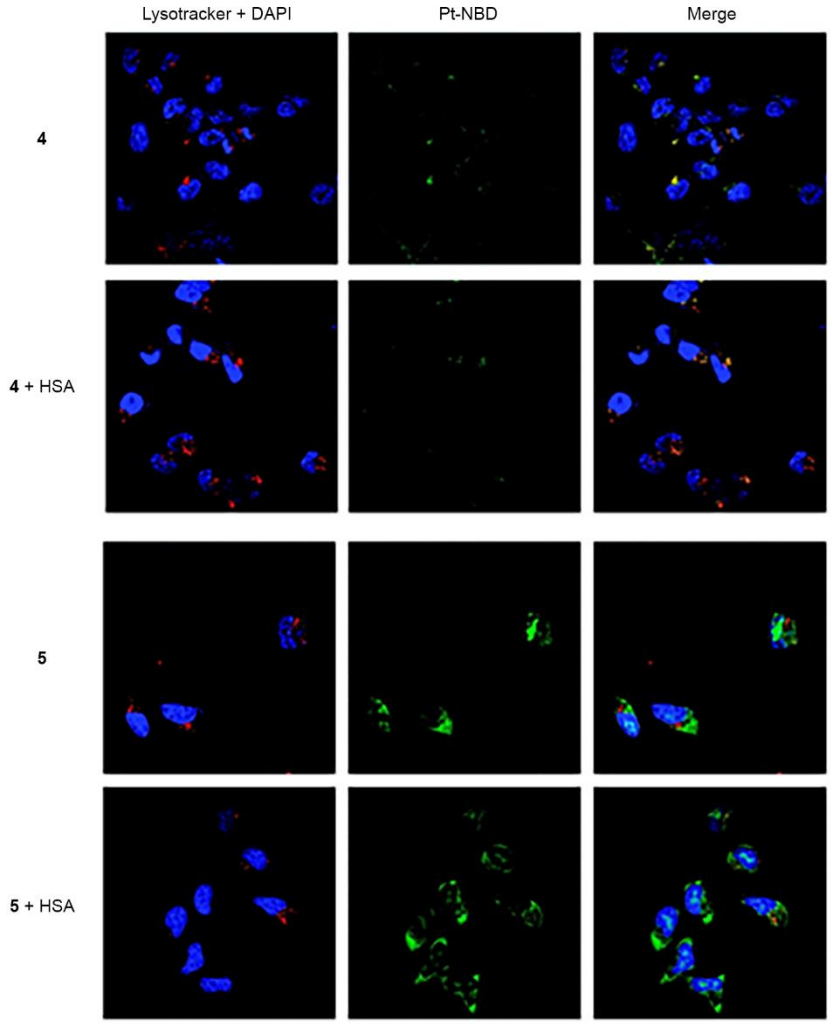

Figure 1.6. A2780 cells labelled with **4** and **5**. The top two panels are cells labelled with **4**, incubated in the presence and absence of human serum albumin (HSA). A significant amount of fluorescence is lost when **4** is incubated with HSA. The bottom two panels are cells labelled with **5**, in the presence and absence of HSA. HSA does not seem to affect the localization of **5**.[5]

Hall and co-workers constructed two BODIPY modified Pt complexes (**6** and **7**) and compared both their localization and ability to induce DNA damage against **1**, cisplatin, and ethylene diamine-Pt (Fig 1.7) in KB3-1 cells, human cervical carcinoma cells[7]. To assess DNA damage, the group monitored phosphorylation of H2A.X by immunofluorescence microscopy (Fig 1.7, images shown in magenta). Even at raised

concentrations (100 µM), **1** and **2** did not appear to induce DNA damage. Complexes **6** and **7** appeared to induce some DNA damage at 50 µM, and this response was also seen in the cisplatin control of 5 µM. The two BODIPY-Pt complexes showed localization within the nucleus and cytoplasm, with punctate staining within the nucleus which could be nucleolar localization.

Furthermore, when the group explored the uptake of **6** and **7** in resistant cell lines (KB-CP.5 and KB-CP20) they noticed a reduction in accumulation (monitored by flow cytometry) in comparison to cisplatin. This could indicate that cellular uptake of Pt-fluorophore complexes might be different to that of cisplatin. Ultimately, this difference could be what is influencing Pt-fluorophore complexes cytotoxicity and targeting.

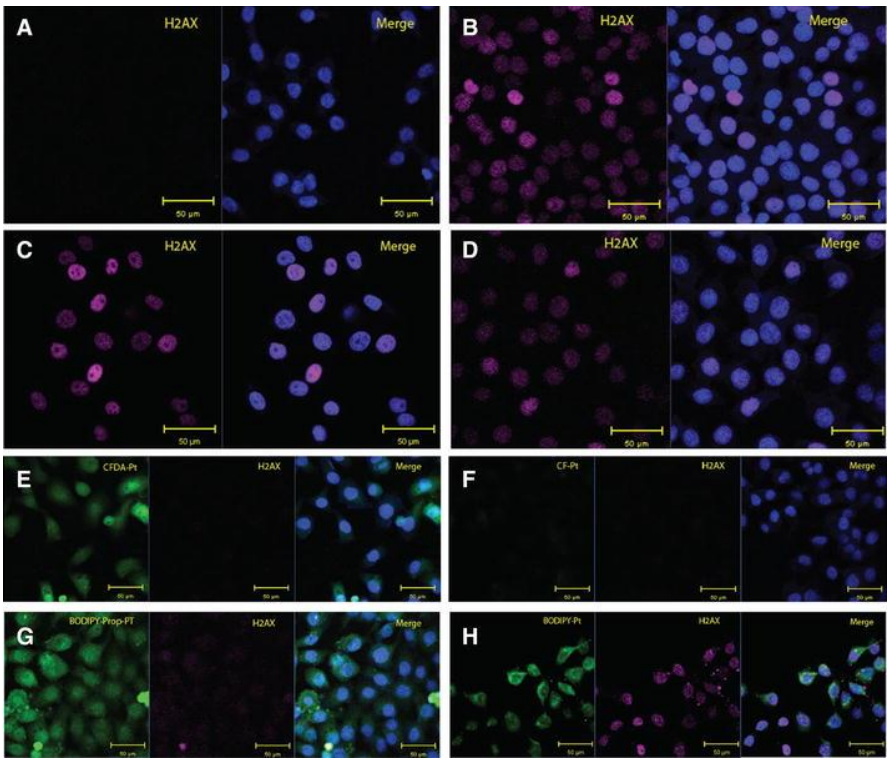

Figure 1.7. KB-3-1 cells treated with Pt-fluorophore conjugates. Panel A is a control set of images with no treatment. Panels B-D are treated with the non-fluorescent Pt species: cisplatin (B), ethylene diamine-Pt (C), **8** (D). Panels E-H are cells treated with **1**, **2, 6,** and **7** respectively. Panels are falsely colored blue for DAPI staining, magenta for H2A.x immunostaining, and green for Pt-fluorophore staining.[6]

Mono-Functional Fluorophore-Tethered Cisplatin-Like Complexes

While cisplatin is a bi-functional crosslinking complex, some groups have also used monofunctional crosslinking complexes to study Pt localization.[8-10] Zhang and co-workers have shown with **9**, a thioflavin modified Pt complex, that targeting of nuclear as well as mitochondrial and lysomal bodies is present (Fig 8).[8] Nair and co-workers were able to construct a turn-on fluorophore appended Pt complex, **10**, that upon DNA-binding elicited a 21-fold increase in emission.[9] Interestingly, in cells **10** does not show any fluorescence at or below its respective IC_{50} value(10 μM). Fluorescence is only present above the IC_{50}

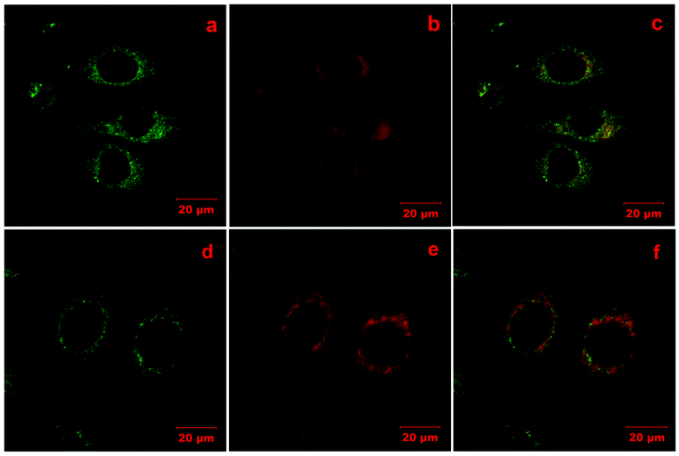

Figure 1.8. Confocal fluorescence images of HeLa cells co-stained with 50 nM MitoTracker Red CMXRos (or 1 μM LysoTracker Red DND-99) and 20 μM **9** for 1.5 h. Panels a/d show the green fluorescence of **9**. Panels b and e show the red fluorescence of Mito Tracker Red and Lyso Tracker Red respectively. Panels c and f show the overlays of their respective rows.[7]

value, which indicated that in order to elicit a fluorescent response the cell's viability had to become greatly decreased. Control studies with serum albumins did not elicit the same increase in emission, indicating the fluorescent turn-on is only present when **10** interacts with DNA. Further studies need to be explored to see if RNA can induce a similar response.

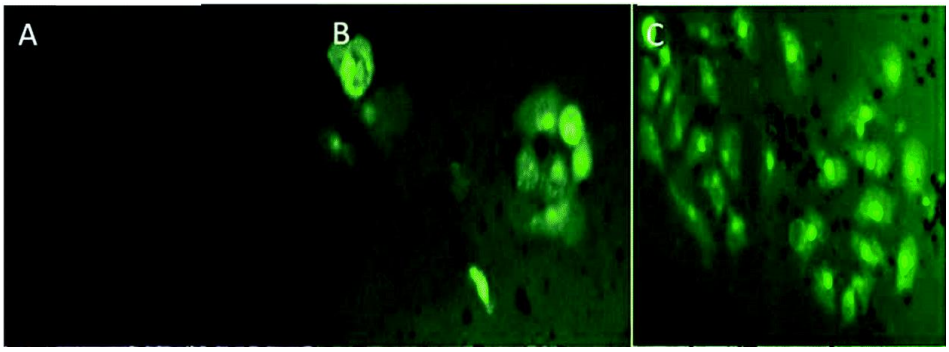

Figure 1.9. Images of HeCat cells treated with **10** at 10 µM (A), 20 µM (B) and 40 µM (C).[9]

Complex **11** was used to show Pt localization within MCF-7 and A549 cell lines, as well as zebrafish larva[10]. In the human cell lines, distinct nucleolar localization is witnessed as well as cytoplasmic localization, most likely due to localization within the mitochondria. In zebrafish larva, fluorescence is present primarily in the liver.

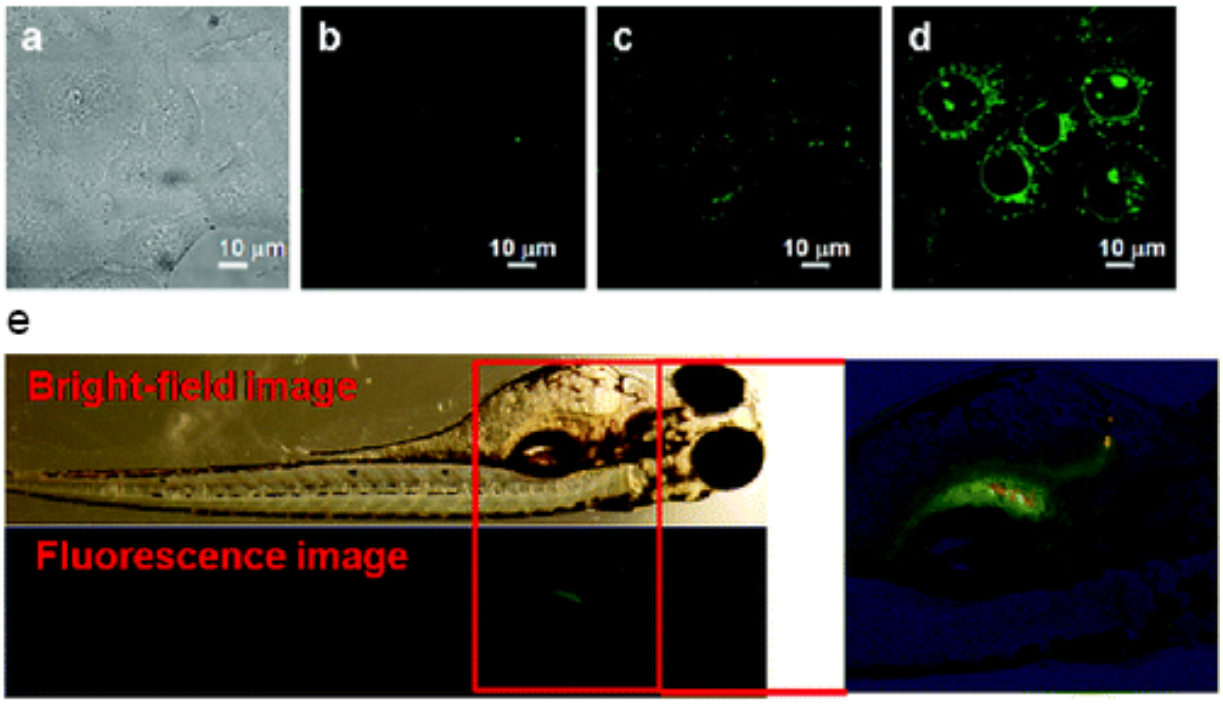

Figure 1.10. Confocal fluorescence imaging of MCF-7 cells incubated with **11** (10 μM): (a) bright-field image; fluorescence image after 0.5 h (b), 3 h (c), and 4 h (d). Also shown are bright-field and fluorescent images of a cross-section of zebrafish larva treated with **11** (e).[10]

Post-treatment fluorophore conjugation

Another approach to ascertaining localization of Pt complexes is the use of post-treatment functionalization. This can be done by installing a group that has tailored reactivity, and will only react with another group appended to a fluorophore. This approach has been pursued by our group as well other groups to ascertain Pt targeting. In short, this method of analysis allows treatment of cells with a Pt complex with a minimally invasive reactive handle (Fig 1.11A). After treatment, the cells are fixed and the localized Pt is conjugated to a fluorophore. The use of this strategy allows for analysis of Pt localization without having the influence of additional steric bulk and/or electrostatic charges from the pended fluorophore. This post-treatment conjugation relies upon the azide-alkyne cycloaddition reaction.[11] In the presence of a Cu catalyst or a strained alkyne species, the

azide will selectively react and form a covalent linkage (Fig 1.11B). Both the azide and alkyne should only react toward each other, reducing other possible side reactions in cells. The relative size and lack of charge in the two species should also help reduce any bias a fluorophore tether may impart.

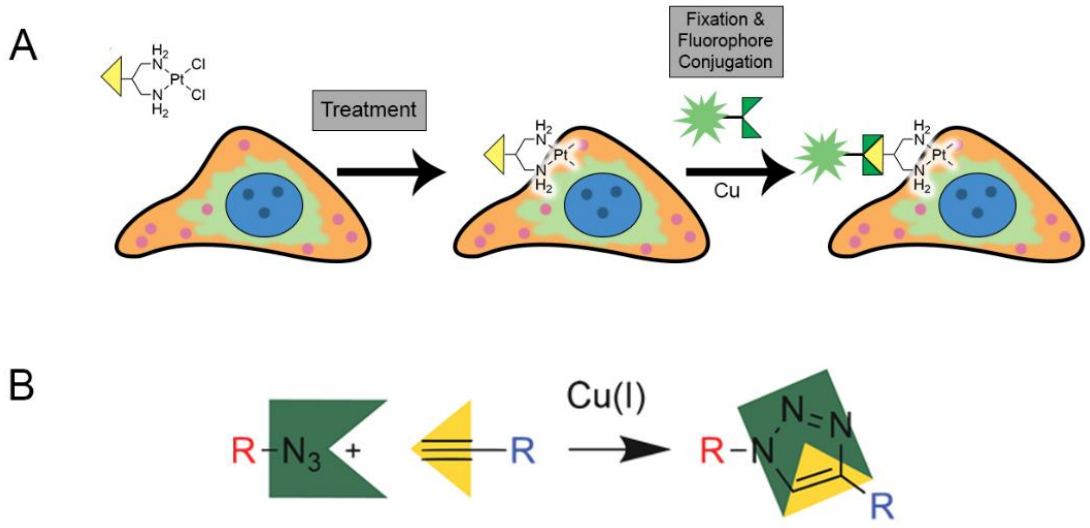

Figure 1.11. Panel A shows the generic scheme for post-treatment fluorophore conjugation. Panel B shows a schematic of the Cu catalyzed azide-alkyne cycloaddition reaction.

Bierbach and co-workers developed a system that combines a DNA intercalator (an acridine unit) and Pt to form a synergetic complex with a raised toxicity (**12**)[12]. This complex has also been modified to contain an azide group, giving the ability to analyze localization without having an effect of the presence of the fluorophore. The appended azide group will have selective reactivity, and for their purposes only will react in the presence of an alkyne and a copper catalyst. The group treated NCI-H460 cells, lung cancer cells, with their complex followed by fixation, permeablization and fluorophore

conjugation. This method of post-treatment conjugation resulted in a fluorescent response in the nucleus and cytoplasm. Most notably the group witnessed punctate staining inside the nucleus ultimately owed to nucleolar localization. Unfortunately, because this method relies on a copper catalyst live cell imaging is not currently possible. However, the use of cell permeable turn-on strained alkyne fluorophores could ultimately lead to this being possible in future studies. At the moment, this method of analysis relies "snapshots" of Pt localization rather than a full fluid motion capture that can be achieved with a pre-tethered fluorophore-Pt complex.

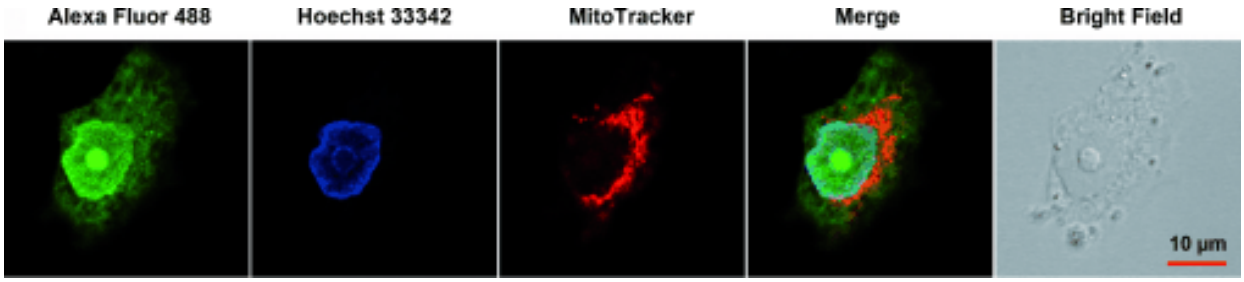

Figure 1.12. Image of NCI-H460 cells treated with **12**, then fixed and post labelled with Alexa Fluor 488 alkyne. Cells were also stained with Hoechst for DNA labelling and Mito Tracker for mitochondrial labelling.[12]

As a means to show that the localization of **12** is not influenced by the azide appendage, Bierbach and co-workers also constructed **12** by labelling **13** with a strained alkyne fluorophore before treatment[13]. By incubating **12** and **13** together, they were able to show that the two species co-localize strongly within cells (Fig 13). They do note that **13** has a decreased ability to target compacted chromatin, most likely due to the steric bulk of the dibenzocyclooctyne (DIBO) group. Furthermore, using this pre-tethered fluorophore Pt complex the group was able to conduct a double labelling experiment within cells using ethynyl modified DNA and RNA constructs (using 5-Ethynyluridine and 5-Ethynyl-2′-deoxyuridine). By using these modified nucleic acids they were able to correlate Pt

treatment with a decreased production of RNA in the nucleus. Ultimately these findings indicate that **12** and **13** lead to a reduction of transcription.

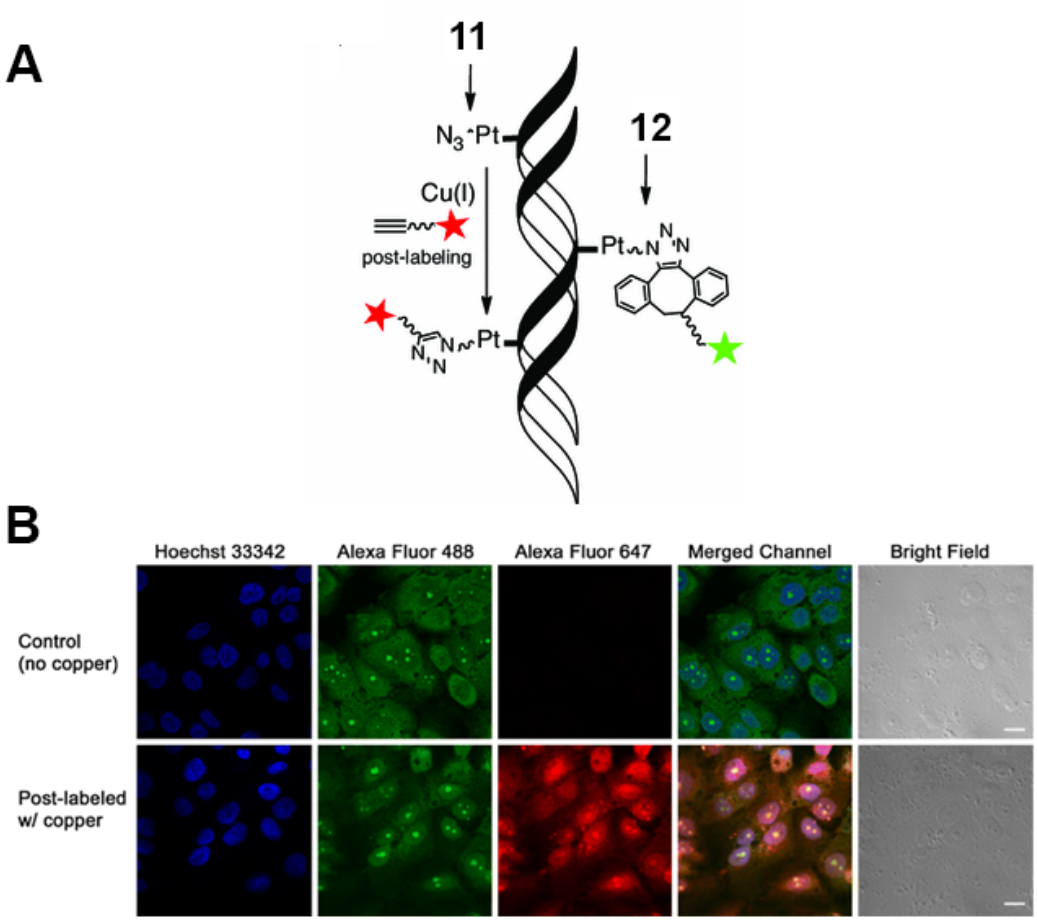

Figure 1.13. Co-localization studies of **12** and **13**. Panel A shows the general scheme of the double labelling technique. In the presence of Cu, **12** can be conjugated to an alkyne-modified Alexa Fluor 647 fluorophore. Panel B shows images of cells incubated only with **12** and **13** in the absence and presence of Cu. Only in the presence of Cu is the group able to see fluorescence in the 647 nm channel. The merged overlay of all channels shows a strong co-localization of the two signals. Both the pre and post-treatment result in a strong nucleolar localization, followed by nuclear and cytoplasmic staining.[13]

It should be noted, the acridine unit can also be heavily influencing localization of the complex as a whole. The synthetic rationale of installing the Pt complex was to increase cytotoxicity by giving the complex as a whole the ability to not only intercalate but to form a covalent linkage as well. The group does note that the azide-free version of **12** shows increased cytotoxicity, which may indicate that the azide may influence drug efflux and

influx as well. Further work needs to be done to ascertain the effect of such reactive handles.

The two approaches listed here can be used to ascertain how these Pt complexes behave *in vivo*. Utilizing a pre-tethered Pt-fluorophore complex we can gain insight on how the localization of Pt changes as a function of time. Use of the turn-on complex **1** can also help mitigate background fluorescence. Ultimately, the question of if the appended fluorophore affects localization is still present. Results in cisplatin resistant cell lines, lowered toxicities, and inconsistent action of DNA damage begs the question of if they behave in the same manner as cisplatin. The use of post-treatment functionalization is also an encouraging route, but the methods currently explore ascertain more the localization of a pro-drug prefaced on intercalation followed by covalent modification of DNA. Our work focuses on the use of post-treatment fluorophore conjugation of systems more similar to the small molecule crosslinking one of cisplatin. Herein, the focus for this body of work will be in the method development and characterization for cellular imaging of azide and alkyne appended complexes for post-treatment analysis.

These chapters include previously published and unpublished coauthored works in the following:

CHAPTER II: CONVENIENT DETECTION OF METAL-DNA, METAL-RNA, AND METALPROTEIN ADDUCTS WITH A CLICK-MODIFIED PLATINUM (II) COMPLEX

- **Moghaddam, A. D.**; White, J. D.; Cunningham, R. M.; Loes, A. N.; Haley, M. M.; DeRose, V. J. *Dalton Trans*. **2015**, *44*, 3536.

CHAPTER III: AZIDE VS ALKYNE FUNCTIONALIZATION IN PT(II) COMPLEXES FOR POST-TREATMENT CLICK MODIFICATION: SOLID-STATE STRUCTURE, FLUORESCENT LABELING, AND CELLULAR FATE

- Wirth, R; White, J. D.; **Moghaddam, A. D,;** Ginzburg, A. L.; Zakharov, L. N.; Haley, M. M.; DeRose, V. J.; *J. Am. Chem. Soc.*, **2015**, 137(48), 15169-15175

CHAPTER IV: DOUBLE POST-BINDING FLUORESCENT CONJUGATION AS A MEANS TO VISUALIZE CELLULAR DISTRIBUTION OF AN AZIDE-APPENDED PT(II) COMPLEX

- *unpublished, Manuscript in prep*
- *co-authors:* Regina M. Wirth, Jonathan D. White, Alison Wallum, Michael M. Haley and Victoria J. DeRose

CHAPTER V: ANALYSIS OF PT LOCALZIATION IN VARIED CELL LINES USING FLUORESCENT MICROSCOPY AND AN AZIDE MODIFIED PT(II) COMPLEX

- *unpublished, Manuscript in prep*

- *co-authors:* Regina M. Wirth, Emily Riester-Morris, Alison Wallum, Michael M. Haley and Victoria J. DeRose

CHAPTER VI: SYNTHESIS AND ANALYSIS OF TWO AZIDE-MODIFIED CARBOPLATIN MIMICS TO BE USED IN POST-TREATMENT FUNCTIONALIZATION

- *unpublished, Manuscript in prep*
- *co-authors:* Matthew M. Cerda, Rachael M. Cunningham, Michael M. Haley and Victoria J. DeRose

CHAPTER II

CONVENIENT DETECTION OF METAL-DNA, METAL-RNA, AND METALPROTEIN ADDUCTS WITH A CLICK-MODIFIED PLATINUM (II) COMPLEX

This chapter has contributions from Dr. Jonathan D. White, Rachael M. Cunningham, Andrea N. Loes, Prof. Michael M. Haley and Prof. Victoria J. DeRose. MMH and VJD provided insight and direction through the course of this investigation. JDW performed the synthesis and prepared samples for Pt-bound DNA samples for dPAGE analysis. RMC performed studies using Pt-bound bovine serum albumin (BSA) and analyzed them via SDS-PAGE, while ANL performed experiments treating *S. cerviscea* and subsequent RNA extractions. All HPLC analysis and mass spectrometry sample preparation were done by myself. This chapter includes material reproduced from Dalton Transactions (2015, 44, 3536-3539, © 2015 Royal Society of Chemistry), co-authored by JDW, myself, RMC, ANL, MMH, and VJD. JDW and I co-wrote this manuscript with extensive input from VJD.

High-Yielding Pt(II) Reagents for Post-Binding Covalent Modifications

Platinum(II)-based drugs are administered in many anticancer treatment regimes;[1] however, a broad identification of Pt-specific cellular targets is still lacking.[2] As Pt(II) compounds are effective nucleic acid crosslinking agents, they also have potential as structure probes in complex RNAs.[3] Click-functionalized Pt reagents provide a reactive handle for post-treatment labelling that would enable broad detection, isolation and

identification of Pt-bound species. We recently described a new pyridine-based Pt click reagent, picazoplatin (**1**, Fig. 2.1).[4] Despite the wide use of click chemistry and importance of platinum therapeutics, only one other recently reported compound, an extended Pt-acridine therapeutic, is available for post-treatment click analysis.[5] In the case of picazoplatin, relatively slow reaction kinetics are built into the design of the parent compound picoplatin wherein the ring methyl shields Pt from substitution reactions.[6] Moreover, although in-cell use was demonstrated, analysis of cellular targets may be complicated by the potential for *trans*-labilization of the azide-functionalized picoline ring. New click-functionalized Pt(II) reagents are of great interest in order to take advantage of bioorthogonal approaches[7] for high-throughput identification of Pt-bound species *in vivo*.

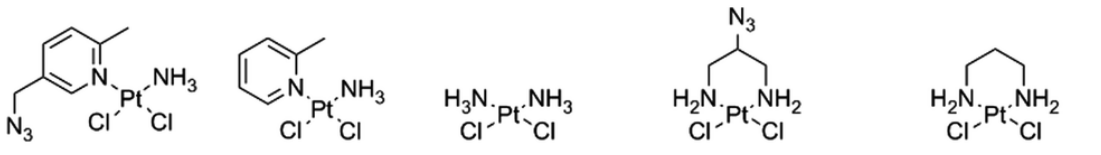

Figure 2.1. Click-functionalized picazoplatin **1** and its parent picoplatin **2**, with cisplatin **3** and the 1,3-propanediamine derivatives **4** and **5**.

To provide a convenient and fast-reacting Pt(II)-azide click reagent, we have explored *cis*-[Pt(2-azido-1,3-propanediamine)Cl_2] (**4**) in nucleic acid binding, protein binding, and click chemistry. While **4** has been previously used to create libraries of diazenecarboxamide–carboplatin conjugates,[8] to our knowledge it has not been applied as an agent for post-treatment labelling by click modification. Herein, we demonstrate efficient click reactivity of the DNA-bound compound and an unusual isomeric

differentiation of **4** when bound to duplex DNA. Click fluorescent labelling of Pt-bound proteins is demonstrated in bovine serum albumin (BSA). The utility of this compound for *in vivo* studies is demonstrated by tracking Pt-bound ribosomes from cells treated with **4**.

DNA binding studies of **4** on a 13-nucleotide DNA containing a single GG site were analysed by dPAGE (Fig. 2.2). A higher yield of **4**-bound DNA is observed in comparison with the sterically-hindered **1**. Subsequent click reactivity with a dansyl alkyne fluorophore is seen in both cases.

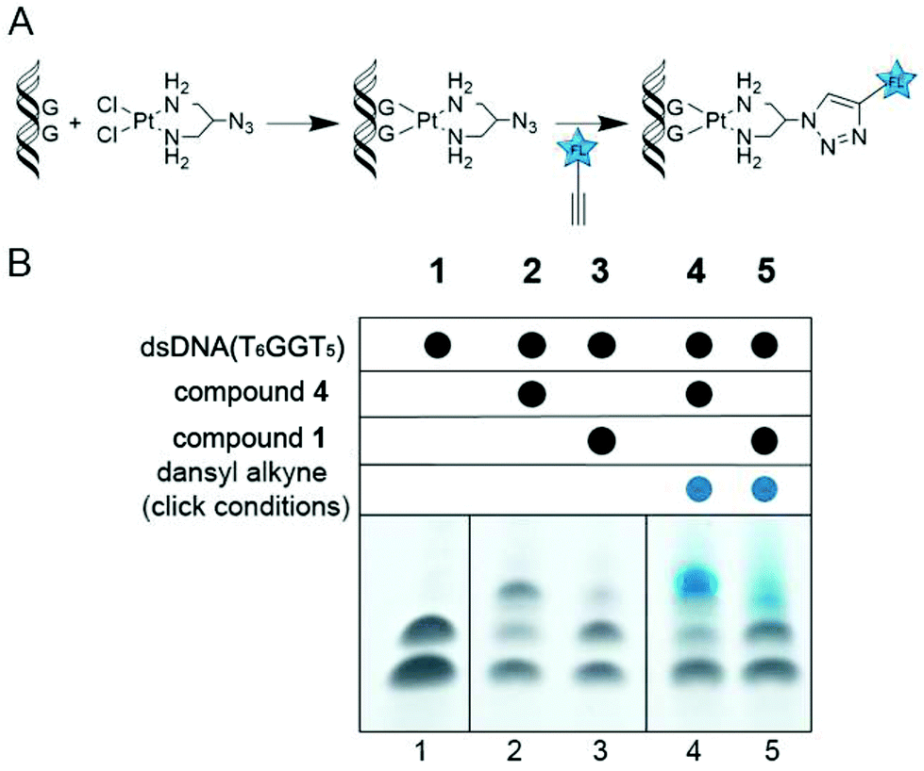

Figure 2.2 (A) Reaction scheme for Pt binding and subsequent click to an alkyne fluorophore. (B) dPAGE analysis of dsDNA bound by picazoplatin (**1**) and *cis*-[Pt(2-azido-1,3-propanediamine)Cl_2] (**4**) and subsequently clicked to a dansyl alkyne fluorophore. The denatured DNA strands are visible in lane 1, while higher molecular weight Pt-bound species are visible in lanes 2 and 3. Click reaction results in fluorescence of the Pt–DNA band under UV light in lanes 4 and 5 (see **Appendix A**).

RP-HPLC Analysis of DNA-Bound Pt Adducts

To further quantify Pt binding and click reactivity of **4**, HPLC analysis was used with a short DNA hairpin sequence (TATGGTATTTTTATACCATA, HP). Upon Pt binding to the single GG site, two product peaks emerge that are distinct from the parent DNA peak. Both new peaks were confirmed by dPAGE to contain hairpin DNA bound by Pt (see **Appendix A**). Both products contain one bound Pt(2-azido-1,3-propanediamine) as confirmed by identical 3+ charged ions in ESI-MS analysis (Fig. 2.3C). When reacted with dansyl alkyne, material in both product peaks yields clicked products as resolved by HPLC and identified by the fluorophore absorbance at 340 nm (>80% yield, see **Appendix A**). Thus, this bimodal product distribution is hypothesized to originate from two different structural isomers of **4** bound to the asymmetric DNA strand. This hypothesis was tested with the analogous azide-free complex **5** (see **Appendix A**).[9] As expected, the HPLC trace of DNA-bound **5** exhibits only one product peak (Fig. 2.3B), indicating that the 2-azido group of **4** creates structural isomers.

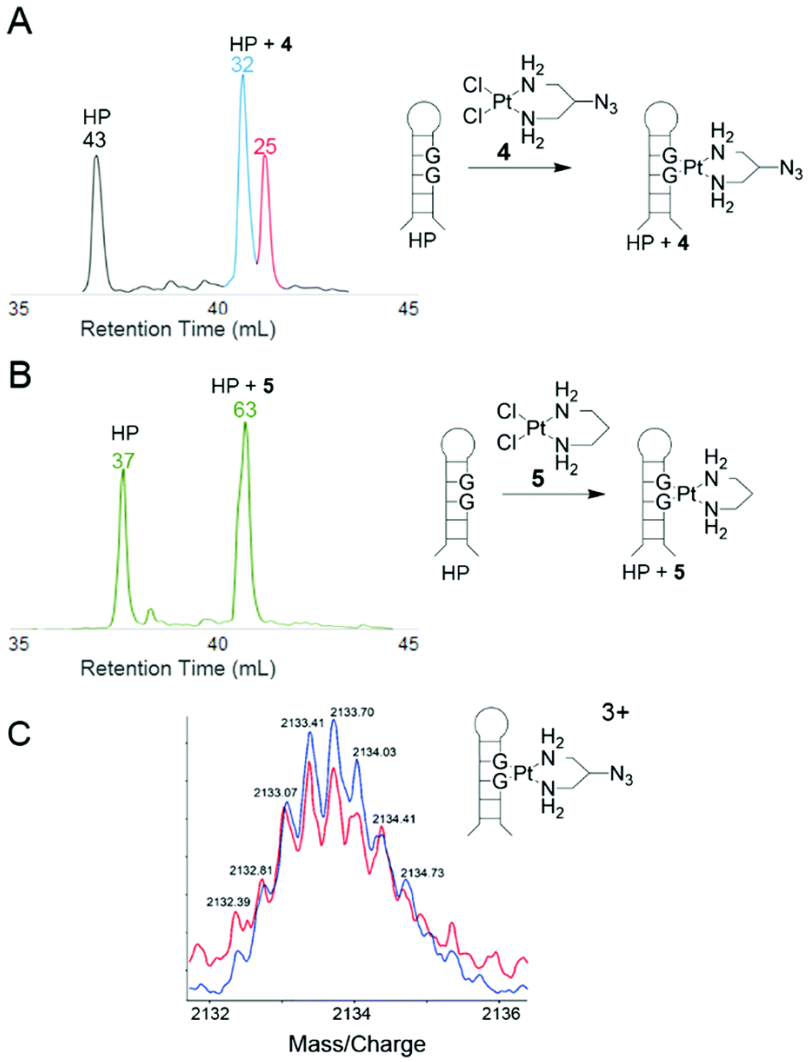

Figure 2.3 HPLC absorbance traces at 260 nm for a short hairpin DNA sequence bound to (A) **4** and (B) **5**. Peaks observed at ~37 mL eluent volume are identified as unbound DNA, and peaks between ~40 and ~42 mL are Pt-bound DNA (55–65% yield). When **4** is bound to DNA, two peaks are resolved indicating the presence of non-equivalent Pt-bound species. Both collected fractions (blue and red traces) were analysed *via* ESI-MS, revealing that they contain the same 3+ charged species of **4**-bound DNA (C). Reaction with azide-free **5** yields a single product band (B, 55–65% yield). Normalized areas are indicated above peaks of interest.

The two isomer products of **4**-treated hairpin DNA consistently yield non-equivalent peak areas, indicating preference of one conformation that is likely being dictated by the orientation of the azide relative to the helix. Supporting this, treatment of single-stranded DNA shows equivalent populations of both isomers (Fig. 2.4C), whereas

the same sequence in duplex returns to an unequal population (Fig. 2.4D, see also **Appendix A**).

Possible conformations of DNA-bound **4** are visualized (Fig. 2.4) in molecular models built by substituting **4** into the crystal structure of cisplatin-bound 12-mer DNA duplex (pdb: 3LPV).[10] Bond lengths and angles around the Pt(II) center were fixed and the position of the DNA was locked (see **Appendix A**), and equilibrium geometries of the two structural isomers were determined using molecular mechanics (MMFF). The resulting models show distinct geometric properties, with the azide oriented either toward the major groove or towards the phosphate backbone. In the denatured strands analyzed by HPLC, these isomers must give rise to slight differences in hydrophobicity; resolution of such minor differences in oligonucleotides has precedent.[11,12] The inequivalent populations of isomers suggest that the helical structure of DNA has a direct impact on the preferred orientation of the azide substituent due to steric and electronic effects. Like the hairpin DNA, upon reaction with the dansyl alkyne fluorophore, **4**-bound T_6GGT_5 is converted into clicked products with yields that range from 80–90% (see **Appendix A**).

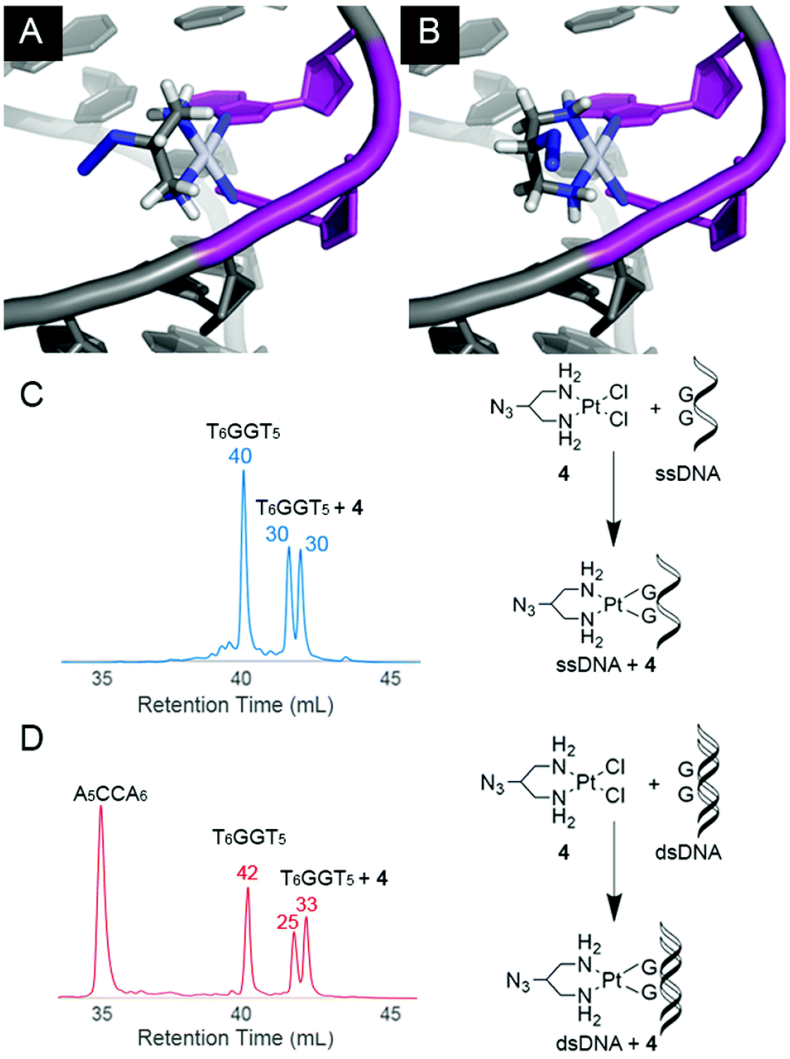

Figure 2.4 Molecular modelling (MMFF) of the two possible isomers of **4**-bound double-stranded DNA with the azide oriented in towards (A) or out from (B) the centre of the helix. In the helical conformation of A as shown, the azide moiety is less solvent exposed than in B. Models were generated by substituting **4** into the crystal structure of cisplatin-bound DNA (PDB: 3LPV, see **Appendix A**). The adjacent Pt-bound guanines of the intrastrand crosslink are shaded purple. HPLC absorbance traces at 260 nm for **4** reacted with (T_6GGT_5) as a single-strand (C, 55–65% yield) or in duplex (D, 55–65% yield). Normalized areas are indicated above peaks of interest. When reacted with the single-strand sequence, isomers of **4**-bound DNA show equal population (ratio = 0.96 ± 0.05; see **Appendix A** for data in triplicate) whereas they are unequal for the duplex (ratio = 1.3 ± 0.09; see also **Appendix A**).

Metal-Protein and Metal-RNA Pt-Binding Analysis

In furthering the analysis of potential targets for Pt(II) compounds, bovine serum albumin (BSA) was also investigated as a model compound for the ability of **4** to bind and participate in post-treatment labelling of proteins. Previous studies have shown Pt-binding to Cys 34[13] following treatment of BSA with cisplatin. Here BSA is incubated with increasing equivalents of **4** followed by click to an alkyne-containing dansyl fluorophore (Fig. 5). Labelled protein was visualized by Coomassie staining and fluorescence imaging. Fluorescence is seen only in the **4**-treated samples and increases in a dose-dependent manner (Fig. 2.5, lanes 2–4). Fluorescence is also only observed in reactions containing both **4** and the Cu catalyst.

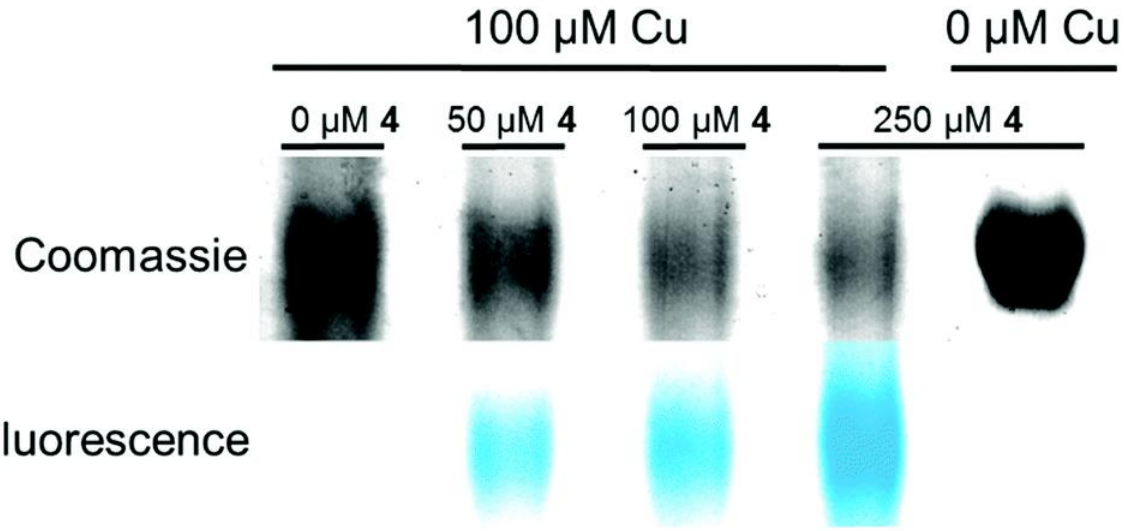

Figure 2.5 Fluorescent labelling by click chemistry of **4**-treated bovine serum albumin (BSA) with a dansyl alkyne fluorophore. Lanes 2–4 contain BSA incubated in the presence of $CuSO_4$ post Pt treatment and show a dose-dependent increase in fluorescent signal with respect to the concentration of **4**. Lanes 1 and 5 shows that fluorescent labelling is also dependent on the presence of both **4** and the Cu catalyst.

Ultimately, the power of clickable Pt compounds is to identify and analyze *in vivo* targets. In contrast to cisplatin, Pt(II) compounds with small chelating amine ligands such as

ethylenediamine and 1,3-propanediamine are better tolerated by cells, making them particularly attractive as potential *in vivo* crosslinking reagents.[14] We have previously shown significant accumulation of Pt on cellular RNA following treatment with cisplatin, with major accumulation being on ribosomal RNA.[15,16] Here, we tracked the lifetime of Pt–RNA adducts using **4**, and find surprising longevity of Pt adducts on ribosomal RNA. *S. cerevisiae* was treated with 0 μM and 250 μM **4** for 6 h and then re-suspended in fresh media. Cells resuspended in drug-free media showed growth similar to untreated control cells, consistent with the relatively low toxicity of **4** and in contrast to treatment with cisplatin.[15] To determine whether Pt–rRNA adducts were quickly degraded or long-lived, RNA was extracted from cells at various timepoints and accumulated Pt detected following click labelling with Alexa Fluor 488 DIBO (Fig. 2.6). Lanes 1–4 contain rRNA isolated from untreated cells subjected to the same click labelling protocol. The absence of fluorescence in these lanes indicates the absence of nonspecific labelling during the DIBO/click procedure. Lanes 5–8 contain rRNA isolated from treated cells after up to 2 h in **4**-free media. The normalized fluorescence per rRNA band shows no significant loss in Pt–RNA adducts, meaning that platinated ribosomes persist in doubling cells and that the majority of them are not targeted for fast degradation. The persistence of the fluorescent labelling even after 120 min post-treatment demonstrates the efficacy of **4** in post-labelling strategies to ascertain possible Pt(II) cellular targets.

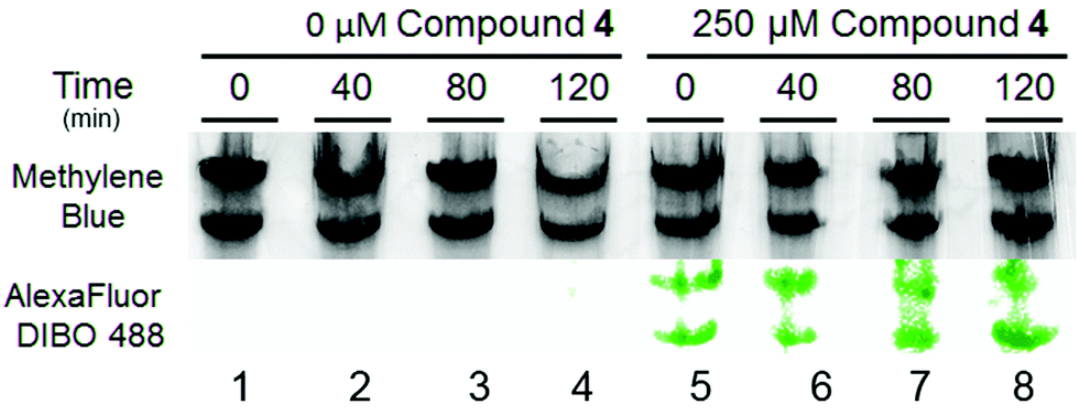

Figure 2.6 Fluorescent labelling by click chemistry of rRNA extracted from **4**-treated *S. cerevisiae*. 25S and 18S rRNA extracted from *S. cerevisiae* treated with 0 μM or 250 μM **4** for 6 h and resuspended in drug-free media for 0–120 min. All samples were subsequently treated with 250 μM Alexa Fluor 488 DIBO (16 h, 37 °C).

Conclusions

This work demonstrates the ability of azide-modified Pt(II) compound **4** to readily bind oligonucleotides and proteins and subsequently undergo click reactions for post-treatment fluorescent labelling. This demonstrated reactivity of **4** expands the array of available azide-modified Pt(II) reagents to be used in post-treatment target analysis. In comparison with recently reported **1**, **4** exhibits greatly increased efficiency in target binding. HPLC analysis and molecular modelling suggest formation of two different isomers of **4**-bound DNA adducts, hypothesized to be biased by the orientation of the azide moiety of **4** in relation to the helical structure of DNA. Efforts to discern differences in click reactivity between the two isomers are currently underway in our laboratory, as well as efforts utilizing clickable Pt(II) reagents as RNA crosslinking agents to quantify and isolate platinum-bound species *in cellulo*.

Summary of Chapter II and Bridge to Chapter III

In this chapter we analyzed the binding of **4** to DNA, RNA and proteins. Complex **4** exhibited a bias in conformational isomers upon binding to DNA. This isomerization was shown to be most likely due to the presence of the azide group on **4**. Furthermore, the isomerization bias seems to be influenced by the higher order structure of DNA. Complex **4** also shows a propensity to form metal-protein and metal-RNA adducts as well. The RNA adducts on rRNA formed *in vivo* appear to be long-lived. Using **4** as a synthon to construct other Pt(II) azide-modified complexes could help give insight on Pt localization within cells. Chapter III uses two different derivatives of **4**, an azide and an alkyne-modified complex, to ascertain differences in binding, reactivity and localization of Pt within cells.

CHAPTER III

AZIDE VS ALKYNE FUNCTIONALIZATION IN PT(II) COMPLEXES FOR POST-TREATMENT CLICK MODIFICATION: SOLID-STATE STRUCTURE, FLUORESCENT LABELING, AND CELLULAR FATE

This chapter contains contributions from Regina M. Wirth, Dr. Jonathan D. White, Aurora L. Ginsberg, Prof. Michael M. Haley and Prof. Victoria J. DeRose. MMH and VJD provided insight and direction through the course of this investigation. Under the advisement of JDW, RMW conducted all synthesis and dPAGE analysis of the Pt compounds. The synthesis of two rhodamine fluorophores and development of the in-cell imaging technique were done by myself. ALG, under my advisement, performed studies using the alkyne-appended Pt complex in HeLa cells while I investigate the azide appended complex within cells. This chapter includes material reproduced from the Journal of the American Chemical Society (2015, 44, 3536-3539, © 2016 American Chemical Society), co-authored by RMW, JDW, myself, ANG, MMH, and VJD.

Introduction

Since the compound cisplatin, *cis*-diamminedichloroplatinum(II), was approved by the FDA for clinical use in 1978, Pt-based therapeutics have become one of the most widely used and successful treatment options for a variety of cancers, including ovarian, testicular, bladder, non-small-cell lung carcinomas, and others.[1-4] Although much progress has been made in understanding the mechanisms of action of Pt compounds as well as their specific cellular targets, a comprehensive molecular-level understanding of their reactivity is still

lacking.[5-8] It is generally accepted that Pt reagents are taken up into the cell via passive and active mechanisms and then undergo aquation, the displacement of labile chloride ligands by water, forming $[Pt(NH_3)_2Cl(OH_2)]^+$ and $[Pt(NH_3)_3(OH_2)_2]^{2+}$ species.[9,10] These highly reactive species form exchange-inert complexes with purine bases of genomic DNA in addition to other biomolecules.[11] *In vivo* and *in vitro* studies have unambiguously identified *cis*-1,2-$\{Pt(NH_3)_2\}^{2+}$-d(GpG), 1,2-d(ApG), and 1,3-d(GpNpG) intra- and interstrand DNA cross-links as products, and these are capable of inhibiting normal transcriptional processes of the cell and initiating apoptotic signaling.[12,13] Importantly, only a very small fraction of Pt (less than 10% in the case of cisplatin) accumulates within genomic DNA.[14] In samples isolated from cells treated with Pt reagents, Pt has been found to bind to a wide variety of additional nucleophilic targets, including different cellular RNAs, proteins, and sulfur-containing compounds such as glutathione. Despite a great deal of work, Pt localization in treated cells and binding properties with non-DNA targets, and their consequences, remain poorly understood.[6,7,15] A better understanding of Pt cellular reactivity is essential in order to design new, more effective therapeutics and methods of delivery.

In addition to identifying molecular targets of Pt reagents, a comprehensive identification of all organelle targets is desired. Such an understanding would shed light on apoptotic and toxicity pathways, as well as differences in efficacy in dissimilar types of cancers. Highlighting the diversity of potential cellular locales, various studies using atom-based techniques as well as fluorescent tagging have obtained evidence for cellular Pt accumulation in ribosomes, the nucleus, nucleoli, mitochondria, and secretory pathways linked to vesicles, lysosomes, and Golgi.[16,18]

Fluorescence detection via confocal microscopy has distinct advantages of sensitivity and resolution and can be coupled with existing fluorescent markers for co-localization studies. An important strategy used to detect Pt in cells comprises the covalent tethering of fluorescent probes to modified Pt-coordinated ligands. In one such study, a fluorescein-linked Pt compound was observed to accumulate in the nucleus and nucleolus 2–3 h post-treatment, followed by punctate localization in the cytoplasm after 7 h. A gradual decrease in total cellular fluorescence was observed over several days, indicating that Pt actively effluxes from the cells.[17] Other Pt–fluorescein conjugates have revealed accumulation in the Golgi and in vesicles, and expression of Cu efflux proteins was demonstrated to affect Pt retention.[18] Other important conclusions regarding the reactivity of Pt compounds have been determined via modification with fluorescent probes, and these have been reviewed recently.[19] While fluorophore-linked Pt probes have been shown to mimic some properties of native Pt complexes, the physical properties of the large, hydrophobic probes and their interactions within the cell are expected to be quite different from those of the small, neutral or positively charged Pt complexes.[8,17-20] These differences may influence the types of interactions that direct localization of the Pt complex, such as intercalation, hydrophobic, or electrostatic-based interactions. It has been shown, for example, that different amino-acid-linked cisplatin analogues exhibit altered specificity for ribosomal RNA (rRNA) compared to the parent compound.[21]

Due to possible undesirable consequences of pre-attaching probes, fluorescence detection of Pt compounds through post-binding modifications would be more attractive. This strategy takes advantage of minimally invasive reactive handles incorporated onto Pt reagents, followed by conjugation to fluorescent probes after the Pt compound has bound

irreversibly to biomolecule targets (Fig 3.1). Using this strategy, we have previously reported use of the Cu-catalyzed azide–alkyne cycloaddition (CuAAC) click reaction,[22] with modified Pt(II) complexes containing azide- and alkyne-reactive "handles".[23-26] We have identified cellular RNAs, including tRNA, as targets of Pt reagents *in vivo*, in addition to identifying other nucleotide and protein targets *in vitro*.[23-27] Recently, Bierbach and colleagues have used post-binding click modification of a monofunctional Pt–acridine hybrid complex to identify its cellular distribution within the nucleus and nucleoli of lung cancer cells.[20a,20b] Herein, we report the design and use of the new click-capable Pt(II)–azide complex **1** and its cellular distribution in HeLa cells, as observed via confocal fluorescence microscopy. The in-cell and *in vitro* reactivity of **1** is also compared with that of the previously reported alkyne-modified congener **2**,[26] demonstrating the utility of the completely complementary pair of Pt–click reagents and rhodamine–fluorophore probes. Both compounds **1** and **2** were designed to mimic the *cis* geometry and difunctional reactivity of cisplatin and other Pt(II)-based FDA-approved chemotherapeutics.

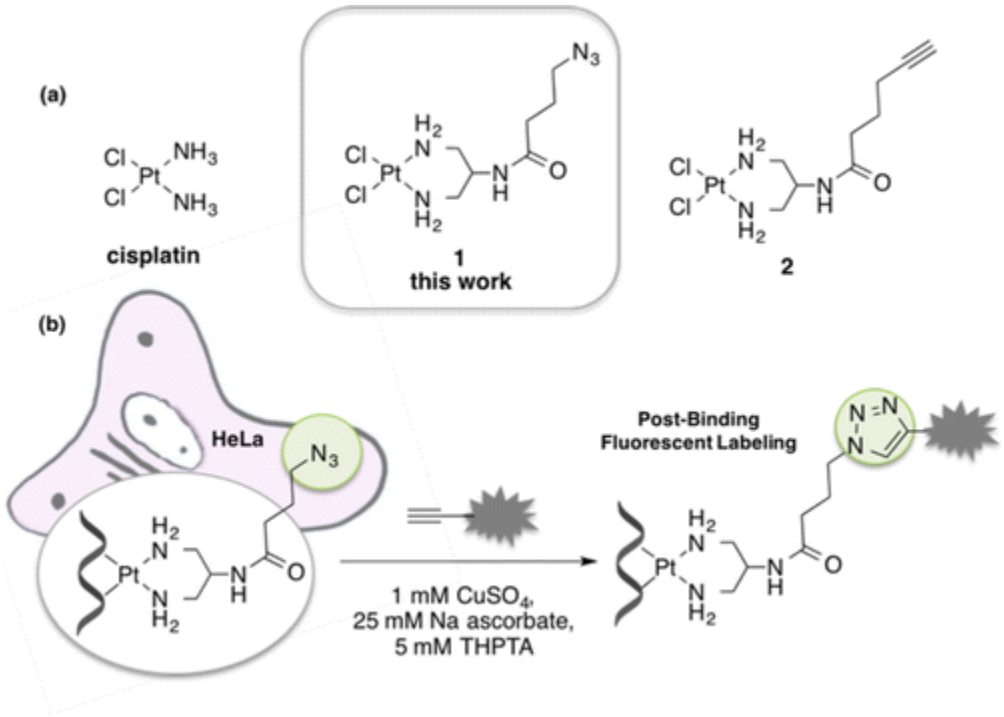

Figure 3.1. (a) Chemical structures of the anticancer drug cisplatin, with the novel azide-appended **1** and alkyne-appended **2**. (b) Reaction scheme of target-bound 1 undergoing post-binding covalent click modification to a fluorescent probe.

Results and Discussion

Compound **1** was synthesized analogously to the preparation of **2**, with the peptide linkage allowing for facile incorporation of different coupling partners (Fig 3.http://pubs.acs.org/doi/10.1021/jacs.5b09108 - fig22). Therefore, di-*tert*-butyl (2-aminopropane-1,3-diyl)dicarbamate was coupled to 4-azidobutanoic acid with 1-ethyl-3-(3-*N*,*N*-dimethylaminopropyl)carbodiimide.[28] Deprotection with anhydrous HCl followed by platination of $[Pt(DMSO)_2Cl_2]$ yielded the final product **1** in 16% overall yield. Both complexes **1**and **2** exhibit identical ^{195}Pt NMR chemical shifts ($\delta = -2286$ ppm, d_7-DMF; see **Appendix B**), indicating no inter- or intramolecular interactions between the Pt center and peptide-linked azide or alkyne groups.[29]

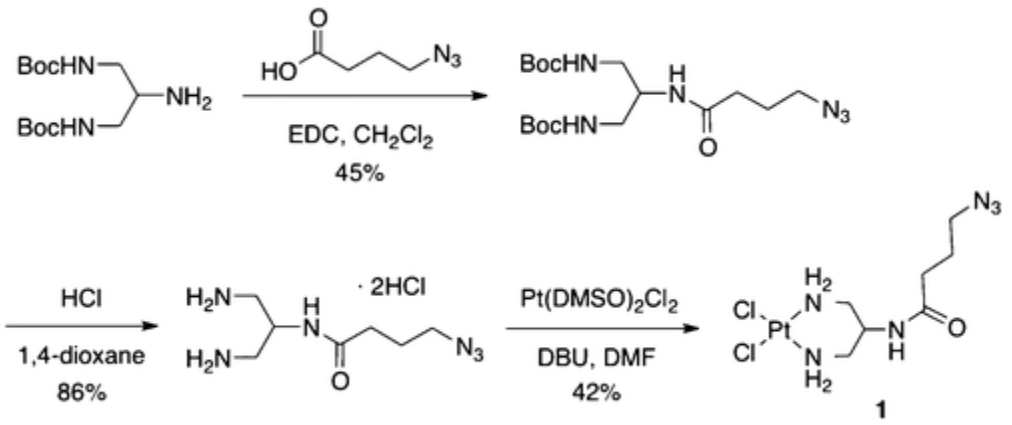

Figure 3.2. Synthesis of Pt complex **1**. Boc = tert-butoxycarbonyl, EDC = 1-ethyl-3-(3-N,N-dimethylaminopropyl)carbodiimide, DMSO = dimethyl sulfoxide, DBU = 1,8-diazabicyclo[5.4.0]undec-7-ene, DMF = N,N-dimethylformamide.

Crystals of **1** suitable for X-ray diffraction were obtained from a chilled DMF/H_2O solution, and the structure obtained confirms that assigned via NMR spectroscopy. The individual bond lengths and angles around the square planar Pt(II) center of the azide-containing **1** are very similar to those of the reported alkyne-appended **2** (see **Appendix B**).[26,30] Both compounds form Pt–Pt dimers (Pt···Pt, 3.46 Å in **1**) connected in the crystal structure by hydrogen bonds (Fig 3 and **Appendix B**).[31, 32] Each chloride acts as a hydrogen bond acceptor for the Pt-coordinated amine groups (Cl···N, 2.53 Å, 2.35 Å in **1**) (Fig 3.3a).[32] In addition, a distance of 2.13 Å between coordinated amine protons and adjacent carbonyl oxygen indicates hydrogen bonding (see **Appendix B**http://pubs.acs.org/doi/suppl/10.1021/jacs.5b09108/suppl_file/ja5b09108_si_001.pdf, Figure S3).

Despite the similarities in the solid state between **1** and **2**, the broader packing arrangement changes drastically upon exchange of the alkyne with the azide moiety. The arrangement of **2** is primarily dictated by CH/π(C≡C) hydrogen bonds, forming a rare, spoke-type arrangement (Figure 3.3c).[26] Arrangement of the azide-containing **1** appears to

be dictated by the formation of the Pt dimer, including both Pt–Pt bonding and hydrogen bonds. The Pt centers are aligned into infinite 1D-zigzag chains with regular alternating distances of 3.46 and 3.98 Å and a Pt···Pt···Pt bond angle of 159.6°. Interestingly, the azide moieties of adjacent Pt "chains" are aligned antiparallel and in close proximity to one another, approximately 3.5 Å apart (Figure 3.3b). This is in agreement with azide−azide packing distances previously reported for several organo-azides and may indicate the presence of a weak dipole–dipole interaction between nitrogen atoms of opposing azides.[33] Finally, N–N bond lengths and angles of the azide moieties themselves are in good agreement with well-established parameters (1.12 and 1.28 Å for the terminal and internal N–N bond distances, respectively, and N≡N–N bond angle of 174.1°).[33, 34]

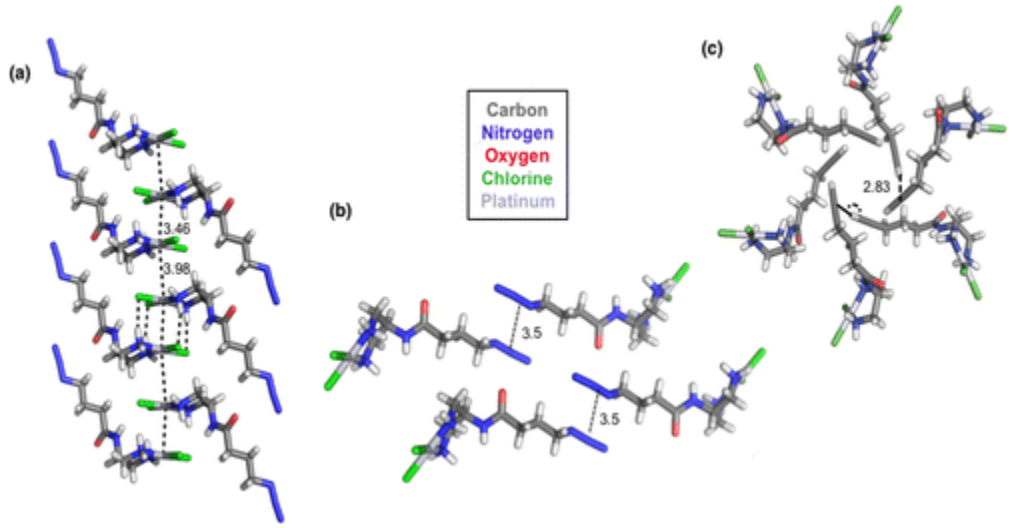

Figure 3.3. (a) Crystal structure arrangement of **1** showing the Pt–Pt dimer formation in a 1D-zigzag chain with a 159.6° angle between the platinum centers as well as Cl···H–N hydrogen bonding. Selected bond lengths and angles: Pt–Cl 2.315(2) Å, 2.334(3) Å; Pt–N 2.016(8) Å, 2.045(7) Å; N≡N 1.117(11) Å; N–N 1.280(12) Å; N≡N–N 174.2(11)°. (b) Antiparallel arrangement of the azide moieties of adjacent Pt chains. (c) Crystal structure arrangement of **2** showing the spoke-type arrangement dictated by CH/π(C≡C) hydrogen bonds. See **Appendix B** for detailed crystallographic data.

To confirm the ability of **1** to bind known targets of Pt and subsequently undergo post-binding click modifications, **1** was bound to a short oligonucleotide sequence containing a 5′-GG-3′ pair and subsequently reacted with an alkyne-functionalized rhodamine fluorophore (**3**) (see **Appendix B**) and subjected to denaturing polyacrylamide gel electrophoresis (dPAGE). Both compounds **1** and **2** undergo facile binding to DNA (18 h, 37 °C), followed by near-complete conversion to the rhodamine-labeled click product ($CuSO_4$–ascorbate, 18 h, rt), the latter complex **2** having been reacted with the analogous azide-functionalized rhodamine fluorophore (**4**) (Fig 3.4).[35] Both complexes appear to bind to DNA in similar yields, which suggests the identity of the click "handle" (i.e., azide versus alkyne) does not significantly affect binding or click reactivity *in vitro*.

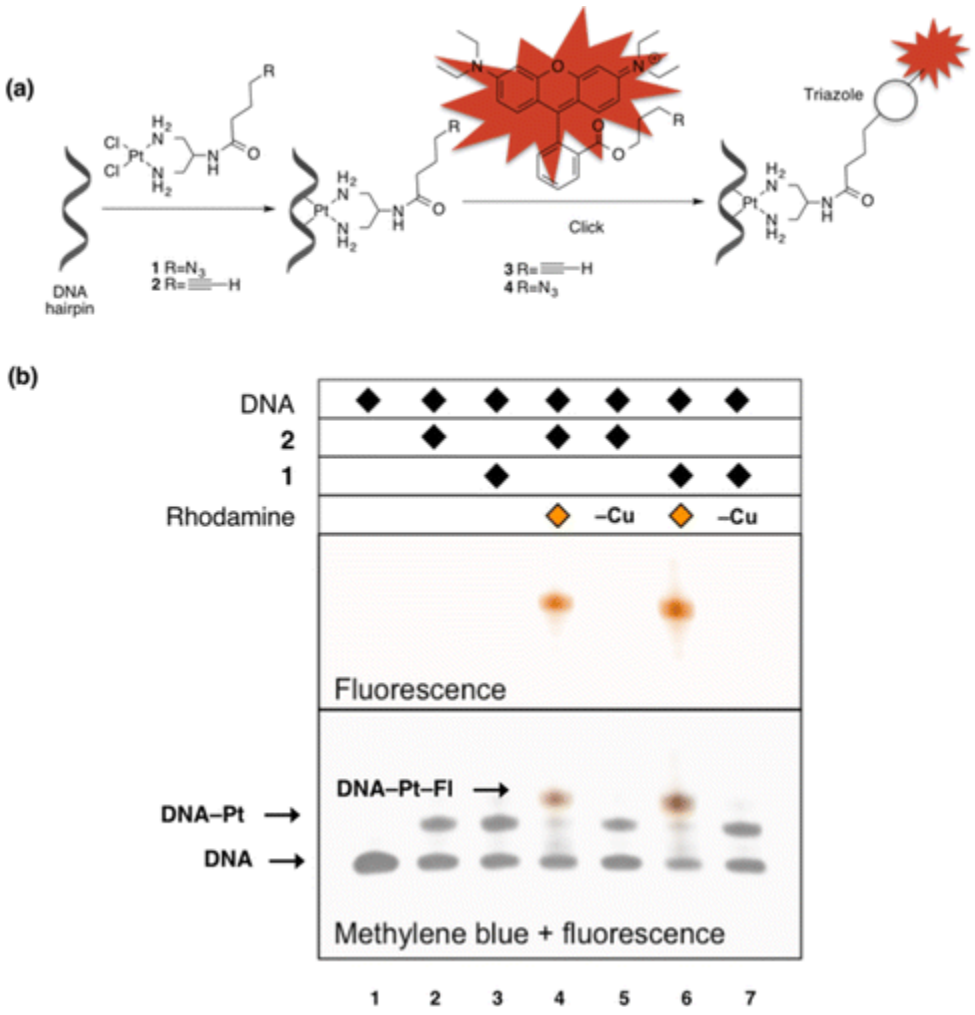

Figure 3.4. (a) Reaction scheme of the binding of **1** and **2** to a DNA hairpin followed by fluorescent click-labeling using complementary alkyne- or azide-rhodamines (**3**,**4**). (b) dPAGE experiment showing the binding of **1** and **2** to a 5′-GG-3′ DNA hairpin (lanes 2 and 3). The click reaction of **1**- and **2**-bound hairpin with the complementary rhodamine fluorophores can be observed by the appearance of a fluorescent band (lanes 4 and 6). Control reactions show no click ligation under Cu-free conditions (lanes 5 and 7).

Further *in vitro* experiments were conducted to obtain deeper insight into the binding and click reactivity of **1**. Since we now possessed two complementary click-appended Pt(II) complexes, we were curious if they could be reacted together to covalently attach two Pt-bound targets. Solutions of **1** and **2** were individually bound to separate 5′-

GG-3′ DNA hairpins, then reacted together under click conditions analogous to the previously described reactions with rhodamine (24 h, rt). The appearance of a band of significantly less mobility indicates the formation of the triazole-linked hairpin DNA dimer (lane 4, Figure 3.5). This result suggests the potential for these Pt compounds to be used in nucleotide cross-linking applications and other diverse nucleotide modification reactions.[36]

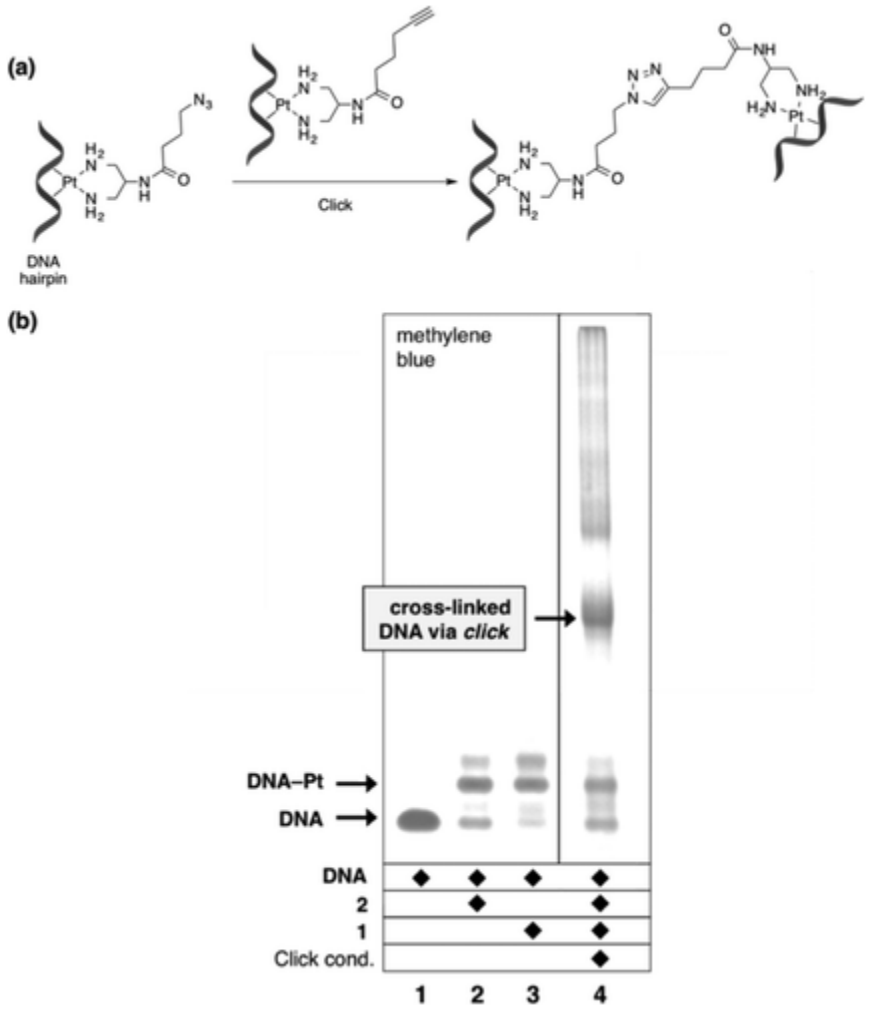

Figure 3.5. (a) Reaction scheme of biomolecule-bound azide **1** clicking to the biomolecule-bound alkyne **2** to form a cross-linked DNA. (b) dPAGE experiment showing **1** and **2** bound to a 5′-GG-3′ DNA hairpin (lanes 2 and 3). Lane 4 shows the click reaction product between **1**- and **2**-bound DNA hairpins, resulting in a triazole-linked DNA dimer (see **Appendix B** for complete conditions).

To assess the influence of the peptide linkage of **1** (and **2**) on DNA binding and click reactivity, we compared **1** to the peptide- and linker-free *cis*-[Pt(2-azido-1,3-propanediamine)Cl_2] (**5**).[37] Compound **5** has been previously utilized by our group for post-treatment fluorescent click labeling of nucleotides and proteins *in vitro*, and rRNA *in vivo*.[25]

For comparison, **1** and **5** were each bound to a 5′-GG-3′ DNA hairpin sequence and subjected to click conditions with a dansyl alkyne fluorophore (Fig 3.6a) and analyzed via dPAGE (Fig 3.6b). Both compounds appear to bind to DNA in similar yields (lanes 2 and 3), indicating binding reactivity independent of the linker moiety. The click reactivity was evaluated by time-dependent (0.5, 3, or 6 h reaction times) treatment of the Pt–DNA complex with the dansyl–alkyne fluorophore under click conditions. Interestingly, **1**-bound DNA is completely converted to clicked product after only 3 h reaction time, whereas even after 6 h click reaction time, unreacted (non-clicked) **5**-bound DNA is observed (Fig 3.6, lane 8). The observed enhanced reactivity of the longer **1** may be due to increased steric accessibility of the azide moiety once bound to DNA. Additionally, non-innocence of the peptide bond participating in the click reaction cannot be ruled out—for example, Ting and colleagues reported an acceleration of the CuAAC reaction using organo-azides that contain internal Cu(I) chelating moieties.[38]

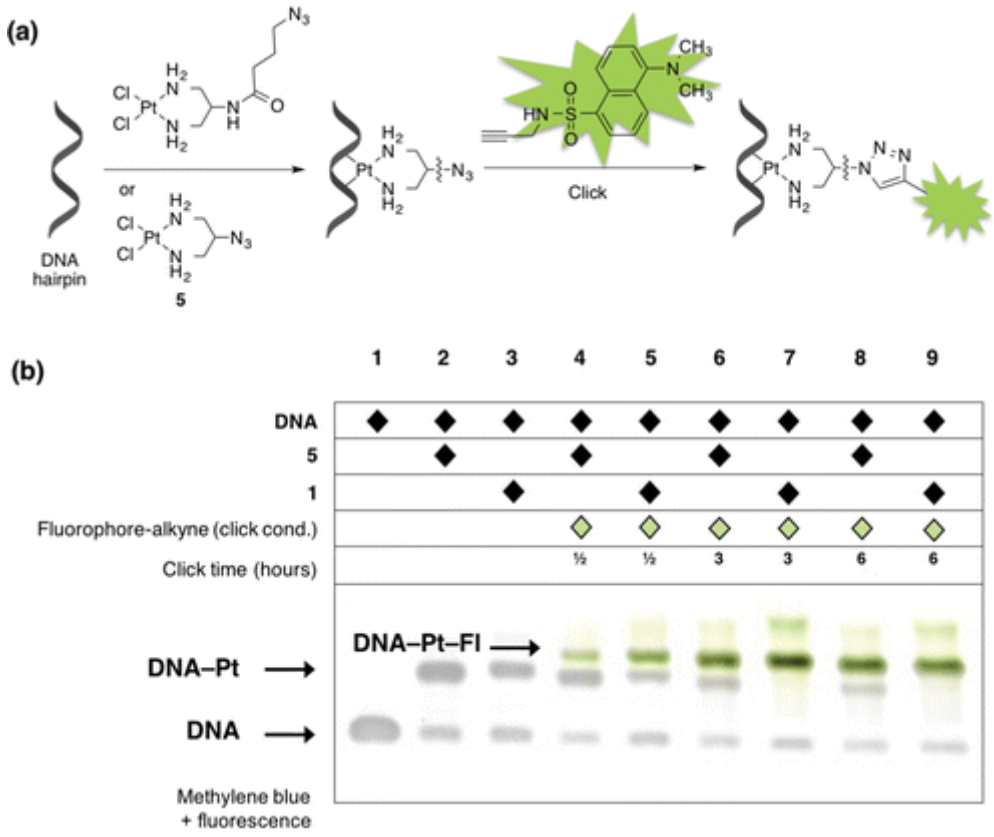

Figure 3.6. (a) Reaction scheme of binding of the azide-modified Pt(II) complexes **1** and **5** to a 5′-GG-3′ DNA hairpin sequence, followed by subsequent CuAAC with dansyl alkyne fluorophore. (b) dPAGE analysis of binding and fluorophore conjugation of **1** and **5** to DNA hairpin (see **Appendix B** for conditions).

Encouraged by its apparent enhanced reactivity, we pursued cellular localization studies using the azide-appended **1** and confocal fluorescence microscopy (Fig 3.7). In initial studies, HeLa cells were treated with **1** (25 μM, 3 h), washed, fixed and permeabilized, and then labeled with the alkyne-containing rhodamine fluorophore **3** (5 μM, 2 h) under CuAAC click conditions (see **Appendix B**). Confocal images of the cells show the highest level of fluorescence in the nucleoli of the HeLa cells, along with broad localization in the nucleus (Fig 3.7b). Importantly, the Cu-free controls show no fluorescence from nonspecific fluorophore interactions (Fig 3.7f and **Appendix B**). These results are consistent with previously reported targets of Pt(II) chemotherapeutics. The high

accumulation of compound **1** in the nucleoli is in agreement with previously identified nuclear DNA adducts of Pt,[10] as well as Pt–rRNA adducts. rRNA has been shown to bind Pt(II) complexes using inductively coupled plasma mass spectrometry and fluorescent labeling in *Saccharomyces cerevisiae*.[24, 27] Pt–protein adducts may also be present. The nucleolus has also been identified as a major target using some fluorophore pre-tethered Pt(II) complexes.[39] Bierbach and colleagues very recently identified localization in the nucleolus using an azide-modified Pt–acridine complex for post-binding fluorescent labeling as well as pre-tethered Pt–fluorophores, although differences between the two approaches were noted.[20a, 20b]

Treatment of HeLa cells using the complementary alkyne-containing complex **2** and the rhodamine-azide **4** (25 μM treatment) shows identical localization (Fig 3.7d), which indicates similar cellular binding of both Pt complexes **1** and **2** independent of the click-functionalized moiety. Interestingly, however, Pt(II)-concentration-dependent post-treatment labeling in the HeLa cell line shows a dramatic difference in the observed fluorescent signal between these two complementary click compounds. Despite the similar localization of **1** and **2**, there is significantly less fluorescent signal following 25 μM cellular treatment with **2**, using identical conditions. HeLa cells were also treated individually with 5 μM complex **1** and **2** for 3 h followed by click labeling with the complementary rhodamine fluorophores. At this lower concentration, cells treated with the alkyne-appended complex **2** show no detectable fluorescent signal above background, but cells treated with azide-containing **1** present bright and distinct fluorescence (Fig 3.7j). Although we have not observed Pt-catalyzed hydration or hydroamination across the triple bond in previous experiments using **2**, it is

well-reported that alkyne-containing compounds can undergo these reactions, which could lead to a decrease in fluorescent signal in-cell.[40] The hydrophobicity of alkynes in comparison to their azide counterparts may also have an effect on accumulation or reactivity in the cell. These promising results show the potential of compound **1** not only for further localization studies in different cancer cell lines, but also for ongoing goals of isolating and identifying Pt(II)-bound targets using click chemistry.

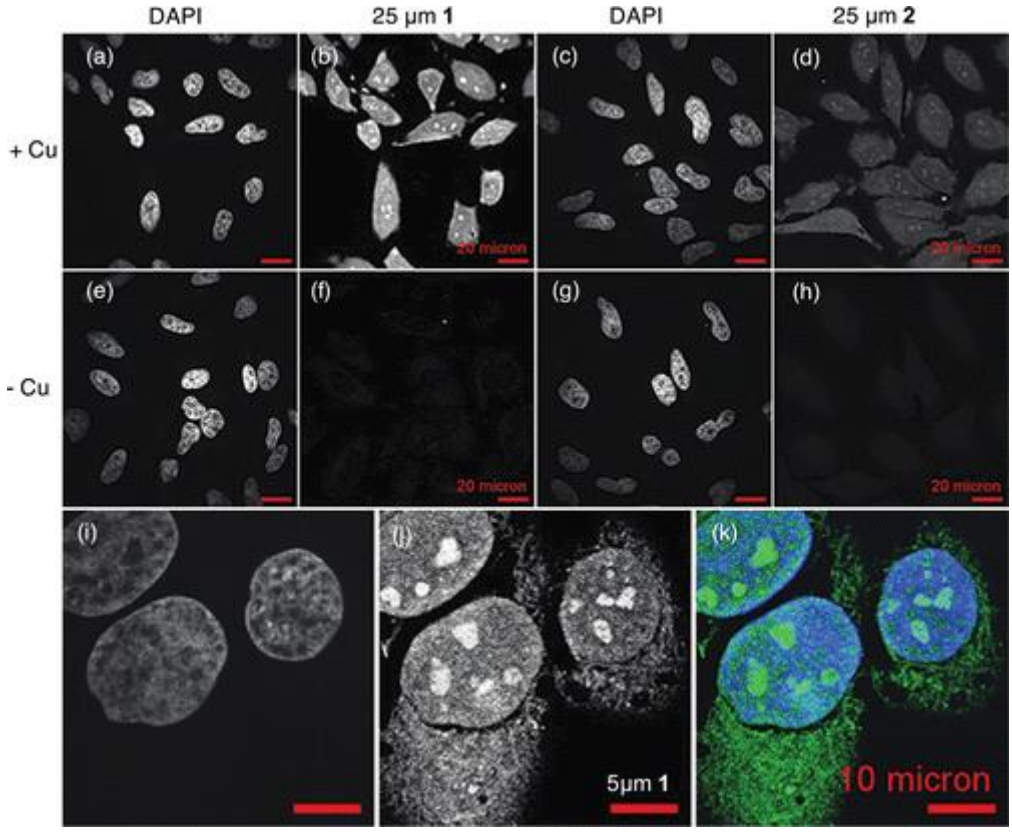

Figure 3.7. Confocal image of fluorescent cellular localization. Panel (b) shows the fluorescent labeling of HeLa cells treated with **1** (25 μm, 3 h) and subsequent click with rhodamine alkyne **3**. The Cu-free control (f) shows no fluorescence. Panel (d) shows the fluorescent labeling of HeLa Cells treated with **2** (25 μm, 3 h) after fixation, permeabilization, and labeling with the rhodamine azide **4** in the HeLa cell line and Cu-free control (h). Panel (j) shows an enlarged image of the fluorescent labeling of HeLa cells treated with **1** (5 μm, 3 h) and subsequent click with rhodamine alkyne**3**. The overlay of the DAPI stain and rhodamine labeling is depicted in (k).

Conclusions

In summary, we have developed a novel azide-containing Pt(II) complex (**1**) and compared it to its alkyne-containing congener (**2**), and we report here for the first time the post-treatment fluorescent labeling of a bifunctional cisplatin-based Pt(II) complex in the HeLa cancer cell line. The exchange of the alkyne to the azide moiety leads to a completely different arrangement in the solid state, with the alkyne-containing **2** forming a circular arrangement dominated by CH/π(C≡C) hydrogen bonds and secondary Pt–Pt dimer interactions. In contrast, the arrangement of the azide analogue is dominated by Pt–Pt dimer formation and hydrogen bonding forming a 1D-zigzag chain. In solution both complexes bind similarly to a DNA hairpin and show similar click reactivity in post-binding fluorescent labeling using complementary click-modified rhodamine fluorophores. Not only were we able to show the utilization of **1** as a cross-linking agent for larger biomolecules, but we also demonstrated its faster click reactivity in comparison to a previously described azide-containing Pt(II) complex. Finally, we report the first post-treatment fluorescent labeling of a cisplatin-like bifunctional Pt(II) complex in HeLa cells, observing Pt(II) localization in the nuclei and distinctively in the nucleoli. Concentration-dependent localization showed stronger fluorescent signals using the azide **1** versus the alkyne**2** Pt complex. These results show the potential of the novel compound **1** for further cell-line-dependent localization studies and the isolation of Pt(II)-bound targets.

Summary of Chapter III and Bridge to Chapter IV

In this chapter we analyzed the binding of **1** and **2** to *in* vitro DNA. Complex **1** shows a similar binding capacity to form Pt-DNA adducts as **2**. Furthermore, **1** shows enhanced

reactivity to fluorophore conjugation in comparison with **2**. When compared to its parent compound **5**, **1** shows a similar increased ability to append a fluorophore by the azide-alkyne click reaction. This difference in reactivity between **1** and **2**/**5** shows that the enhanced reactivity of **1** is most likely due to its longer linker to the azide substituent. Treatment of HeLa cells reveals that **1** and **2** show strong localization within the nuclei, most likely the nucleoli, with localization also present in the cytoplasm. These initial results within an imaging context are encouraging, but we were then motivated to improve the ability to detect Pt species at even lower concentrations. For this reason, in Chapter IV we explored the idea of appending two fluorophores in place of one, for double-post binding fluorescent conjugation.

CHAPTER IV

DOUBLE POST-BINDING FLUORESCENT CONJUGATION AS A MEANS TO VISUALIZE CELLULAR DISTRIBUTION OF AN AZIDE-APPENDED PT(II) COMPLEX

This chapter contains contributions from Regina M. Wirth, Dr. Jonathan D. White, Alison Wallum, Prof. Michael M. Haley and Prof. Victoria J. DeRose. MMH and VJD provided insight and direction through the course of this investigation. RMW conducted the synthesis of the Pt complex and the Si-Rhodamine fluorophore under the advisement of JDW. All cell studies and analyses were conducted by myself. Under my advisement, AW performed all HPLC analysis and *in vitro* fluorescent characterization of the doubly conjugated fluorophore-Pt-DNA species. This chapter contains material reproduced from portions of a manuscript being prepared for submission to Nature Chemical Biology, co-authored by myself, RMW, JDW, AW, MMH, and VJD.

Introduction

Since the discovery of their biological activity in the mid-1960s, Pt(II)-based chemotherapeutics have been used ubiquitously in anticancer treatment regimes. Their anti-proliferative effects are broadly ascribed to interactions with genomic DNA, causing inhibition of transcription and other processes.[1-3] Used in ~50% of prescribed chemotherapies, effective use of this vanguard class of metal-based therapeutics is hampered by relatively severe side effects as well as both intrinsic and acquired resistances.[7] In addition to binding genomic DNA, Pt drugs form exchange-inert adducts

with a wide variety of biological nucleophiles, including proteins, RNAs, and small molecules such as glutathione. The extent and timing of these interactions, and their consequences on cytotoxicity, cellular resistance mechanisms, and alternative apoptotic signaling, are poorly understood.[1-3,8,9] A comprehensive description of organelle-specific cellular Pt localization is currently incomplete, and new strategies to study the reactivity of Pt drugs and identify all cellular targets of Pt are needed.[10]

To better track Pt compounds *in vivo*, we have developed Pt(II) reagents modifed with small, minimally invasive bioorthogonally reactive handles that allow post-treatment labeling by alkyne-azide cycloaddition 'click' reactions for visualization and identification.[11] Here, we report a new method to improve resolution of Pt-bound species *in cellulo* that includes a double-click reaction to add multiple fluorophores per Pt reagent (Fig 4.1). This method is extended to a near-IR 'turn-on' silicon-rhodamine-azide fluorophore that eliminates background signal through quenching and reduced autofluorescence.

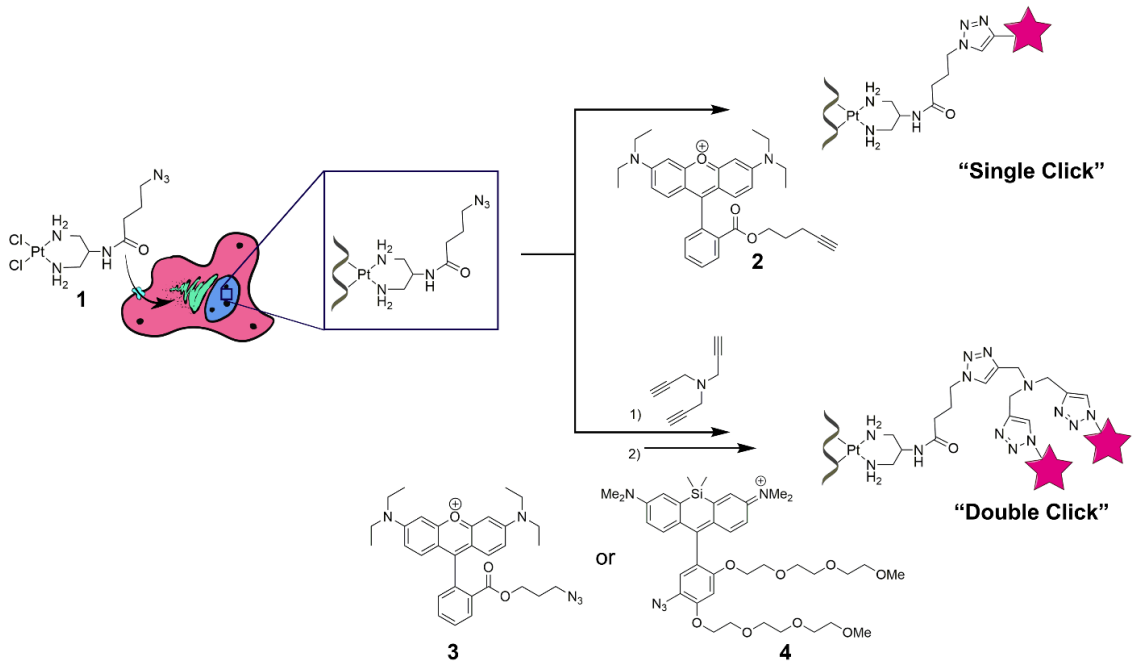

Figure 4.1. Post-treatment covalent modification of **1** with rhodamine B (**2** and **3**) or 'turn-on' silicon-rhodamine fluorophores (**4**). HeLa cells treated with 5 μM **1** are subsequently fixed, permeabilized, and then reacted with either alkyl-rhodamine B (**2**) or tripropargylamine under click conditions. In the double-click protocol, the latter are further reacted with either the Si-rhodamine-azide or rhodamine-B-azide under click conditions and imaged via confocal microscopy. See **Appendix C** for full experimental conditions.

Applications of post-binding fluorescent labeling reactions using modified Pt complexes have been limited. Using a monofunctional azide-modified Pt-acridine complex, Bierbach and colleagues observed nuclear and intense nucleolar accumulation in cultured lung carcinoma cells after 3 h treatment.[16] Previous work from our group has shown rRNA to act as a *de facto* Pt sponge,[17] making it all the more interesting that intense Pt accumulation is seen at the site of ribosome biogenesis in the nucleoli. Using click-enabled Pt(II) reagent **1** and its alkyne counterpart, we have recently imaged Pt-bound species in HeLa cells,[15] also finding intense nucleolar localization along with intensity in the nucleus and cytoplasm. In an attempt to increase brightness of these images, we envisioned an intermediate click reaction to attach multiple fluorophores to a Pt target. In this approach we first reacted the Pt-azide-bound target with tripropargylamine, and then

performed a second click ligation with azide fluorophores to afford two fluorophores per Pt (Fig 1). Such "double" and "tandem" click reactions have been used in diverse contexts,[18,19] however, to our knowledge, multi-click strategies have not been used for in-cell imaging.

Results

To demonstrate our double-click method, we first compared the confocal fluorescence images of **1** with single- and double-rhodamine B labeling. After treating HeLa cells with the bifunctional Pt compound **1** followed by standard post-treatment click labeling with alkyne- fluorophore (**2**), we observe intense nucleolar fluorescence (Fig 4.2A). Fluorescence intensity is dramatically increased, however, in cells treated with the 'double-click' protocol (Fig 4.2B). Pt distribution in both sets of images appears to be quite similar, with intense localization in the nucleoli, along with tight localization around the nucleus and additional fluorescence in non-nuclear regions. In the brighter double-click images we are able to better resolve fine detail of Pt localization (Figure 4.2 C and D). The images acquired using the double click method show more detail even after post-acquisition processing to equalize the brightness across all panels (Figure S1, see **Appendix D**). As demonstrated by intensity line plots, images captured using the double-click method are not only brighter than those with single fluorophore attachment, but also show better resolution between nucleoli and nuclear regions (Figures 4.2E and F). This double-label method with rhodamine fluorophores does not result in fluorophore self-quenching, as demonstrated by fluorescence yield measurements on in vitro DNA constructs separated via HPLC (SI Figure 3, see **Appendix D**).

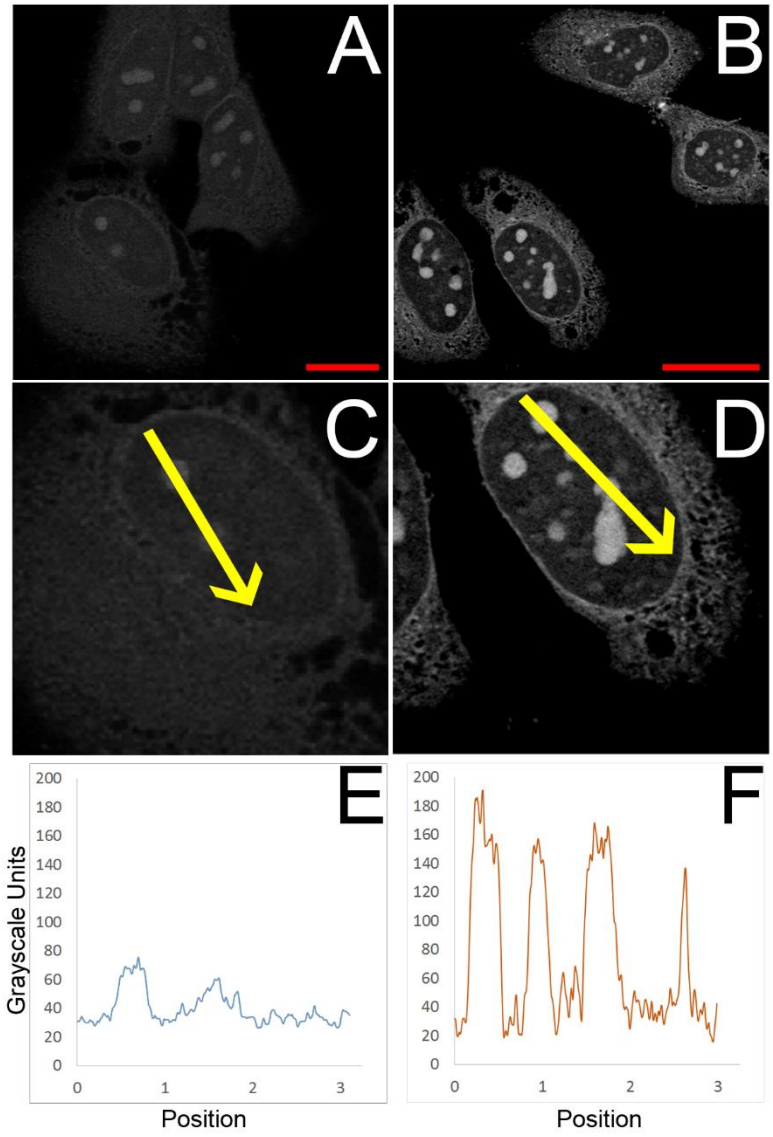

Figure 4.2. HeLa cells treated with **1** and then subjected to 'single'- (A) or 'double'- (B) click (Figure 1) with rhodamine fluorophores. (A) 5 µM treated HeLa cells post-labelled with the single-click protocol. (B) 5 µM treated HeLa cells post-labelled with the double-click protocol. Scale bars 10 µm. Panels (E) and (F) show intensity line plots for the arrows drawn in 2x magnified images (C) and (D). Images were acquired using the same laser and similar acquisition settings (**Appendix C**) and shown unprocessed for comparison. Images that are processed post-acquisition to have equal brightness are compared in **Appendix C**.

To reduce background in the imaging of Pt-bound species we then pursued use of a turn-on near IR Si-Rhodamine fluorophore (**4**), first synthesized by Bertozzi and colleagues.[15] The N_3-Si-Rho fluorophore has low fluorescence intensity that exhibits a 50-fold turn-on upon triazole formation, with absorbance and emission at 655/668 nm respectively.[15] In the double-click reaction using **1**-treated cells and standard N_3-RhoB, in the absence of extensive washing, significant background fluorescence is observed in the –Cu control sample (Figure 3B,D). The azide-quenched Si-Rho fluorophore, however, shows no background fluorescence under the same conditions (Figure 3A). Following reaction with the Si-Rho fluorophore, brighter nucleolar intensity is observed than with RhoB (Figures 4.3C,D). In addition to bright nucleolar fluorescence, the comparison of Figures 4.3C,D with 2C,D also shows a brighter general nuclear fluorescence. Unlike the standard protocols for post-treatment labeling, the protocol used in Figures 4.3C,D minimizes the washing steps that are usually needed to remove unbound fluorophore (see **Appendix D**). The nuclear fluorescence in Figure 4.3C, fully absent in the unclicked control sample (4.3A), is brighter than that observed with the standard double-click protocol (Fig 4.2) and suggests that use of the turn-on fluorophore allows imaging of some nuclear Pt-bound species that are more soluble and lost under extensive washes.

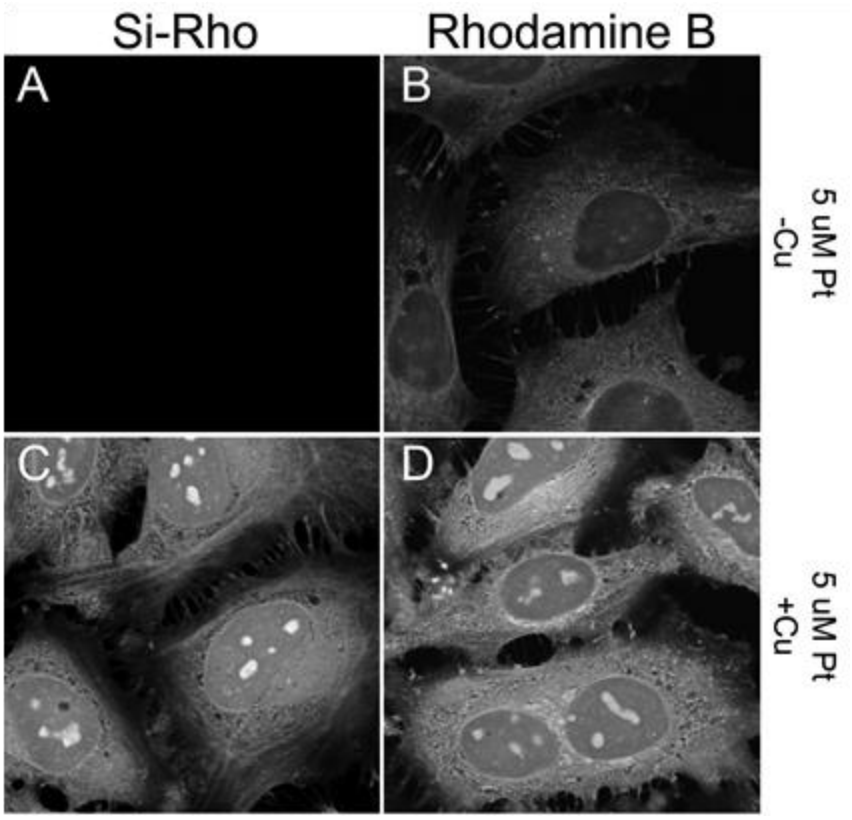

Figure 4.3. HeLa cells treated with 5 μM **1** and then labelled with either rhodamine B azide fluorophore (B) or Si-Rhodamine fluorophore (A) using the double-click protocol with minimized washing steps. Panels A and B show the extent of the background fluorescence due to unbound fluorophore. Panels C and D reveal similar Pt localization, with the most abundant signal present in the nucleolus.

Conclusions

In summary, the double-click fluorescence labeling method presented here significantly improves visualization of azide probes within cells. Use of the double-click method in comparison to the traditional click conjugation shows similar localization of Pt-bound biomolecules but with images that have improved detail and higher overall brightness. The ability to use azide-quenched fluorophores to locate azide-labeled probes significantly broadens opportunities for turn-on click labeling This method can easily be exported to other applications of azide detection as well as other means of visualization outside of microscopy.

Summary of Chapter IV and Bridge to Chapter V

In this chapter we showed the ability of **1** to be post-modified with two fluorophores after treating HeLa cells for 3 h. Localization of the doubly-conjugated species showed a similar profile to what was previously seen with single fluorophore conjugation, except that double conjugation images showed greater brightness and contrast than singly conjugated species. *In vitro* experiments reveal that the doubly conjugated species does not exhibit strong fluorescent quenching, as its quantum yield is similar to that of the parent fluorophore. Use of a previously reported turn-on fluorophore **4** led to similar localization as was observed with **3**, but with greatly reduced background. Ultimately, this work motivated us to explore if the localization present with these complexes depends on the identity of the cell type. In Chapter V, we explore the differences in localization of **1** in three different cell lines.

CHAPTER V

ANALYSIS OF PT LOCALIZATION IN MULTPLE CANCER CELL LINES USING FLUORESCENT MICROSCOPY AND AN AZIDE MODIFIED PT(II) COMPLEX

This chapter contains contributions from Regina M. Wirth, Emily Reister-Morris, Alison Wallum, Michael M. Haley and Prof. Victoria J. DeRose. MMH and VJD provided insight and direction through the course of this investigation. RMW was responsible for all Pt synthesis. ERM was responsible for maintenance of all cell lines. AW, under my advisement, performed in-cell labeling of Pt in C6 cells. All cell studies utilizing the HCC 1143 and MDA MB 468 cell lines were done by myself. This chapter contains material reproduced from portions of a manuscript being prepared for submission to American Chemical Society Chemical Biology, co-authored by myself, RMW, AW, ERM, MMH, and VJD.

Introduction

Platinum-based therapeutics are ubiquitous in cancer treatments[1-3], and the need to understand and eliminate the deleterious effects of these drugs remains critical. Our lab has developed methods to modify platinum reagents with a reactive handle to track and extract Pt targets within cells[4-7]. Most recently, we have shown that post-treatment functionalization of Pt compounds with fluorophores reveals intense Pt localization within the nucleoli[7] of HeLa human cerivical cancer cells. Building on these results, here we probe localization of these complexes in other cell types.

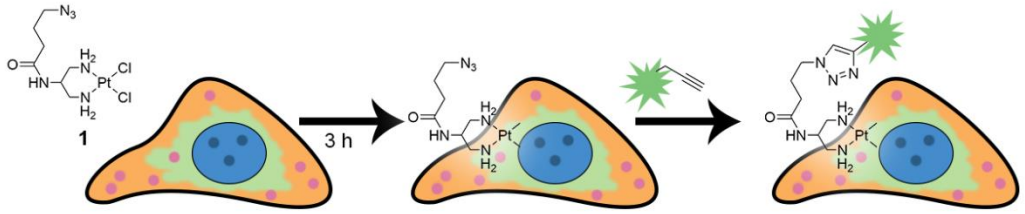

Figure 5.1. Workflow for cellular imaging studies. Cells are incubated in 5 μM **1** for 3 h and then fixed, permeabilized and conjugated with Alexafluor 488 alkyne fluorophore through click chemistry. Cells are then washed and imaged via confocal microscopy.

Cisplatin has shown particularly high promise in the treatment of triple negative breast cancer (TNBC), an aggressive subtype consisting of ~15% of all breast cancers. TNBC is characterized by fast tumor growth and metastasis, and frequent relapse after treatment. TNBC cells lack estrogen and progesterone receptors as well as lack overexpression of her2/neu,[8] all of which are important therapeutic targets. Since TNBC cells lack the ability to be treated through hormone therapy[8] other methods using small molecule crosslinking agents such as Pt reagents are an important treatment route. Information about the drug response to cisplatin in TNBC cells can provide insight into mechanisms by which the drug functions as well as lead to improvement in therapeutic approaches. Because of this, we decided to investigate the localization of our azide-modified complex **1** within two different TNBC cells, HCC 1143 and MDA MB 468 cells[8]. These cell lines have been previously well-characterized with respect to drug response. In examining a number of different TNBC cell lines, we chose these two lines because of their reported responses to Pt treatment. While both sensitive to cisplatin, these cell lines differ in that HCC1143 cells are reported to have a slightly lower response to cisplatin than MDA MB 468 cells. As a comparison, we also chose to investigate Pt localization with C6 glioma cells. C6 cells have a relatively high resistance to cisplatin when compared to other cell

types[9]. Some gliomas in both the human and rat cell lines have shown an increased glutathione response upon cisplatin treatment[10]. Glutathione, a tripeptide bearing a thiol moiety, is known to contribute to Pt resistance in cancer cells[11]. C6 cells have been shown to have greater amounts per cell of both glutathione and other antioxidants, of which could contribute to their resistance to Pt[12]. Differences in localization of the drug within this cell type could help elucidate what affects drug resistance.

Results

Imaging the Pt localization in the two TNBC cell lines after 3-hr treatment with **1** revealed quite varied results. The MDA MB 468 cells had localization differences within its own population (Fig. 5.2). All cells within the MDA MB 468 cell line exhibited strong fluorescence in the nucleolus, but some cells showed similar intensity within the nucleus as well. All cells also showed some localization in regions outside of the nucleus.

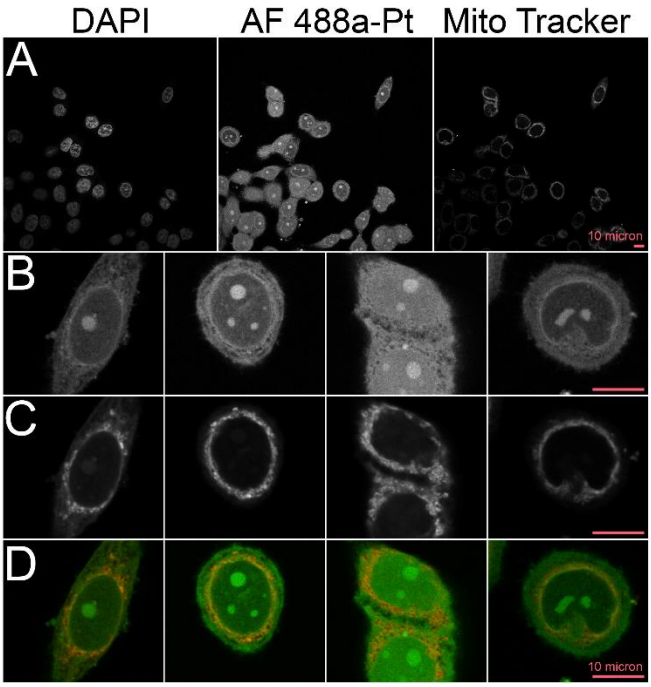

Figure 5.2. MDA MB 468 cells labeled with DAPI, Alexa Fluor 488 alkyne and Mito Tracker Deep Red. The top panel shows the DAPI, Alexa Fluor 488/Pt and the Mito Tracker Deep Red images in greyscale. Images from the Alexa Fluor and Mito Tracker Deep Red channels are shown as well as an overlay of those two channels (Alexa Fluor in green and Mito Tracker Deep Red in red).

In particular, the Pt signal appears somewhat brighter in a ring around the nucleus. We postulated that this region might be mitochondria. Indeed, mitochondria stained with Mito-Tracker Deep Red (Invitrogen) do appear as a ring around the nucleus in these MDA cells (Figure 2C) and there is overlap between the fluorophore-labeled Pt and the Mito-Tracker signal (Figure 2D). To determine if localization was more pronounced in the mitochondria than in other regions of the cells (outside of the nuclei), we quantified average fluorescence intensity across the selected areas inside and outside the mitochondria (see **Appendix E**) (Table 1).

Cell Type (Location)	Average Fluorescence
MDA MB 468 (inside Mito)	660 ± 91
HCC 1143 (inside Mito)	480 ± 100
MDA MB 468 (outside Mito)	568 ± 189
HCC 1143 (outside Mito)	522 ± 194

Table 5.1. Average fluorescence of Alexafluor 488 channel inside and outside of Mito-Tracker stained mitochondria.

The data in Table 1 indicate that the average Pt-Alexafluor fluorescence is not statistically higher inside the regions stained by Mito-Tracker, indicating that substantial localization to other extra-nuclear cell structures is occurring.

As a comparator, this experiment was repeated using HCC 1143 cells (Fig. 5.3). Unlike the MDA MB 468 cells, the HCC 1143 cells appear to be more homogenous in morphology and in Pt localization. HCC 1143 cells exhibited intense nucleolar Pt localization, and then broad localization within the nucleous and cytoplasm. Mito-Tracker staining reveals a more dispersed mitochondrial morphology for HCC cells than the tighter nuclear 'ring' observed in MDA cells. Interestingly, in the cytoplasm there are dark areas where Pt localization is not present. These areas do not seem to coincide with the mitochondria as the fluorescence inside and outside of the mitochondria are roughly similar.

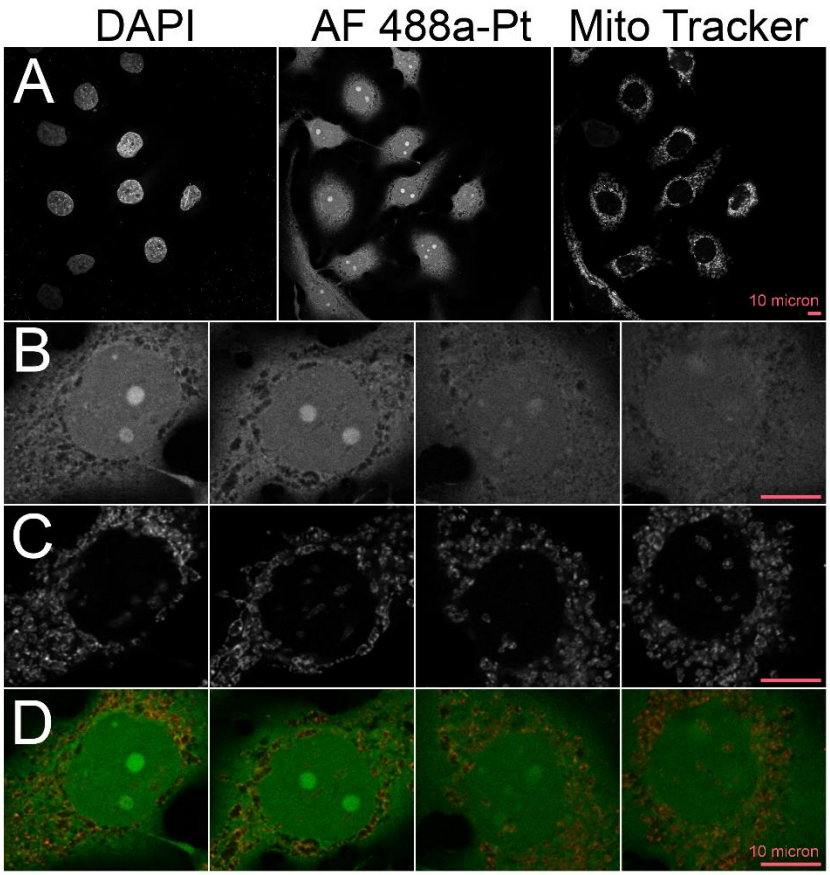

Figure 5.3. HCC 1143 cells labeled with DAPI, Alexafluor 488 alkyne and Mito Tracker Deep Red. The top panel shows the DAPI, Alexafluor 488/Pt and the Mito Tracker Deep Red images in greyscale. Images from the Alexa Fluor and Mito Tracker Deep Red channels are shown as well as an overlay of those two channels (Alexa Fluor in green and Mito Tracker Deep Red in red).

For further comparison, we measured Pt localization in the C6 glioma cell line. Unlike the HeLa, HCC 1143 and MDA MB 468 cells, the C6 cells have less well-defined nucleoli. While Pt is observed to localize to the nucleus, a strong nucleolar localization is not observed (Fig 5.4). This could be due to differences in C6 cell morphology and response to Pt when compared to other cell lines[10]. Upon Pt treatment, C6 cells undergo changes in nuclei morphology, stemming from expansion to segregation of nucleoli.

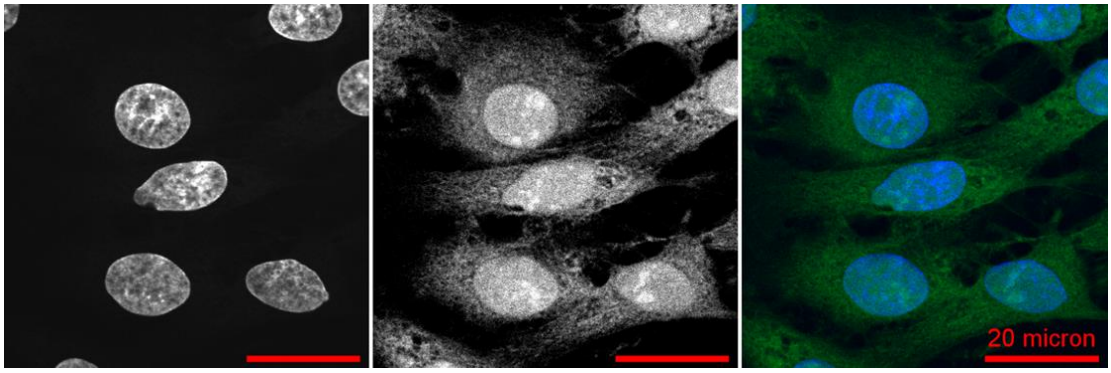

Figure 5.4. C6 cells labeled with DAPI and Alexa Fluor 488 alkyne. The left panel shows a greyscale image of the DAPI stain, the middle panel Alexa Fluor 488 alkyne, and the right panel shows an overlay of the two (DAPI in blue and Alexa Fluor 488 in green).

Conclusions

Cellular imaging of TNBC cells reveal intense localization of **1** within the nucleoli of both cell lines. MDA MB 468 cells exhibited variance in localization, with localization intensity differences between the cytoplasm and nucleus. HCC 1143 cells exhibited more homogenous localization across the population of cells. C6 did not appear to have the same intense nucleolar localization. This could be due in part to the varied morphological response that C6 cells have to Pt treatment. C6 cells pre-treated with cisplatin have shown elevated glutathione levels which could influence this cell type's elevated resistance. Moreover, longer treatment times with cisplatin have been shown to result in nucleolar segregation within C6 cells. Glutathione depletion within glioma cells has been shown to increase cisplatin sensitization[12]. The lack of strong nucleolar localization could be due to either factor, or a combination of the two. Further studies need to be done to ascertain if nucleoli are still intact, or if **1** is causing nucleolar segregation.

Summary of Chapter V and Bridge to Chapter VI

In this chapter we explored the localization of **1** within three different cell types. In the TNBC cells, **1** exhibited a similar localization as it did within HeLa cells, ultimately showing a strong targeting of the nucleoli. MDA MB 468 cells showed varied morphological differences. While all cells within that line showed strong nucleolar localization, there were variations in localization in the cytoplasm and nuclei. HCC 1143 cells showed much more homogenous localization, still favoring the nucleoli. C6 glioma cells did not show a strong nucleolar localization. This could be due to differences in morphology of the cell line with respect to HeLa/HCC 1143/MDA MB 468 cells, or it could be due a glutathione response. For this reason, we wanted to pursue the construction of another Pt-azide derivative based on a carboplatin scaffold. Carboplatin has shown slower kinetics in comparison to cisplatin and it may have a greater resistance to react and form side products in sulfur-rich cell lines.

CHAPTER VI

SYNTHESIS AND ANALYSIS OF TWO AZIDE-MODIFIED CARBOPLATIN MIMICS TO BE USED IN POST-TREATMENT FUNCTIONALIZATION

This chapter contains contributions from Matthew M. Cerda, Rachael M. Cunningham, Michael M. Haley and Prof. Victoria J. DeRose. MMH and VJD provided insight and direction through the course of this investigation. MC, under my advisement, was responsible for the synthesis of **1** and **3**. The synthesis of **2** and **4** were carried out by myself. RCM was responsible for the binding of **2**/**4** in bovine serum albumin as well as the SDS-PAGE analysis.

Introduction

Despite its clinical success, cisplatin has also suffered from a number of toxicity issues such as nephrotoxicity, ototoxicity, and overall dose-limiting toxicity.[1] To reduce these effects, other drugs such as carboplatin were developed.[1] The relative toxicity of cisplatin in part stems from its aquation kinetics, as the aquated complex is considered to be the active form of the drug. The design rationale for carboplatin is to create a drug that resists aquation by installing a chelating leaving group.[2] This resistance will slow reaction kinetics with biomolecules, and lower the overall toxicity.[2] Carboplatin also maintains the same exchange-inert ammonia ligands such that the active form of carboplatin should still be the same as cisplatin. Overall, this has created a complex that targets the same types of cancers as cisplatin, while still reducing the other types of toxicities previously discussed. However, in terms of treatment for testicular germ-cell cancers, squamous cell carcinoma

of the head and neck and bladder cancers carboplatin has shown limited efficacy.[2] The question remains, is this limited efficacy caused by the lowered toxicity or differential biomolecule targeting by these two Pt complexes.

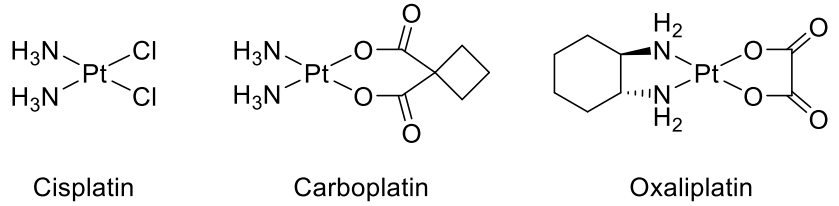

Figure 6.1. FDA-approved Pt-based anticancer drugs: cisplatin, carboplatin and oxaliplatin.

In an effort to understand localization of Pt(II) reagents in cells, our lab has developed a number of derivatives that have been modified with either an azide or alkyne reactive handle for post-treatment fluorescent labelling.[3-6] Recently, we endeavored to synthesize a carboplatin derivative with similar structure to our cisplatin mimics and compare the localization and behavior of the two complexes. Work toward this end would help answer the question of whether the slower aquation kinetics induced by the cyclobutanedicarboxylate substituent has an effect on localization and targeting of the Pt compound in cells.

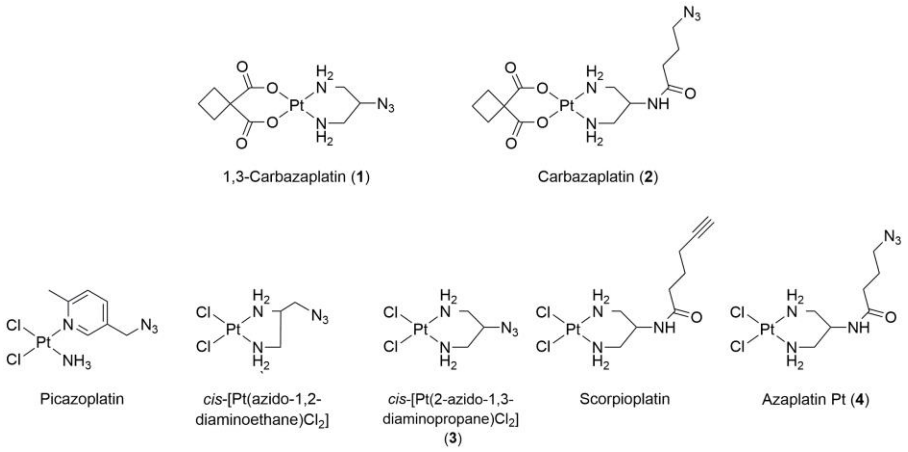

Figure 6.2. Azide and alkyne modified Pt(II) complexes synthesized in our lab.

Results

We had previously reported on the use of **3** for post-treatment analysis and its interesting isomerization bias as revealed by RP-HPLC[2]. Uranker and co-workers developed the synthesis of **3** as well as the synthesis of **1**.[11] Interestingly, in attempting to make **1** by the methods listed, we encountered issues of low yield and intractable Pt impurities; the treatment of cyclobutanedicarboxylic acid with base (sodium hydroxide or DBU) in the presence of **3** did not generate appreciable amounts of **1**, and hydroxide coordination of Pt may have been taking place over coordination by the carboxylic acid. This led us to pursue a different synthetic route using a silver salt of the acetate. The silver salt eliminates the need for base, and accelerates the reaction by precipitating the chloride ligands. This route afforded us both complex **1** and the novel compound **2** in moderate yields (Fig 2).

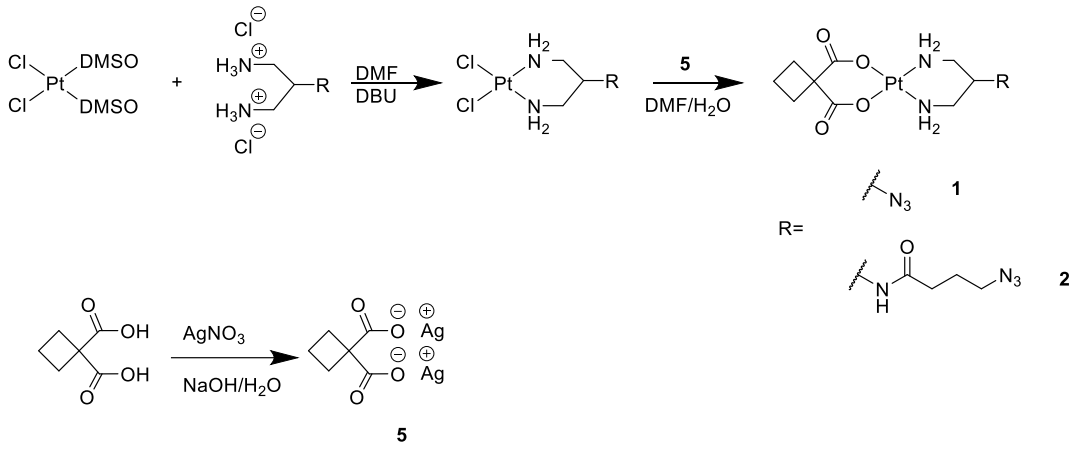

Figure 6.3. Synthetic scheme for **1** and **2**.

Complex **1** was further used to demonstrate post-treatment analysis *in vitro* using a hairpin DNA construct (Fig 6.3). Utilizing the scheme in Figure 6.4A we used **1** to bind and then functionalize the DNA-Pt species with a rhodamine B fluorophore (Fig 6.4C) using the copper-catalyzed click reaction. As shown in Figure 3B, dPAGE analysis shows a mass shift of the hairpin DNA upon binding of **1** and again another mass shift upon fluorophore conjugation. Further studies need to be pursued to ascertain the influence of the leaving group by comparing binding kinetics of **1** relative to **3**.

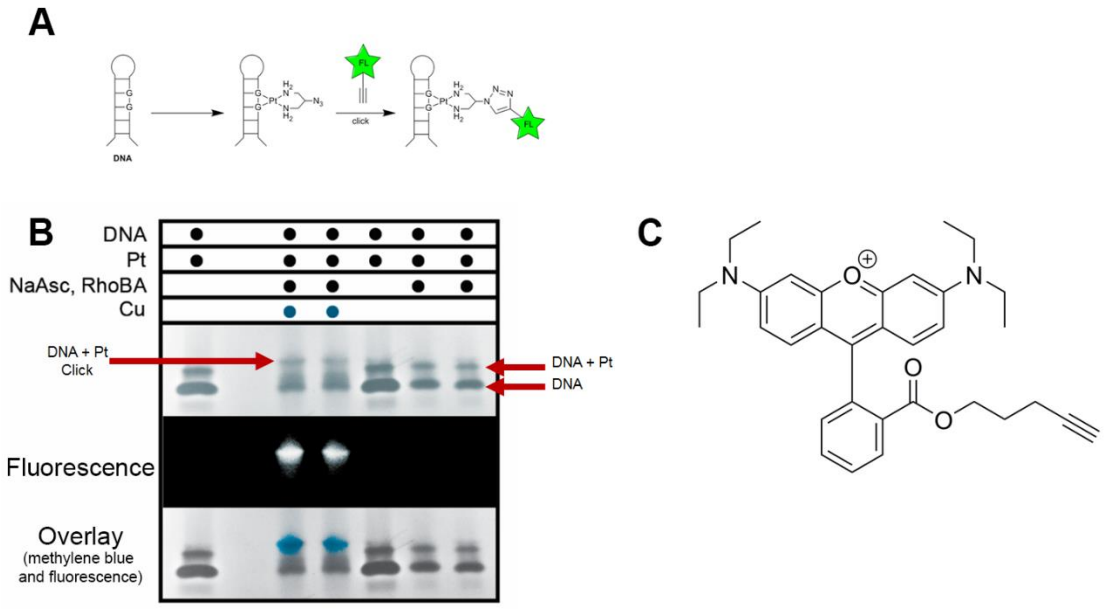

Figure 6.4. General scheme for binding of **1** to HP-DNA (A) and dPAGE analysis (B). For the click reaction, a rhodamine B alkyne-modified fluorophore was used (C).

We also investigated the ability of **2** to bind to bovine serum albumin (BSA), followed by fluorophore conjugation. After 6 and 24 h of incubation of BSA with **2,** we are able to see the presence of fluorophore-Pt-BSA species via SDS PAGE. Furthermore, when we compare it to **4** at the same time points we see a similar response. Interestingly, we do not see a pronounced decrease in reactivity of **2** as might be expected if slower aquation kinetics were governing the yield of the Pt-BSA conjugate. More studies need to be done to fully elucidate reaction kinetic differences between the two complexes.

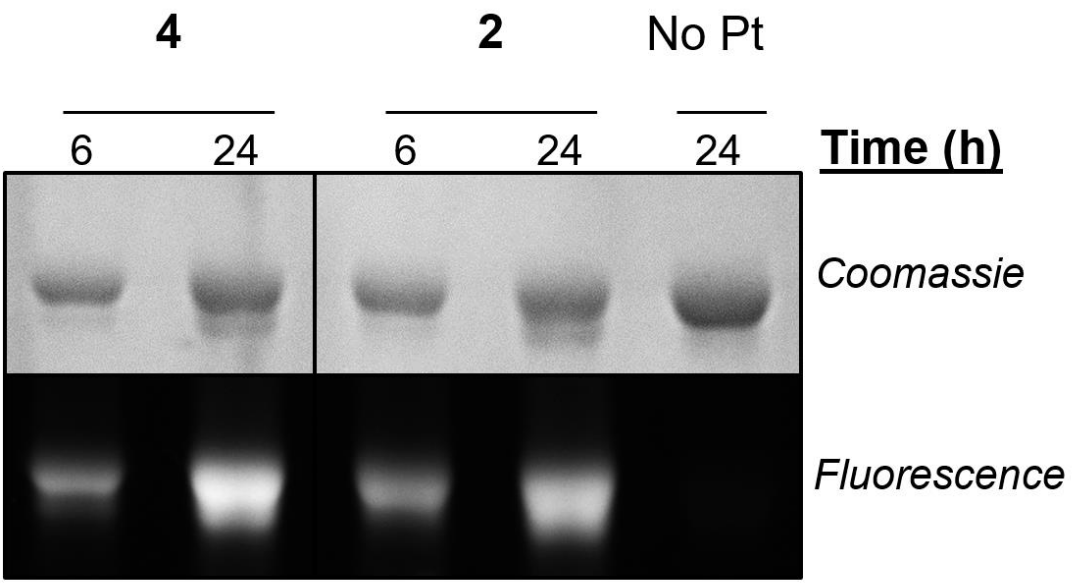

Figure 6.5. SDS PAGE analysis of **2** and **4** bound to BSA and conjugated to a rhodamine B fluorophore after incubation for 6 and 24 h.

Conclusions and Future Directions

We were able to successfully synthesize two azide-modified Pt complexes bearing cyclobutanedicarboxylate as leaving group through a newly explored synthetic route generating the Ag-carboxylic acid salt as a precursor. Preliminary studies have shown that **1** is able bind DNA in a similar manner to its parent compound **3**, and is able to undergo post-treatment fluorophore conjugation through Cu-catalyzed click chemistry. Treatment of BSA with **2** shows similar results as **4**, indicating its efficacy to be used in post-treatment analysis. Further studies need to be done to ascertain the relative reactivity between **1** and **3**, as well as the general reactivity of **2** to biomolecules. It is also of interest to see if the same isomerization bias witnessed with **3** is present with **1**. This bias could be influenced by the size and aquation ability of the respective Pt complexes. Lastly, it is important to see if these four species all have similar localization within cells. Using the reactive handles

present on them could give insight on the relative in cell kinetics of cisplatin and carboplatin, including but not limited to uptake, processing, and efflux.

CHAPTER VII

CONCLUDING REMARKS

Having developed a wide array of different click-enabled Pt(II) complexes, in this work we have explored how we can visualize their distribution in cells, improve certainty of their localization, and categorize their localization differences in different cell types. The use of the newly synthesized Carbazaplatin could help us gain insight to how other Pt drugs like Carboplatin interact with cells, and could help elucidate resistance pathways and mechanisms. Ultimately, using these constructs we can also better pinpoint Pt specific targets through post-treatment biotinylation followed by enrichment and identification by sequencing or proteomics, a task our group is currently investigating. Also, another important task is understanding the behavior of Pt as a function of time, in terms of target identification and binding preferences in a cell. This ultimately could be aided by the use of cell permeable strained alkyne fluorophores, although the literature is currently lacking in that regard. A “snapshot” approach at varied time points could still help us understand what events are taking place. Another point of study could be correlating relative Pt-fluorophore fluorescence to states in cell cylces of different cell types via flow cytometry.

APPENDIX A

Experimental Details

General Comments. Materials were purchased from commercial vendors and used without further purification. Anhydrous N,N'-dimethylformamide (DMF) was purchased from EMD Millipore (DriSolv). 1,3-Propanediamine was purchased from TCI America, KI and KCl were purchased from EMD, and $AgNO_3$ was purchased from Strem Chemicals, Inc. K_2PtCl_4 was purchased from Sigma Aldrich and deuterated solvents were purchased from Cambridge Isotope Laboratories. ^1H, ^{13}C, and ^{195}Pt NMR spectra were recorded in d_7-DMF using a Varian Mercury 300 MHz (^1H: 300.09 MHz) or Bruker Advance III HD 600 MHz (^1H: 600.02 MHz, ^{13}C: 150.87 MHz, ^{195}Pt: 128.99 MHz) NMR spectrometer with a Prodigy multinuclear broadband cryoprobe. Chemical shifts (δ) are expressed in ppm relative to the residual DMF (^1H: 8.03 ppm, ^{13}C: 29.76) or the external reference K_2PtCl_4 (^{195}Pt: –1604 ppm). Gels were visualized with methylene blue stain and UV exposure (AlphaImager HP System). All DNA substrates were purchased directly from Integrated DNA Technologies, Inc., dissolved in nanopure ddH_2O to a final stock concentration of 1 mM, and used directly without further purification.

***cis*-[Pt(2-azido-1,3-propanediamine)Cl_2] (4)**. The azide-containing **4** was prepared according to the method of Urankar et al. (reference 8b in **Chapter II**).

***cis*-[Pt(1,3-propanediamine)Cl_2] (5)**. The azide-free **5** was prepared following the method described by Dhara for cisplatin (reference 9a in manuscript). Briefly, to a clear-red solution of K_2PtCl_4 (0.54 g, 1.31 mmol) in H_2O (15 mL) was added KI (1.31 g, 7.87 mmol) in H_2O (5 mL) and the reaction was stirred in the dark for 20 min. 1,3-Propanediamine (0.01 g, 1.32 mmol) in H_2O (10 mL) was added dropwise over ca. 15 min. and stirred for

another 2 h in the dark. The resulting yellow precipitate was then filtered and washed thoroughly with H_2O and dried in a desiccator. All of the yellow solid (0.61 g, 1.17 mmol) was suspended in H_2O (8 mL) to which $AgNO_3$ (0.38 g, 2.22 mmol) in H_2O (2 mL) was added at once. The mixture was stirred in the dark overnight (16.5 h). The opaque-tan mixture was filtered through a 0.2 μm syringe filter to reveal a clear-yellow filtrate. One drop of 1 M HCl was added to the filtrate, followed by 1.01 g KCl. The mixture was allowed to sit for 2 h in the dark at rt, after which a yellow solid was filtered from a clear-yellow filtrate. The yellow solid was rinsed with H_2O and dried in a desiccator to furnish the desired product (0.28 g, 0.83 mmol, 63%). ^{1}H NMR (300 MHz, d_7-DMF): δ 4.99 (Pt–NH_2–, s, 4H, $^3J_{Pt\text{-}H}$ = ~60 Hz), 2.88-2.60 (Pt–NH_2–CH_2–, m, 4H, obscured by residual DMF solvent peak), 1.78 (CH_2–CH_2–, m, 1H); ^{13}C NMR (151 MHz, d_7-DMF): δ 43.2 (–NH_2–*C*H_2–), 28.3 (–CH_2–*C*H_2–); ^{195}Pt NMR (129 MHz, d_7-DMF): δ –2256 (Pt). HRMS (ESI) m/z calculated for $C_3H_{11}N_2Cl_2Pt$, 339.9947 (M^++H); found, 339.9932.

5-(Dimethylamino)-N-(2-propynyl)-1-naphthalenesulfonamide (dansyl alkyne fluorophore). The dansyl alkyne was synthesized according to previously published methods (F. Bolletta, D. Fabbri, M. Lombardo, L. Prodi, C. Trombini, N. Zaccheroni, *Organometallics*, 1996, ***15***, 2415-2417).

Platinum Activation (aquation). Picazoplatin (**1**), *cis*-[Pt(2-azido-1,3-propanediamine)Cl_2] (**4**), or *cis*-[Pt(1,3-propanediamine)Cl_2] (**5**) (5 μmol) was added to a solution of $AgNO_3$ in ddH_2O (10 mM, 1 mL). The solution was incubated at 50 °C for 4 to 18 h with stirring, at which time AgI precipitated as a white solid and was separated by centrifugation (10,000 rpm for 10 min). The resulting supernatant was removed and used

for DNA and RNA binding studies. Solutions were stored in the dark at 4 ℃ and used for up to one week.

Platinum–DNA Binding (HPLC analysis). The DNA duplex (280 μM each of 5'-T_5GGT_6-3' and 5'-A_6CCA_5-3', typically 28 nmol) or the DNA hairpin (280 μM of 5'-TATGGTATTTTTATACCATA-3', typically 28 nmol) was folded by rapid heating to 90 °C and slow cooling to 4 °C in 10 mM Na_2PO_4 (pH 7.1), 0.1 M $NaNO_3$, and 10 mM $Mg(NO_3)_2$. An activated solution of **4** or **5** was added in equimolar proportions (for HPLC) or two-fold excess (for click reactions) and the solution was incubated at 37 °C for approx. 16 h. Pt-bound DNA was purified with Sephadex G-25 Medium size exclusion resin (GE Healthcare) on laboratory-prepared spin columns (BioRad) to remove unbound Pt.

Platinum–DNA Binding (PAGE analysis). The DNA duplex (280 μM each of 5'-T_5GGT_6-3' and 5'-A_6CCA_5-3', typically 28 nmol) was folded by rapid heating to 90 °C and slow cooling to 4°C in 10 mM Na_2HPO_4/NaH_2PO_4 buffer (pH 7.1), 0.1 M $NaNO_3$, and 10 mM $Mg(NO_3)_2$. An activated solution of **1** or **4** was added in twofold excess and the solution was incubated at 37 °C for 16 h. Pt-bound DNA was purified with Sephadex G-25 Medium size exclusion resin (GE Healthcare) on laboratory-prepared spin columns (BioRad) to remove unbound platinum.

Platinum–DNA Click Reactions. Sodium ascorbate (18 μL, 10 mM), CuI (18 μL, 10 mM), dansyl alkyne (10 μL, 2mM), and Et_3N (10 μL, 7.2 M) were added to a solution water:acetonitrile (98:2) of Pt-bound DNA (18 μL, 180 μM). The samples were incubated at 50 °C for 30 min to 4 h. The samples were then purified with Sephadex G-25 Medium spin columns. The samples were dried *in vacuo* and then re-suspended in an equal volume mixture of ddH_2O and formamide for dPAGE or ddH_2O for HPLC analysis.

HPLC Conditions. DNA was separated using reverse-phase HPLC (Akta purifier; Amersham Biosciences) on a C18 column (Hypersil GOLD, 5 mm 4.6/250 mm; Thermo Scientific). A mobile phase of 10 mM triethylammonium acetate (TEAA) and 80% acetonitrile/20% 10 mM TEAA were used. A multistep gradient was used that provided baseline separation of major peaks.

Molecular Modeling. DFT calculations were performed using a model from an NMR solution structure of cisplatin-bound DNA (pdb: 3LPV, reference 9 in manuscript) in Spartan '10 (Wavefunction Inc.) Version 1.1.0. The ammine ligands of cisplatin were replaced with 2-Azidopropane-1,3-diamine, and the bond angles and bond distances resulting from **4** bound to the two guanine residues were restricted (see below). The DNA atoms were held static while the equilibrium geometry of Pt was calculated using molecular mechanics (MMFF). The structures were then imported into PyMOL for visualization.

Bovine Serum Albumin Platination and Click Reaction Conditions. BSA (50 μM) was incubated with 0, 50, 100, or 250 μM **4** in 10 mM Na_2HPO_4/NaH_2PO_4 buffer (pH 7.0), 10 mM $NaNO_3$, and 100 μM $Mg(NO_3)_2$ at 37 °C for 16 h. Pt-bound BSA was purified with Sephadex G-25 Medium size exclusion resin (GE Healthcare) on laboratory-prepared spin columns (BioRad) to remove unbound Pt. To perform the click reaction, 100 μM dansyl-alkyne fluorophore, 100 μM $CuSO_4$, and 2 mM sodium ascorbate was added to platinated BSA and allowed to react at 37 °C for 1 h. Free fluorophore was removed using Sephadex G-25 spin-columns. Purified protein was then analyzed by 10% SDS-PAGE.

S. cerevisiae **Treatment with 4.** Liquid cultures of *S. cerevisiae* strain BY4741 (MATa; his3Δ1; leu2Δ0; met15Δ0; ura3Δ0), a gift from the Tom Stevens laboratory at the University of Oregon, were grown at 30 °C with shaking at 200 rpm in synthetic dextrose

medium (0.67% yeast nitrogen base and 2% glucose supplemented with amino acids and nucleotide bases). Overnight cultures were diluted to OD_{600} ~0.25 in synthetic dextrose medium supplemented with 0 or 250 µM 2-ADAP Pt. Cells were grown at 30 °C for 6 h with aeration, harvested by centrifugation at 4000 rpm at 4 °C, resuspended in fresh medium, and returned to shaker at 30 °C. At 0, 40, 80, and 120 min post treatment, aliquots were harvested by centrifugation at 4000 rpm, supernatant was discarded, and pellets were stored at –20 °C. Total RNA was extracted with the MasterPure Yeast RNA Purification Kit (Epicentre) according to a modified manufacturer's protocol. RNA concentration was calculated using absorbance at 260 nm. For the click reaction, 8-14 µg of total RNA (normalized to OD_{600} of initial culture at timepoint collected) was incubated overnight at 37 °C in a 10 µL reaction mixture containing 20 U RiboGuard RNAse Inhibitor and 0.25 mM Alexa Fluor 488 DIBO. Unbound fluorophore was removed using an RNeasy Mini Kit (Qiagen) according to a modified manufacturer's protocol. Samples were diluted 2-fold in formamide and analyzed on an 8% (29:1) mono/bis polyacrylamide gel. Fluorescence signal intensities from Fig. 6, normalized to RNA (methylene blue stain) and culture OD, are shown below indicating significant retention of Pt-rRNA adducts after 2 h in **4**-free media.

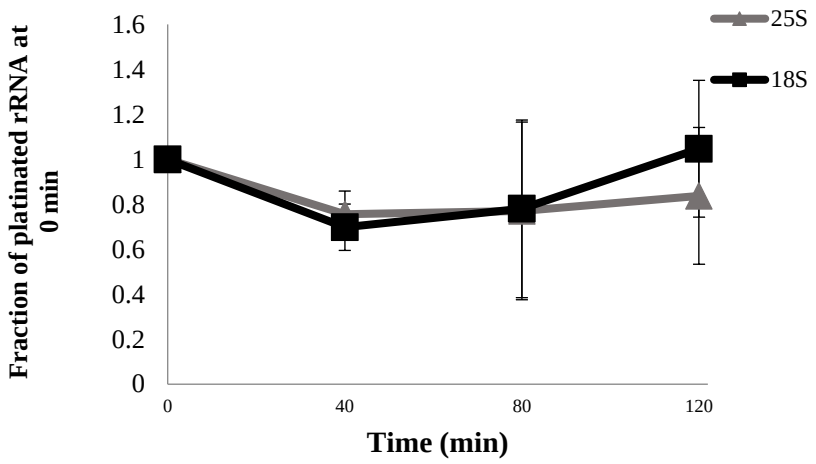

Figure A.1. Normalized Pt-rRNA signal over time. Fluorescence signal from click reaction was normalized to total loaded RNA (methylene blue stain) and OD_{600} of initial culture at timepoint collected.

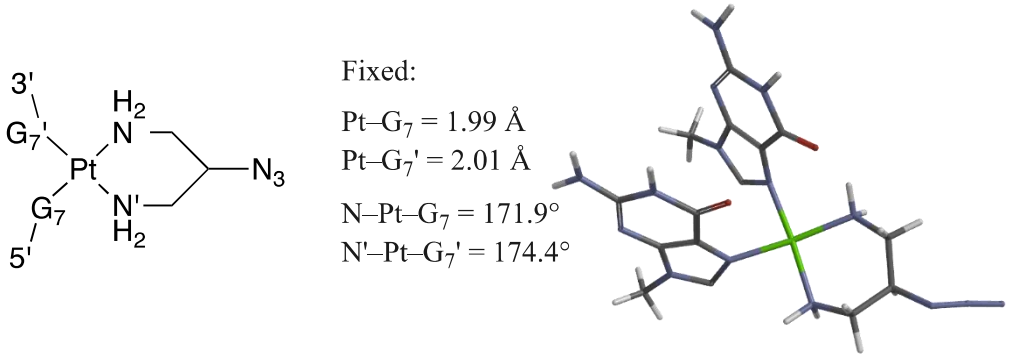

Figure A.2. Results of DFT calculations of **4** bound to DNA. DFT-calculated (B3LYP 6-31G* with pseudopotentials) minimized ground-state geometry of **4** bound to the guanines of double-stranded DNA (3LPV)

^{195}Pt

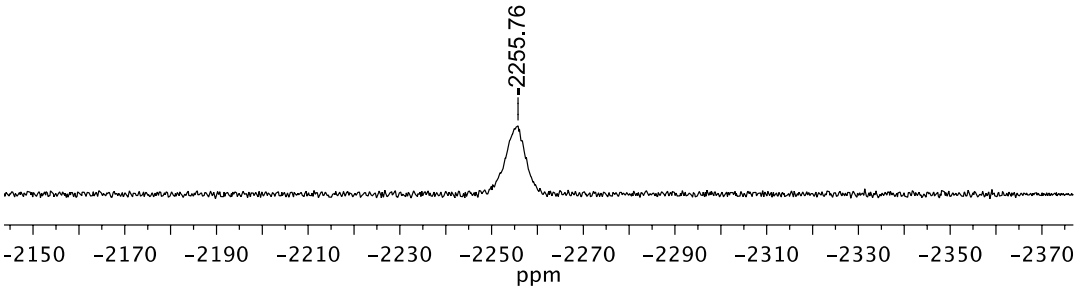

^{13}C

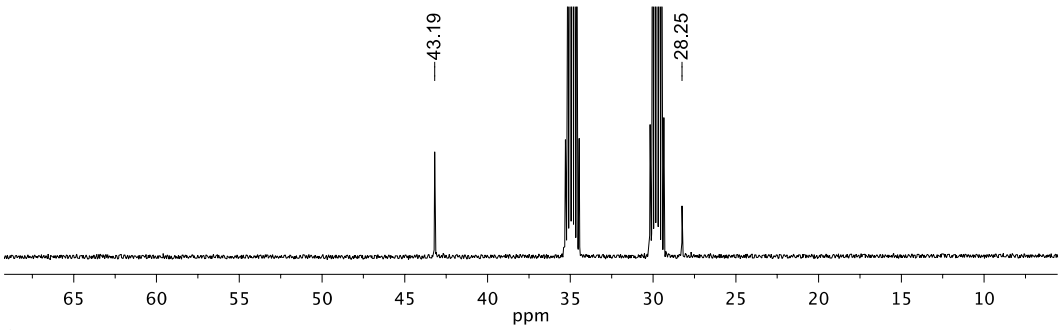

^{1}H

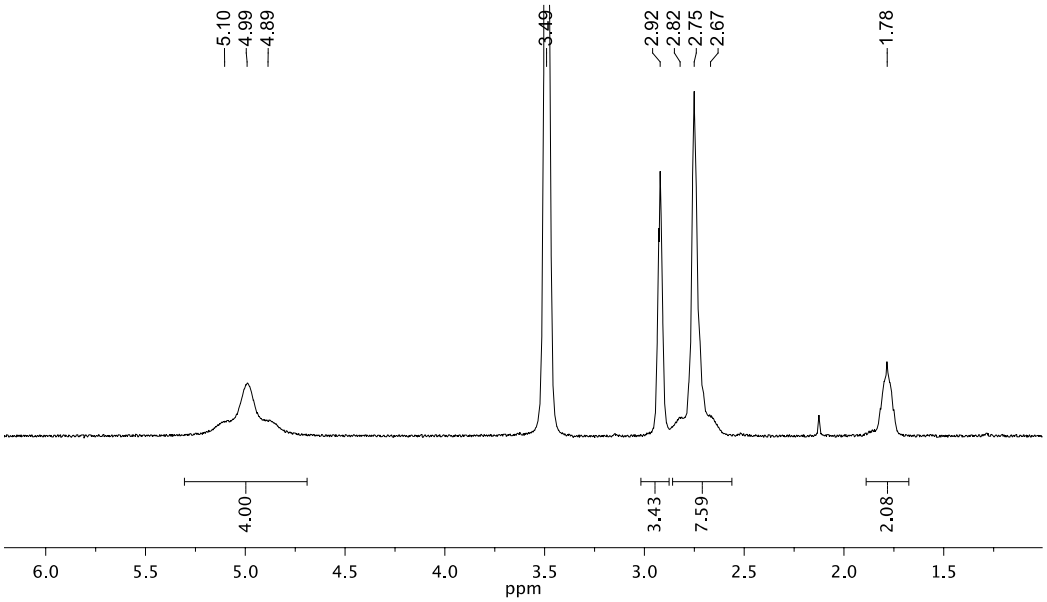

Figure A.3. NMR (^{195}Pt, ^{13}C, ^{1}H) Spectra of **5**

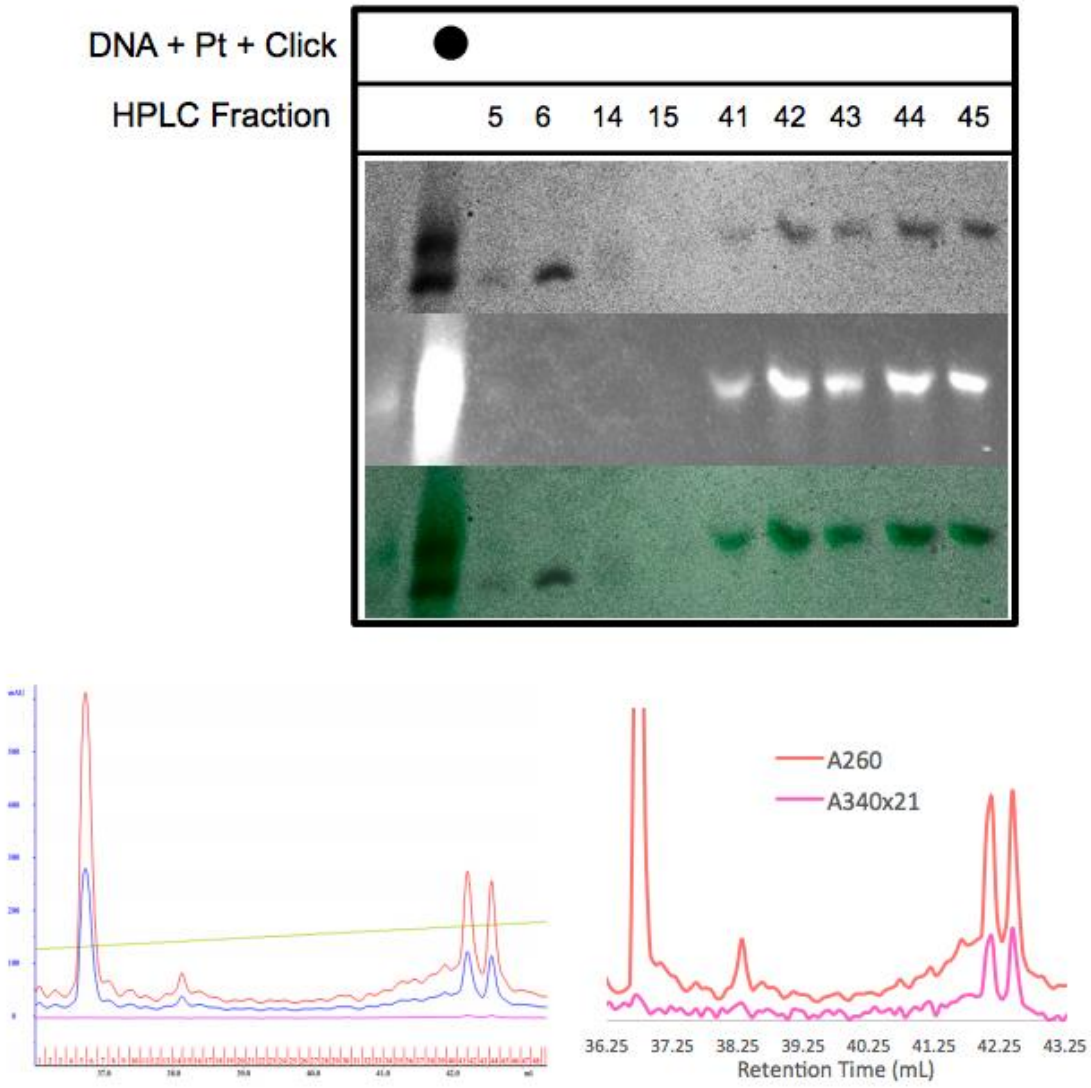

Figure A.4. HPLC and dPAGE analysis of **4**-bound hairpin DNA-Pt adduct following click reaction with dansyl alkyne. HPLC peaks at 5, 6, 14, 15, and 41-45 mL were isolated, rotary evaporated and then re-suspended for dPAGE analysis. In the first lane of the gel above is the crude reaction mixture, in lanes 2-9 are the corresponding HPLC fractions. The HPLC chromatogram on the right reveals that when the absorbance values for the fluorophore are multiplied by a factor of 21 the absorbance of the fluorophore bound to the clicked product can be easily seen and correlated to the corresponding click peaks. This multiplication is based upon the ratio between the extinction coefficient of the dansyl fluorophore and that of the 21 base hairpin.

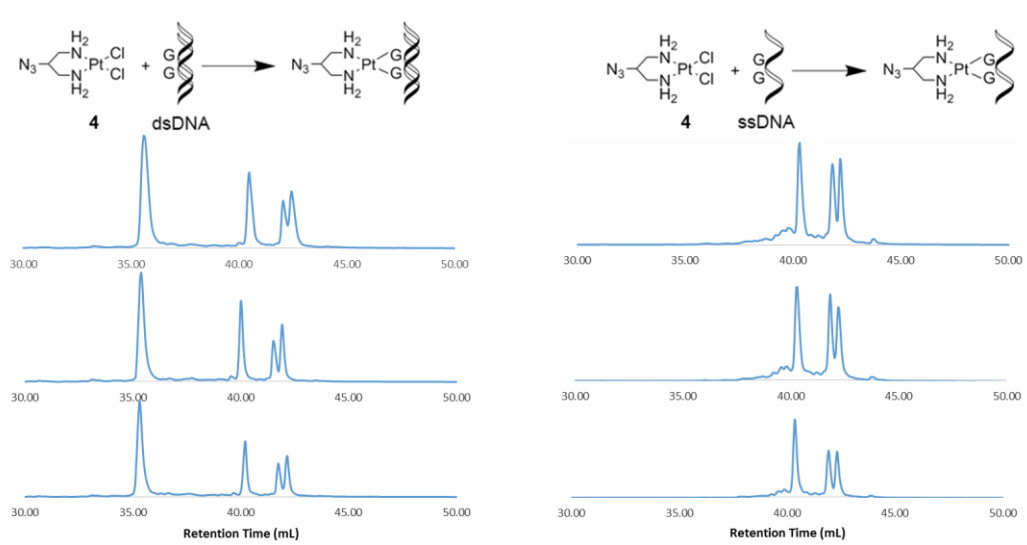

ssDNA			Ratio Pt2/Pt1
DNA	Pt1	Pt2	
48	28	25	0.90
46	27	27	1.00
41	30	29	0.97
		AVG	0.96
		STD	0.05

dsDNA			Ratio Pt2/Pt1
DNA	Pt1	Pt2	
43	23	34	1.49
45	24	32	1.33
42	25	33	1.33
		AVG	1.38
		STD	0.09

Figure A.5. HPLC chromatograms of the single stranded construct (ssDNA) and the double stranded construct (dsDNA) bound by **4**. Normalized areas of DNA parent peaks, first and second platinum binding peaks are listed. The ratio of the Pt-DNA peaks are listed along with the average for each construct and their respective standard deviations.

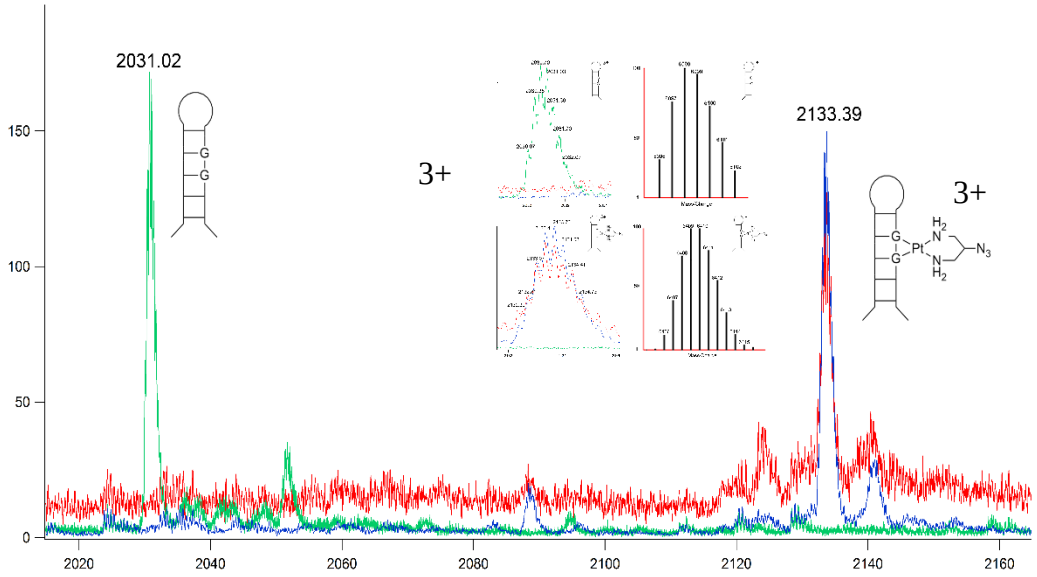

Figure A.6. Results from ESI-MS experiment. Traces for the parent DNA strand (green) and the two isolated **4** bound to DNA (blue and red traces) are shown. Peaks in the spectrum are attributed to the 3+ DNA strand (2031) and the 3+ **4**-DNA strand (2133). Inset shows a zoomed in image of data as well as the predicted isomeric distributions.

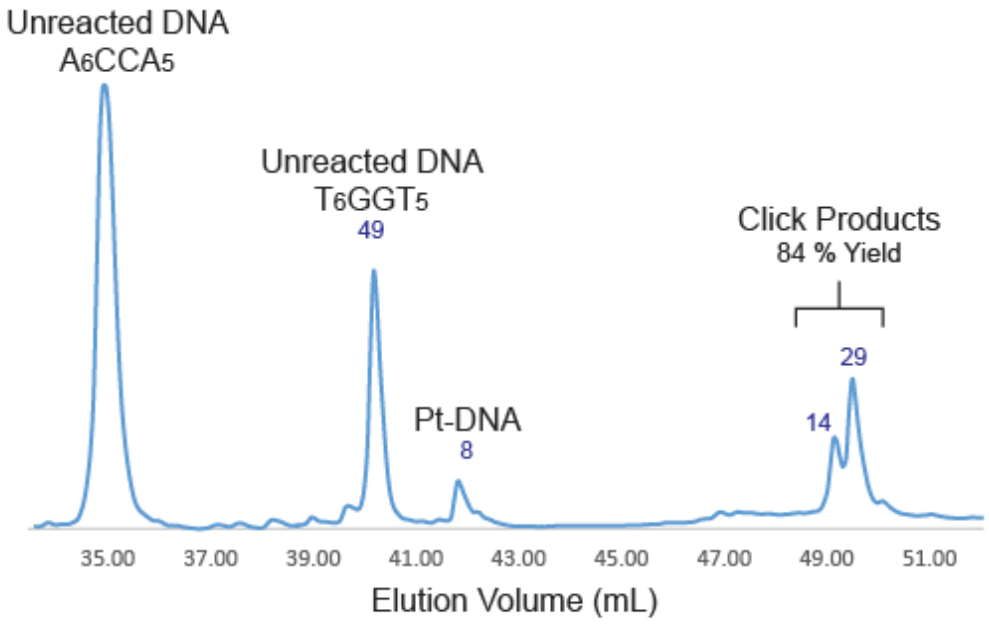

Figure A.7. HPLC chromatogram for dsDNA bound by **4** and clicked to a dansyl alkyne fluorophore. Peaks near 35 and 40 mL elution volume correlate to unbound DNA A_6CCA_5 and T_6GGT_5 respectively. Peak near 42 mL elution volume correlates to **4** bound DNA. Peaks near 49 mL elution volume correlate to the clicked products. The yield of the click reaction is approximately 84 %.

APPENDIX B

Materials and Methods

Materials were purchased from commercial vendors and used without further purification unless noted otherwise. Column chromatography was performed on Silica Gel Premium R_f (Sorbent Technologies, 75–200 μm). ^{1}H, ^{13}C, and ^{195}Pt NMR spectra were recorded in $CDCl_3$, d_6-DMSO, or d_7-DMF using a Varian Inova 500 MHz (^{1}H: 500.11 MHz, ^{13}C: 125.76 MHz, ^{195}Pt: 107.49 MHz) or a Varian Mercury 300 MHz (^{1}H: 300.09 MHz) NMR spectrometer. Chemical shifts (δ) are expressed in ppm relative to the residual $CHCl_3$ (^{1}H: 7.26 ppm, ^{13}C: 77.23 ppm), d_6-DMSO (^{1}H: 2.50 ppm, ^{13}C: 39.52 ppm), d_7-DMF (^{1}H: 8.03 ppm, ^{13}C: 163.15 ppm) or the external reference K_2PtCl_4 (^{195}Pt: –1604 ppm).

dPAGE experiments were visualized with methylene blue stain and UV exposure (AlphaImager HP System). Fluorescent images were obtained using an Olympus FluoView™ FV1000 confocal microscope.

DNA substrates were purchased directly from Integrated DNA Technologies, Inc., dissolved in nanopure ddH_2O to a final stock concentration of 1 mM and used without further purification. Substrates were stored in aliquots at –30 °C.

2 Experimental Procedure and Characterization Data

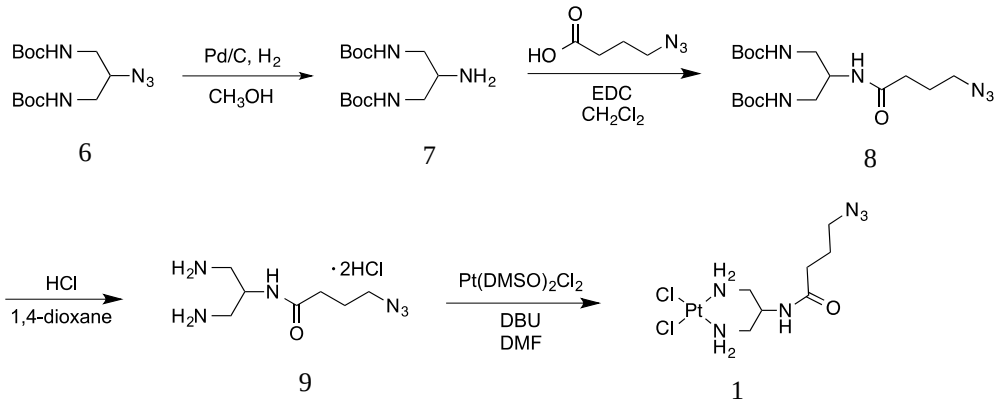

Figure B.1. Synthesis of complex **1**.

Di-*tert*-butyl (2-aminopropane-1,3-diyl)dicarbamate (7):

The dicarbamate **7** was synthesized according to methods in **Appendix A**.

Di-*tert*-butyl [2-(4-azidobutanamido)propane-1,3-diyl]dicarbamate (8):

To a 0° C solution of 4-azidobutanoic acid (0.77 g, 5.96 mmol) and 1-ethyl-3-(3-dimethylaminopropyl)carbodiimide hydrochloride (1.27 g, 6.64 mmol) in dry CH_2Cl_2 (28 mL) was added dropwise a solution of di-*tert*-butyl (2-aminopropane-1,3-diyl)dicarbamate (**7**) (1.20 g, 4.15 mmol) in dry CH_2Cl_2 (40 mL). The reaction was allowed to warm to rt and was stirred for 4 d. The reaction was then quenched with H_2O (20 mL) and allowed to stir for ca. 45 min. The organic phase was separated and washed with basic ($NaHCO_3$) H_2O (3 x 50 mL), then mildly acidic H_2O (ca. 1 M HCl, 3 x 50 mL), then dried with $MgSO_4$ and evaporated *in vacuo* to give a white solid. The solid was recrystallized from boiling EtOAc to reveal another white solid (0.74 g, 45%). ^{1}H NMR (500 MHz, $CDCl_3$): δ 7.05 (CON*H*,

s, 1H), 5.35 (N*H*, s, 2H), 3.74 (C*H*, s, 1H), 3.50-3.04 (NHCH_2, m, 4H), 3.34-3.31 ($CH_2CH_2CH_2$, m, 2H), 2.25 (CH_2N_3, t, J = 7.3 Hz, 2H), 1.90 ($CH_2CH_2CH_2$, p, J = 6.9 Hz, 2H), 1.44 (*t*-Boc, s, 18H). ^{13}C NMR (500 MHz, $CDCl_3$): δ 172.5, 157.7, 80.1, 53.0, 51.0, 40.9, 33.6, 28.5, 24.9.

4-Azido-*N*-(1,3-diaminopropan-2-yl)butanamide dihydrochloride (9):

To a flask charged with di-*tert*-butyl [2-(4-azidobutanamido)propane-1,3-diyl]dicarbamate (**8**) (0.32 g, 0.82 mmol) chilled on ice was added 4M HCl in 1,4-dioxane (7 mL). The mixture was stirred until all the solid had dissolved, then a new, white precipitate formed (ca. 1 h). The solid was filtered, rinsed with 1,4-dioxane followed by Et_2O, then dried *in vacuo* overnight to furnish a white solid (0.175 g, 83%). ^{1}H NMR (500 MHz, d_6-DMSO): δ 8.50-8.00 (NH_3/CON*H*, m, 7H), 4.20 (C*H*, s, 1H), 3.36 (NHCOCH_2, t, J = 5.0 Hz, 2H), 3.10-2.85 (NH_3CH_2, m, 4H), 2.26 (CH_2N_3, t, J = 7.4 Hz, 2H), 1.79 ($CH_2CH_2CH_2$, p, J = 7.1 Hz, 2H). ^{13}C NMR (500 MHz, d_6-DMSO): δ 172.5, 50.4, 45.3, 39.9-39.8 (obscured by solvent peak), 32.4, 24.0.

***cis*-[Pt(2-(4-azidobutyl)amido-1,3-propanediamine)Cl_2] (1):**

To a solution of 4-azido-*N*-(1,3-diaminopropan-2-yl)butanamide dihydrochloride (**9**) (0.045 g, 0.17 mmol) and 1,8-diazabicycloundec-7-ene (50 μL, 0.33 mmol) in dry DMF (1.26 mL) was added *cis*-[$Pt(DMSO)_2Cl_2$] (0.070 g, 0.17 mmol). The reaction was sealed with a septum and stirred in the dark for 2 d. The clear-yellow reaction mixture was added to chilled H_2O (4 mL) and the precipitate was isolated by filtration. The solid was washed with H_2O and dried in a desiccator, yielding a pale-yellow solid (0.032 g, 42%). ^{1}H NMR

(500 MHz, d_7-DMF) δ (ppm) = 8.05-7.97 (N*H*, m, 1H, partially obscured by residual solvent peak), 5.38-5.08 (CH_2NH_2, m, 4H), 4.20-4.10 (($CH_2)_2CHNH$, m, 1H), 3.41 (CH_2N_3, t, *J* = 7.5 Hz, 2H), 2.85-2.69 (CH_2NH_2, m, 4H), 2.31 ($COCH_2$, t, *J* = 7.5 Hz, 2H), 1.85 ($CH_2CH_2CH_2$, p, *J* = 7.5 Hz, 2H). ^{13}C NMR (500 MHz, d_7-DMF): δ 172.3, 51.9, 48.4, 47.4, 33.6, 25.7. ^{195}Pt NMR (500 MHz, d_7-DMF): δ –2287.

4-Pentynyl Rhodamine-B Ester (Rhodamine alkyne) (5):

To a solution of rhodamine-B (2.01 g, 4.20 mmol) in dry CH_2Cl_2 (50 mL) was added 4-pentyn-1-ol (0.47 g, 5.59 mmol), *N*,*N*'-dicyclohexylcarbodiimide (1.34 g, 6.50 mmol), and 4-dimethylaminopyridine (0.06 g, 0.49 mmol) and the reaction was stirred in the dark for 18 h at rt. The purple reaction mixture was washed with H_2O (3 x 50 mL) and the organic layer was evaporated to dryness *in vacuo*. The purple oil was purified via flash column chromatography on silica gel (100:10:1 $CHCl_3/CH_3OH/CH_3COOH$, Rf ≈ 0.4). The combined fractions were evaporated *in vacuo* and purified again via flash column chromatography on silica gel (100:100:1 $CHCl_3/CH_3OH/CH_3COOH$, Rf ≈ 0.8). The combined fractions were dried with $MgSO_4$, filtered, and evaporated in vacuo to reveal a purple oil (801 mg, 35%). ^{1}H NMR (500 MHz, $CDCl_3$): δ 8.30-8.23 (Ar, m, 1H), 7.85-7.66 (Ar, m, 2H), 7.32-7.27 (Ar, m, 1H), 7.09-7.01 (Ar, d, *J* = 9.4 Hz, 2H), 6.92 (Ar, dd, *J* = 9.5 Hz, 2.2 Hz, 2H), 6.86 (Ar, d, *J* = 2.3 Hz, 2H), 4.12 ($COCH_2$, t, *J* = 6.2 Hz, 2H), 3.62 (NCH_2, q, *J* = 7.2 Hz, 8H), 2.05 (CH_2CCH, td, *J* = 7.7, 2.6 Hz, 2H), 1.90 (CC*H*, t, *J* = 2.6 Hz, 1 H), 1.69 ($CH_2CH_2CH_2$, p, *J* = 6.6 Hz, 2H), 1.32 (NCH_2CH_3, t, *J* = 7.1 Hz, 12H). ^{13}C NMR (500 MHz, $CDCl_3$): δ 165.2, 158.9, 157.9, 155.8, 133.7, 133.3, 131.5, 131.4, 130.6, 130.5, 130.1, 114.4, 113.7, 96.7, 82.7, 69.4, 64.4, 46.4, 27.5, 15.3, 12.9.

3 Denaturing Polyacrylamide Gel Electrophoresis – Experiments

DNA Folding (Figure 3.4-6):

The DNA (typically 5 nmol, 5'- TATGGTATTTTTATACCATA-3') was folded by rapid heating to 90 °C and slow cooling to 4 °C in a 10 mM Na_2HPO_4 (pH 7.0), 100 mM $NaNO_3$, and 1 mM $Mg(NO_3)_2$ solution to give a final volume of 13 μL.

Platinum-DNA Hairpin Binding (Figure 3.4):

A 2.5 mM solution of **1** or **2** in DMF was individually added to the folded hairpin (equimolar amount vs. DNA), the solution diluted with 3 μL of ddH_2O and incubated at 37 °C for 18 h. The solution of **1**-bound DNA or **2**-bound DNA was purified with Sephadex G-25 Med. size exclusion resin (GE Healthcare) on laboratory-prepared spin columns (BioRad) to remove unbound **1** or **2**. The eluent was dried to completion by SpeedVac and stored at –30 °C until use.

Platinum-DNA Hairpin Click Reaction (Figure 3.4):

The **1**- or **2**-bound DNA pellet was re-suspended in H_2O (18 μL) and Na_2HPO_4 (pH 7.0, 3.7 μL, 100 mM), to which was added rhodamine alkyne/azide (2 μL, 5 mM), sodium ascorbate (5 μL, 10 mM), and finally $CuSO_4$ (5 μL, 1 mM). The reaction was left for 18 h at rt. Upon completion of the reaction the mixture was purified with Sephadex G- 25 Med. resin on laboratory-prepared spin columns to remove Cu and to quench the reaction. The eluent was dried to completion by SpeedVac and re-dissolved in H_2O (18 μL) and 70% *v/v* formamide (12 μL) for analysis by dPAGE (20%, 29:1).

Platinum-DNA Hairpin Binding (Figure 3.5):

A 5 mM solution of **1** or **2** in DMF was individually added to the folded hairpin (twofold access vs. DNA), the solution diluted with 3 μL of ddH_2O and incubated at 37 °C for 48 h. The solution of **1**- or **2**-bound DNA was purified with Sephadex G-25 Med. size exclusion resin (GE Healthcare) on laboratory- prepared spin columns (BioRad) to remove unbound Pt. The eluent was dried to completion by SpeedVac and stored at –30 °C until use.

Platinum-DNA Hairpin Click Reaction (Figure 3.5):

The **1**- and **2**-bound DNA pellets were re-suspended in ddH_2O (18 μL), Na_2HPO_4 (pH 7.0, 3.7 μL, 100 mM) and both solutions were combined. Sodium ascorbate (10 μL, 10 mM), and $CuSO_4$ (10 μL, 1 mM) were added and the reaction left for 24 hours at rt. The mixture was purified with Sephadex G-25 Med. resin on laboratory-prepared spin columns to remove Cu and to quench the reaction. The eluent was dried to completion by SpeedVac and re-dissolved in H_2O (18 μL) and 70% *v/v* formamide (12 μL) for analysis by dPAGE (20%, 29:1).

Platinum-DNA Hairpin Click Reaction with Dansylalkyne/azide as internal control (Figure B.2):

The **1**- or **2**-bound DNA pellet was re-suspended in H_2O (18 μL) and Na_2HPO_4 (pH 7.0, 3.7 μL, 100 mM), to which was added dansyl alkyne/azide (5-(dimethylamino)-*N*-(2-propynyl)-1-napthalenesulfonamide, 5-(Dimethylamino)naphthalene-1-sulfonyl azide) (2 μL, 10 mM), sodium ascorbate (5 μL, 10 mM), and finally $CuSO_4$ (5 μL, 1 mM). The reaction was left for 24 h at rt. Upon completion of the reaction the mixture was purified with Sephadex G- 25 Med. resin on laboratory-prepared spin columns to remove Cu and

to quench the reaction. The eluent was dried to completion by SpeedVac and re-dissolved in H_2O (18 μL) and 70% *v/v* formamide (12 μL) for analysis by dPAGE (20%, 29:1).

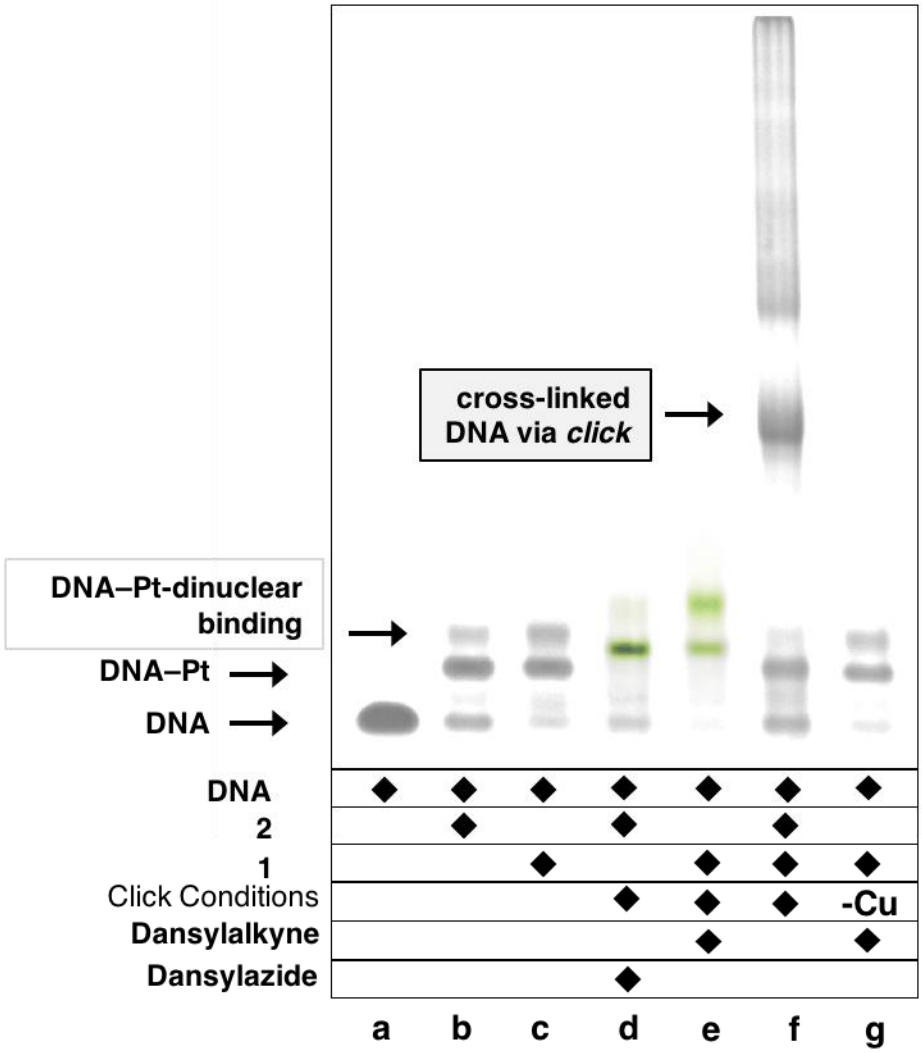

Figure B.2. dPAGE experiment showing the crosslinking of 1 and 2 bound to a 5'-GG-3' DNA hairpin sequence (f). The internal controls are depicted in lane d and e (Platination of the DNA with **1** or **2** followed by subsequent CuAAC with dansyl alkyne/azide fluorophore). The copper free control is depicted in lane g.

Platinum-DNA Hairpin Binding (Figure 3.6):

A 2.5 mM solution of **1** or **5** in DMF was individually added to the folded hairpin (equimolar amount vs. DNA), the solution diluted with 3 μL of ddH_2O and incubated at 37 °C for 48 h. The solution of **1**- or **5**-bound DNA was purified with Sephadex G-25 Med. size exclusion resin (GE Healthcare) on laboratory- prepared spin columns (BioRad) to remove unbound Pt. The eluent was dried to completion by SpeedVac and stored at –30 °C until use.

Platinum-DNA Hairpin Click Reaction (Figure 3.6):

The **1**- or **5**-bound DNA pellet was re-suspended in H_2O (18 μL), Na_2HPO_4 (pH 7.0, 3.7 μL, 100 mM), to which was added dansyl alkyne (5 μL, 10 mM in DMF), sodium ascorbate (5 μL, 10 mM), and finally $CuSO_4$ (5 μL, 1 mM). The reaction was left for 30 min. to 6 hours at rt. Upon completion of the reaction the mixture was purified with Sephadex G- 25 Med. resin on laboratory-prepared spin columns to remove Cu and to quench the reaction. The eluent was dried to completion by SpeedVac and re-dissolved in H_2O (18 μL) and 70% *v/v* formamide (12 μL) for analysis by dPAGE (20%, 29:1).

4 Crystallographic Data

X-ray Crystallography. Diffraction intensities were collected at 173 K on a Bruker Apex2 CCD diffractometer using MoKα radiation, λ= 0.71073 Å. Space group was determined based on intensity statistics. Absorption correction was applied by SADABS.[9] Structure was solved by direct methods and Fourier techniques and refined on F^2 using full matrix least-squares procedures. All non-H atoms were refined with anisotropic thermal parameters. H atoms were refined in calculated positions in a rigid group model. All calculations were performed by the Bruker SHELXTL (v. 6.10)[10] and SHELXL-2013 packages.[11]

Crystallographic Data for **1**: $C_7H_{16}Cl_2N_6OPt$, M = 466.25, 0.07 x 0.04 x 0.03 mm, T = 173 K, triclinic, space group *P*-1, a = 7.330(2) Å, b = 7.583(2) Å, c = 11.831(3) Å, α = 85.465(5)°, β = 86.040(5)°, γ = 86.498(5)°, V = 653.1(3) Å^3, Z = 2, D_c = 2.371 Mg/m^3, μ(Mo)= 11.147 mm^{-1}, F(000) = 440, $2\theta_{max}$ = 50.0°, 7931 reflections, 2287 independent reflections [R_{int} = 0.0774], R1 = 0.0403, wR2 = 0.0644 and GOF = 1.011 for 2287 reflections (154 parameters) with I>2σ(I), R1 = 0.0627, wR2 = 0.0704 and GOF = 1.011 for all reflections, max/min residual electron density +1.423/–1.283 eÅ^3.

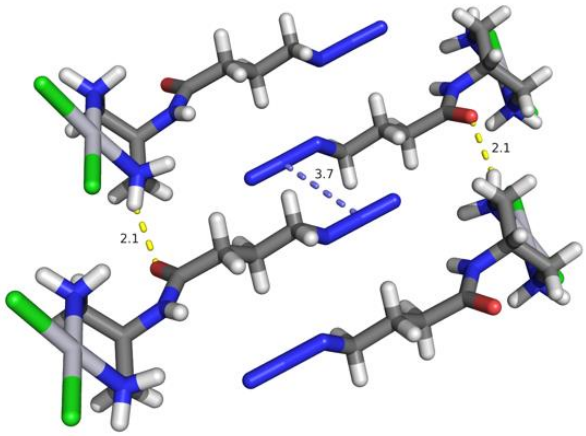

Figure B.3. Crystal structure arrangement of **1** showing the antiparallel arrangement of the azide moiety and hydrogen bonding between the amine protons and adjacent carbonyl group (2.13 Å)

5 Confocal fluorescence microscopy

Cell Maintenance:

The human cervical cancer cell line, HeLa, was obtained from the American Type Culture Collection (Rockville, MD, USA) and was cultured in DMEM media (gibco) containing 4.5 g L D-glucose and 110 mg L sodium pyruvate supplemented with 10% fetal bovine serum (FBS) and 10% antibiotics. Cells were incubated at a constant temperature at 37 °C in a humidified atmosphere containing 5% CO_2 and were subcultured every 2 to 3 days in order to maintain cells in logarithmic growth.

Cell Treatment and Cu-Catalyzed Click:

HeLa cells were seeded onto microscope cover slips with 1.5 x 10^5 cells/mL in 2 mL of media per well. Cells were incubated overnight and then treated with 5 μM or 25 μM **1** and **2** for 3 h. Cells were then rinsed with PBS, fixed with 4% paraformaldehyde (in PBS pH 7.4) for 20 min, and then permeabilized with Triton-X 100 (**Figure 7**) for 20 min. After permeabilization, cells were washed with 3% BSA (in PBS, pH 7.4) twice for 10 min., and

then incubated with 1 mM $CuSO_4$, 5 mM THPTA, 5 μM Rhodamine, 25 mM sodium ascorbate, and 100 mM phosphate buffer for 2 h at room temperature. Cells were then rinsed with 3% BSA in PBS (5 min), and then washed extensively with Triton X (2 x 10 min) and then PBS 2x10 min. Slides were then mounted using ProLong Diamond anti-fade reagent with DAPI stain.

6 NMR Spectra

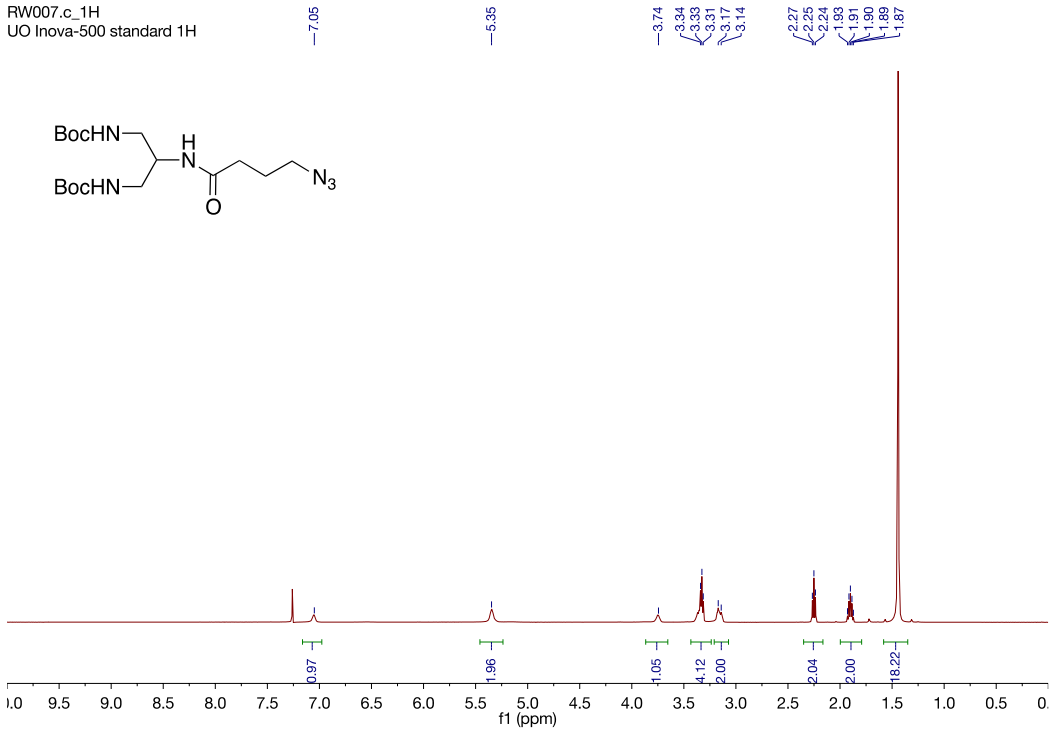

Figure B.4. ^{1}H-NMR spectrum of **8** in $CDCl_3$ (500 MHz).

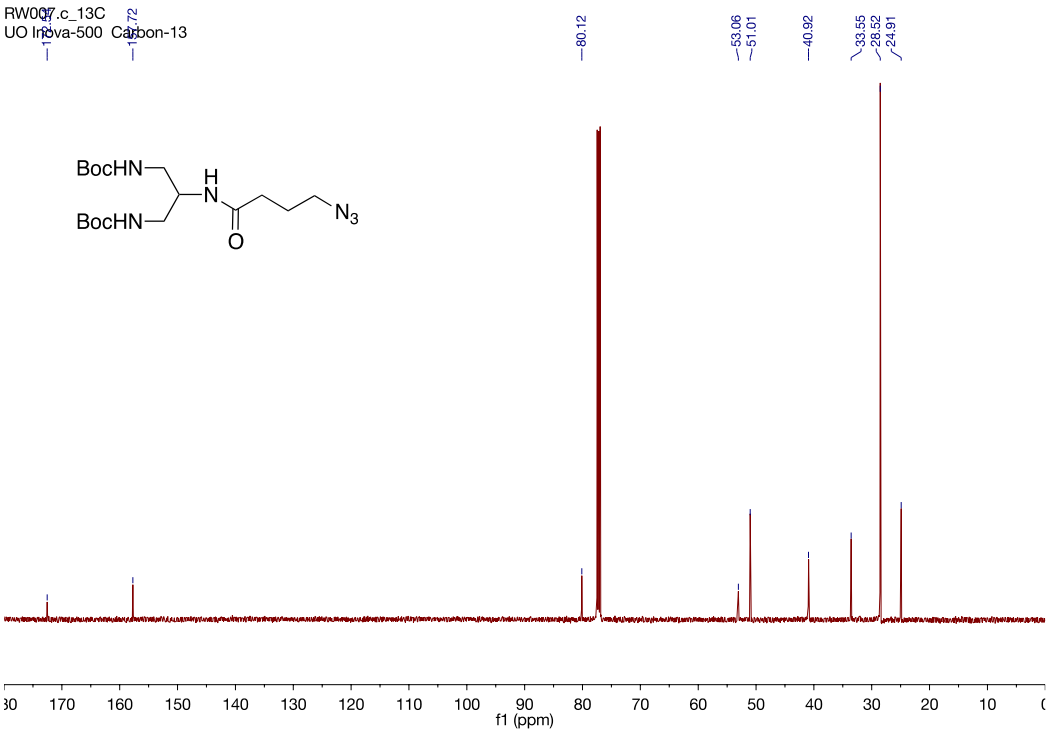

Figure B.5. ^{13}C NMR spectrum of **8** in $CDCl_3$ (500 MHz).

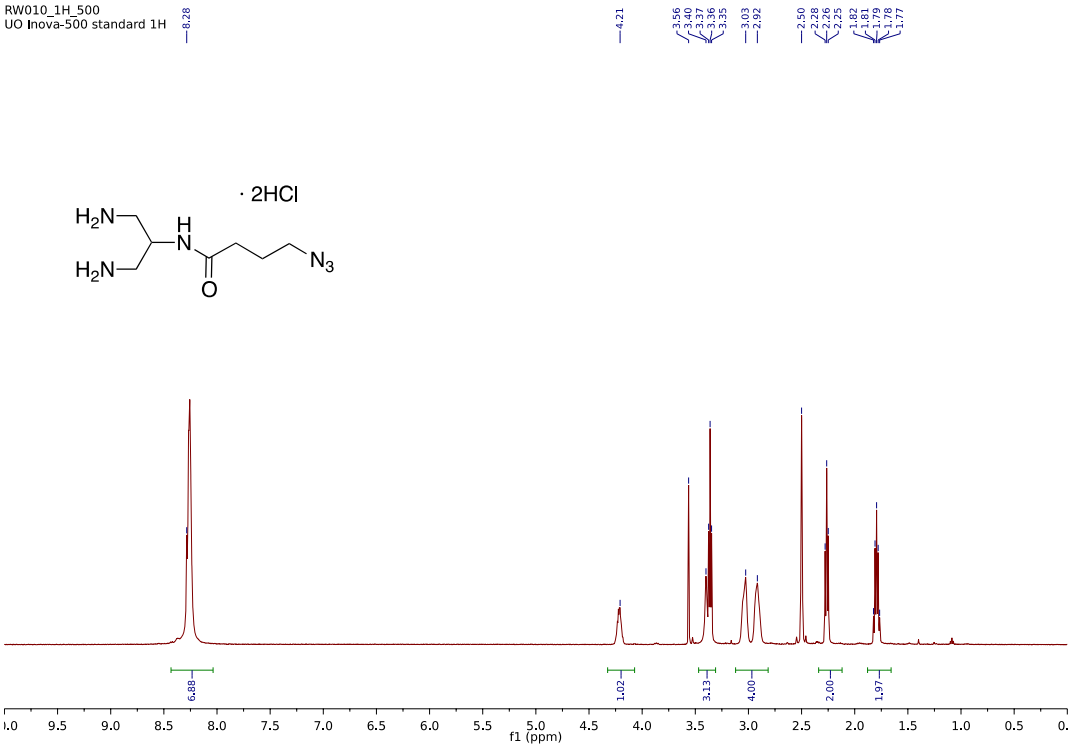

Figure B.6. ^{1}H-NMR spectrum of **9** in d_6-DMSO (500 MHz).

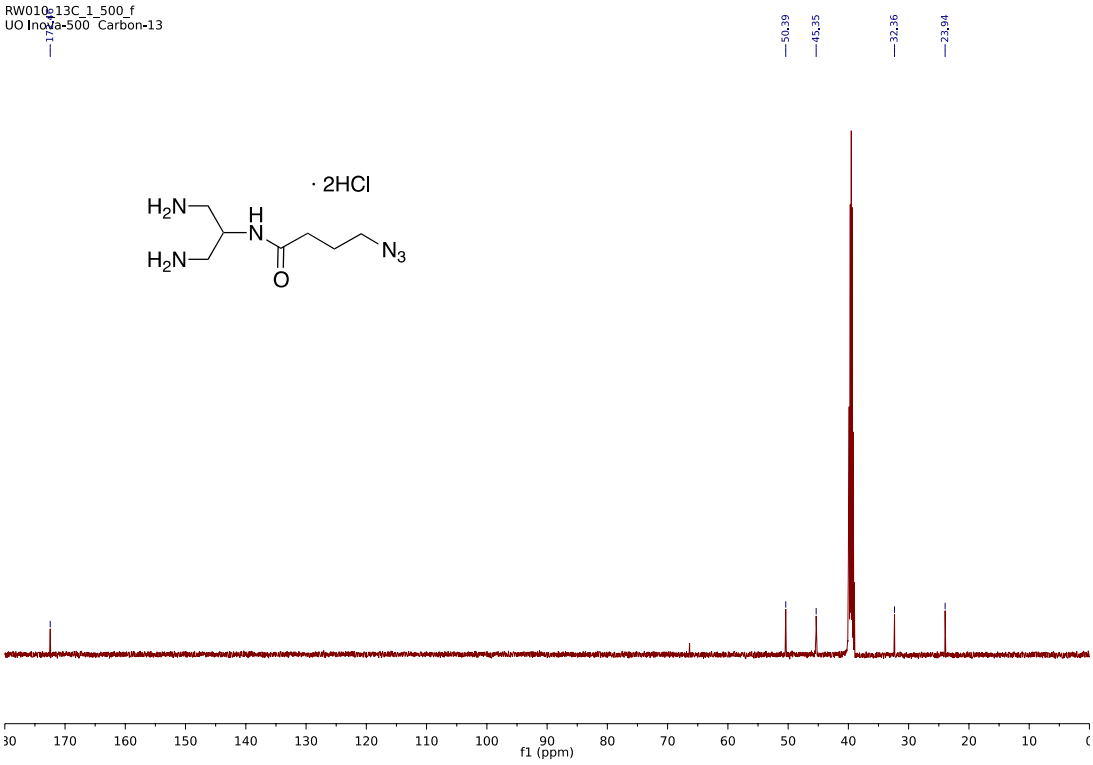

Figure B.7. ^{13}C NMR spectrum of **9** in d_6 -DMSO (500 MHz).

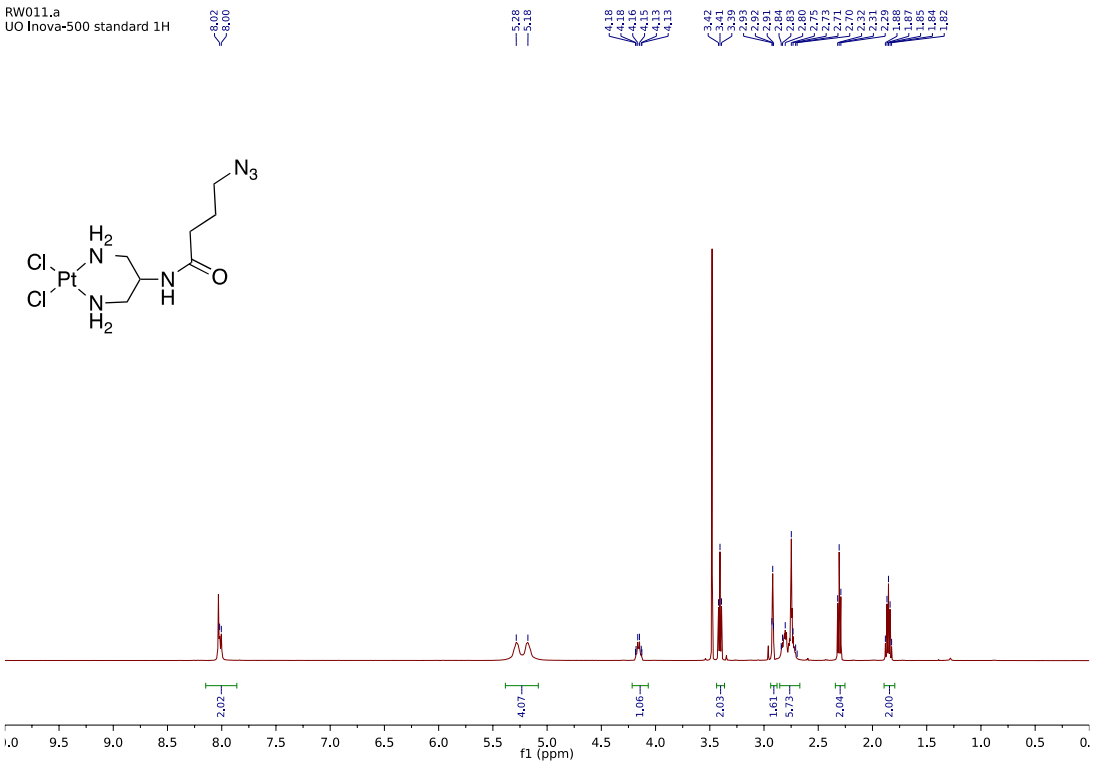

Figure B.8. ^{1}H NMR spectrum of **1** in d_7-DMF (500 MHz).

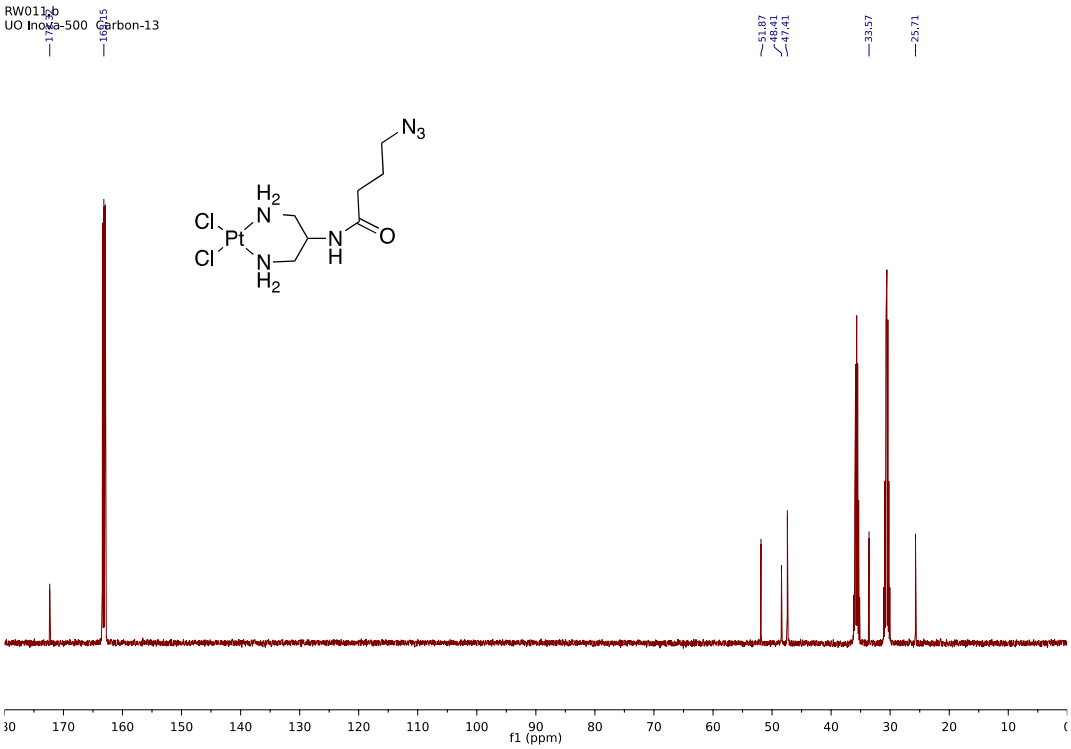

Figure B.9. ^{13}C NMR spectrum of **1** in d_7-DMF (500 MHz).

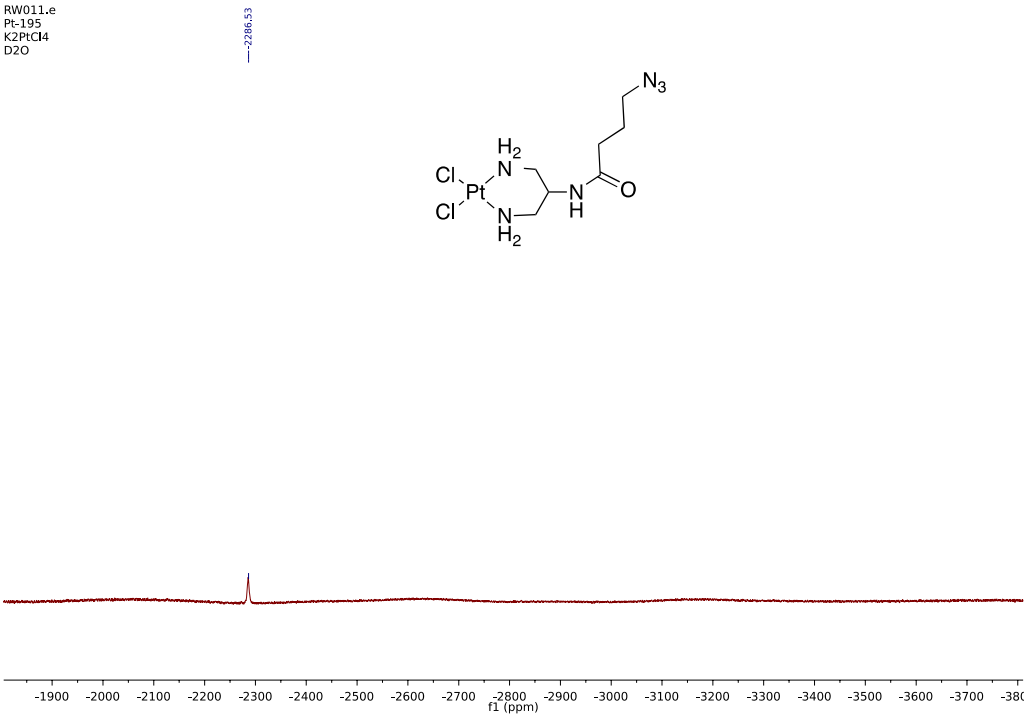

Figure B.10. ^{195}Pt NMR spectrum of **1** in d_7-DMF (500 MHz).

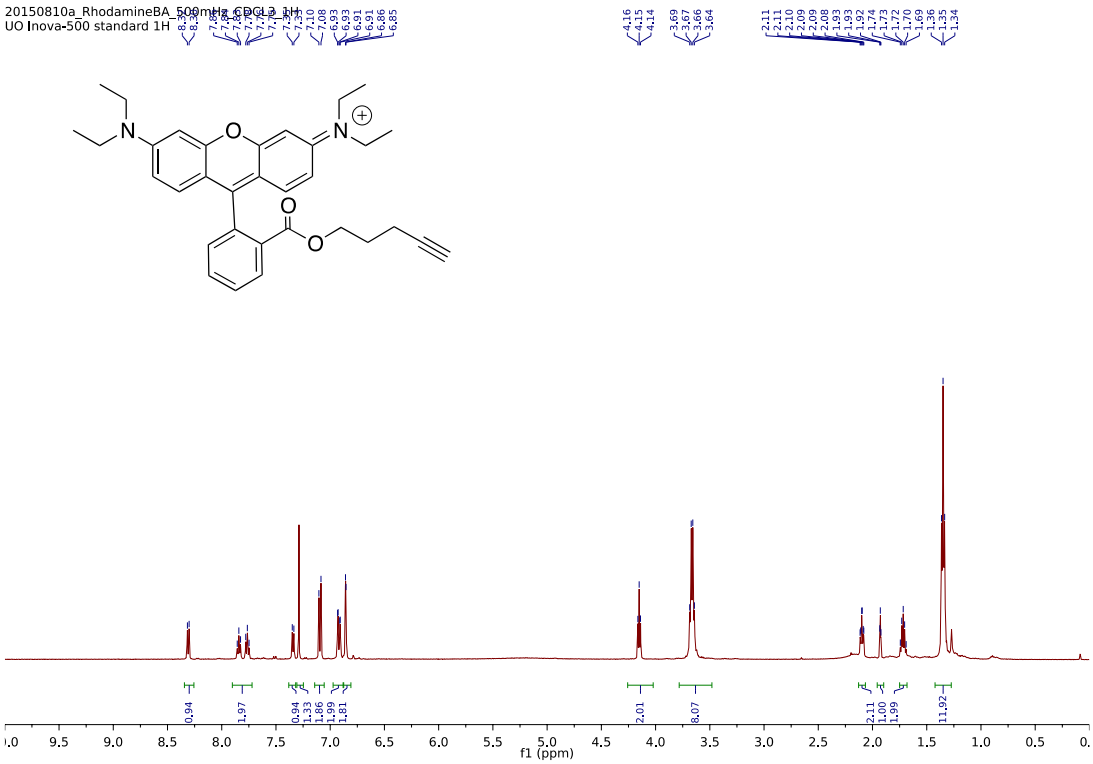

Figure B.11. ^{1}H NMR spectrum of 4-pentynyl Rhodamine-B ester (**5**) in $CDCl_3$ (500 MHz).

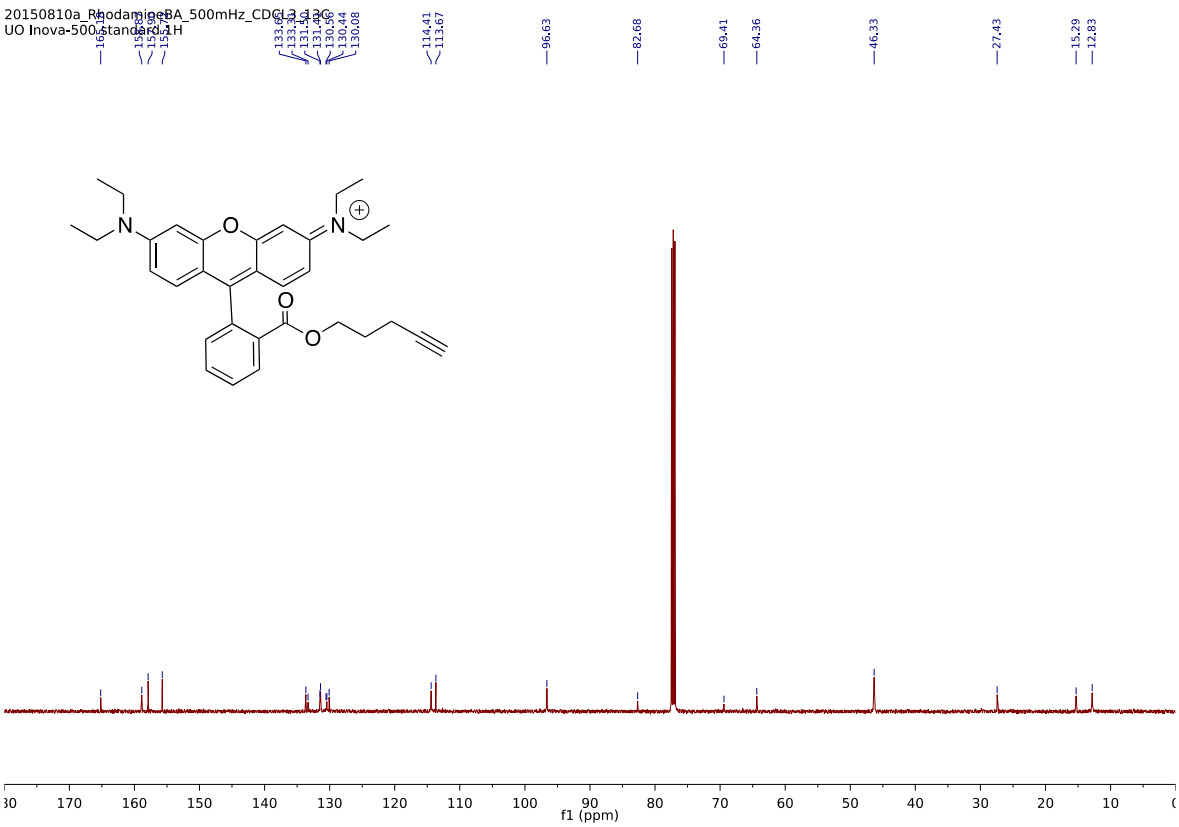

Figure B.12. ^{13}C NMR spectrum of 4-pentynyl Rhodamine-B ester (**5**) in $CDCl_3$ (500 MHz).

APPENDIX C

Materials and Methods

For general HPLC methods refer to **Appendix A**. For general synthetic methods of **1** refer to **Appendix B**.

Platinum–DNA Click Reactions (HPLC analysis). Sodium ascorbate (18 µL, 100 mM), a solution of $CuSO_4$ (20 µL, 5mM) and tris(3-hydroxypropyltriazolylmethyl)amine (THPTA) (20 µL, 25 mM), tripropargylamine (10 µL, 2 mM) and **3** (10 µL, 2 mM) were added to a solution of water containing Pt-bound DNA (18 µL, 180 µM). The samples were incubated overnight at room temperature and then were fractionated via HPLC (see below). HPLC fractions were combined and dried in vacuo. Fractions corresponding to clicked product were again subjected to click reaction with **3** (10 µL, 2mM) in sodium ascorbate (18 µL, 25 mM), (20 µL, 5mM) and THPTA (20 µL, 25 mM). The samples were dried in vacuo and then resuspended in a 3:2 v/v mixture of ddH_2O and formamide, respectively, for dPAGE analysis. Alternatively, the dried samples were dissolved in ddH_2O for HPLC analysis. dPAGE experiments were visualized with methylene blue stain and UV exposure (AlphaImager HP System).

Cell Maintenance

The human cervical cancer cell line, HeLa, was obtained from the American Type Culture Collection (Rockville, MD, USA) and was cultured in DMEM media (gibco) containing 4.5 g/L D-glucose and 110 mg/L sodium pyruvate supplemented with 10% fetal bovine serum (FBS) and 10% antibiotics. Cells were incubated at a constant temperature at 37 °C in a humidified atmosphere containing 5% CO_2 and were subcultured every 2 to 3 days in order to maintain cells in logarithmic growth.

Cell Treatment and Cu-Catalyzed Click

HeLa cells were seeded onto microscope cover slips with 1.5 x 10^5 cells/mL in 2 mL of media per well. Cells were incubated overnight and then treated with 5 μM **1** for 3 h. Cells were then rinsed with PBS, fixed with 4% paraformaldehyde (in PBS, pH 7.4) for 20 min, and then permeabilized with Triton-X 100 for 20 min. After permeabilization, cells were washed with 3% BSA (in PBS, pH 7.4) twice for 10 min, and then incubated with 1 mM $CuSO_4$, 5 mM THPTA, 5 μM tripropargylamine or **2**, 25 mM sodium ascorbate, and 100 mM phosphate buffer for 30 min at room temperature. Cells were then rinsed with 3% BSA in PBS (5 min), and then washed extensively with Triton X (2 x 10 min) and then PBS (2 x 10 min). For the double-click procedure, cells were incubated again with 1 mM $CuSO_4$, 5 mM THPTA, 5μM **3** or **4**, 25 mM sodium ascorbate, and 100 mM phosphate buffer for 30 min at room temperature and then washed again extensively using BSA and Triton-X as noted above. Cells in Figure 3 were not washed after the second click reaction. Slides were then mounted using ProLong Diamond anti-fade reagent with DAPI stain.

Fluorescent images were obtained using an Olympus FluoView^{TM} FV1000 confocal microscope using a 63x (PLAN APO 1.2 NA) objective lens. A 405 nm laser with an emission range of 430-470 was used to image DAPI staining in cells. For fluorophores **2** and **3** a 543 nm laser with an emission range of 560-660 nm was used. For fluorophore **4** a 635 nm laser with an emission range of 655-755 nm was used. All images were acquired at an 8 μs/pixel scan rate and 4x line averaging at 800 x 800-pixels. Images were acquired at an 8-bit sampling. All images were processed using ImageJ (National Institutes of Health) and figures were prepared using Adobe Photoshop CC 2015. All images were held

to the same excitation power, PMT voltages, offset values and pinhole settings for each respective channel.

3 Supplementary Figures

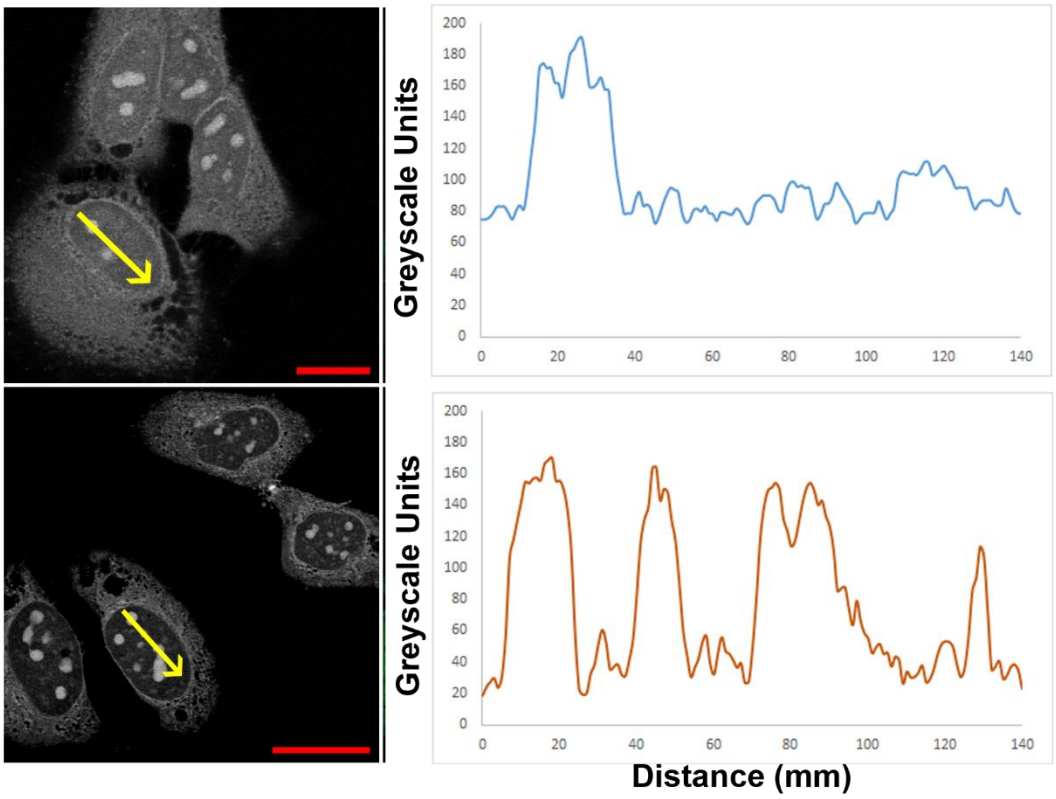

Figure C.1. Line plots of the double and single clicked species with brightness levels enhanced post-acquisition. The lower panel shows a line plot of the double-clicked cells as shown in Figure 1. The top panel shows the single-clicked species line plot with brightness levels enhanced to match the maximum observed in the double-click experiment.

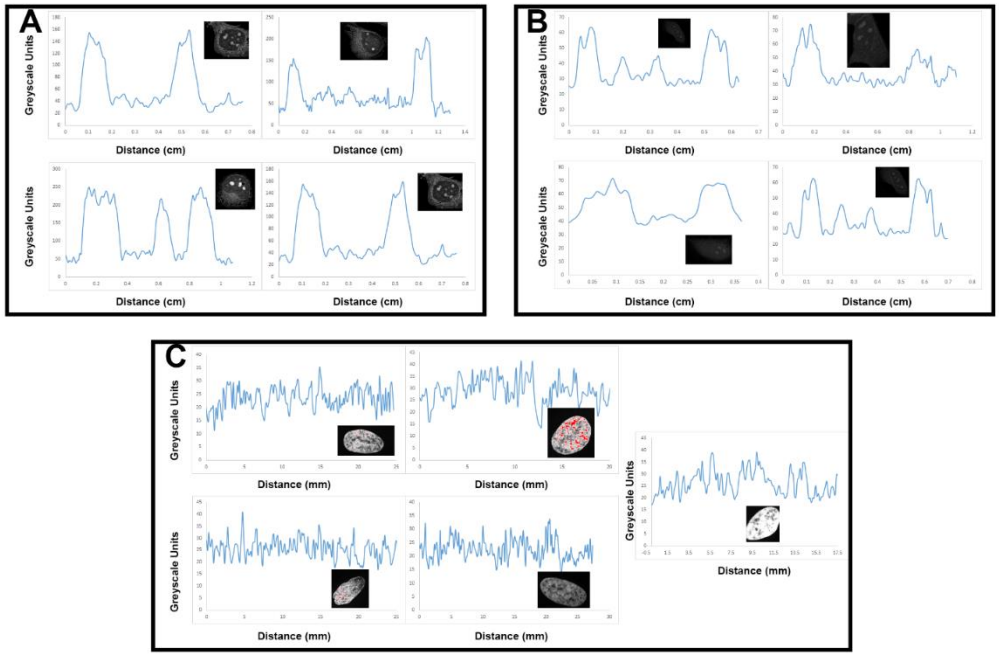

Figure C.2. Line plots comparing intensities in several double-clicked (panel A) and single-clicked (panel B) cells. Panel C shows background fluorescence for control cells treated with fluorophore but no Cu catalyst. In panel C the DAPI channel is shown in place of the rhodamine B channel.

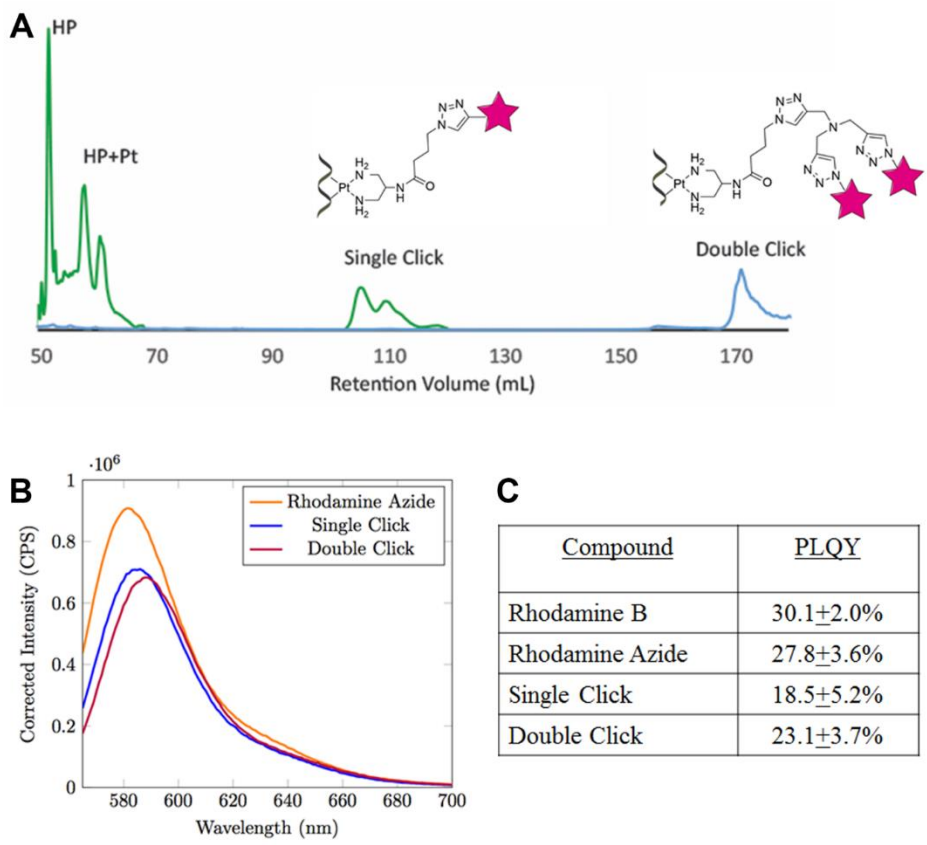

C

Compound	PLQY
Rhodamine B	30.1±2.0%
Rhodamine Azide	27.8±3.6%
Single Click	18.5±5.2%
Double Click	23.1±3.7%

Figure C.3. Fluorescence quantum yield measurements for **1**-treated DNA hairpin with single- or double-fluorophore attachment. Panel A shows the HPLC chromatogram separating products from the single-click reaction (green) and product of the subsequent double-click reaction (blue). Products of **1**-bound DNA include two isomers, as previously observed.[9] Panel B shows the relative fluorescence intensities of the rhodamine azide, the DNA-Pt hairpin with a single rhodamine fluorophore, and the DNA-Pt hairpin with two attached rhodamine fluorophores. Fluorescence is normalized to the fluorophore concentration. Panel C shows the fluorescence quantum yield (PLQY) of each species, with errors calculated from measurements performed in triplicate.

APPENDIX D

Materials and Methods

For general synthetic methods of **1** refer to **Appendix B**.

Cell Maintenance

All cell lines, HCC 1143, MDA MB 468, and C6 cells were obtained from the American Type Culture Collection (Rockville, MD, USA) and were cultured in recommended media (Gibco) at 37 °C in a humidified atmosphere containing 5% (HCC 1143 and C6) or 1% (MDA MB 468) CO_2 and were subcultured every 2 to 3 days in order to maintain cells in logarithmic growth.

Cellular Imaging

Cells were seeded onto microscope cover slips with 1.5 x 10^5 cells/mL in 2 mL of media per well. Cells were incubated overnight and then treated with 5 μM **1** for 3 h. Cells were then rinsed with PBS, fixed with 4% paraformaldehyde (in PBS, pH 7.4) for 20 min, and then permeabilized with Triton-X 100 for 20 min. After permeabilization, cells were washed with 3% BSA (in PBS, pH 7.4) twice for 10 min, and then incubated with 1 mM $CuSO_4$, 5 mM THPTA, 5 μM Alexafluor 488 alkyne (Invitrogen), 25 mM sodium ascorbate, and 100 mM phosphate buffer for 30 min at room temperature. Cells were then rinsed with 3% BSA in PBS (5 min), and then washed extensively with Triton X (2 x 10 min) and then PBS (2 x 10 min). For co-localization experiments, before fixation the media was removed and cells were treated with 100 nM Mito-Tracker Deep Red (Invitrogen) for 30 min in FBS free media. Slides were mounted using ProLong Diamond anti-fade reagent with DAPI stain.

Fluorescent images were obtained using an Olympus FluoViewTM FV1000 confocal microscope using a 63x (PLAN APO 1.2 NA) objective lens. A 405 nm laser with an emission range of 430-470 was used to image DAPI staining in cells. For Alexafluor 488 alkyne a 488 nm laser with an emission range of 500-570 nm was used. For Mito-Red tracker a 635 nm laser with an emission range of 655-755 nm was used. All images were acquired at an 8 µs/pixel scan rate and 4x line averaging at 800 x 800-pixels. Images were acquired at an 8-bit sampling. All images were processed using ImageJ (National Institutes of Health) and figures were prepared using Adobe Photoshop CC 2015. All images were held to the same excitation power, PMT voltages, offset values and pinhole settings for each respective channel.

Co-localization Analysis

For co-localization analysis, cell images were loaded into ImageJ (National Institutes of Health) and images were masked using the fluorescence present in the channel for Mito Tracker Deep Red. The average fluorescence intensity for the masked Alexafluor 488 channel was calculated and then an inverse selection was made. Bounds for cells were set by the fluorescent image in Alexafluor 488 channel and the nucleus was masked using the DAPI channel and removed from analysis of fluorescence outside of the mitochondria.

APPENDIX E

Methods

For general synthetic methods of **3** refer to **Appendix A**. For general synthetic methods of **4** refer to **Appendix B**.

*Synthesis of **1**.* To a stirred solution of **3** (48.6 mg) in H_2O (5 mL), **5** (46.4 mg) was added and shielded from light for 48 h. The solution was then filtered through celite, and the celite column was rinsed 3 times with H_2O (5 mL). The filtrate was placed under rotary vacuum to afford **1**, a brown solid (31.3 mg, 53% yield). ^{1}H NMR (500 MHz, d_7-DMF): δ 4.99 (Pt–N*H*$_2$–, s, 4H, $^3J_{Pt\text{-}H}$ = ~60 Hz), 2.88-2.60 (Pt–NH$_2$–C*H*$_2$–, m, 4H, obscured by residual DMF solvent peak), 1.78 (CH$_2$–C*H*$_2$–, m, 1H); ^{195}Pt NMR (129 MHz, d_7-DMF): δ –1950 (Pt).

*Synthesis of **2**.* To a stirred solution of **4** (15 mg) in a 50:50 mixture of H_2O:DMF (10 mL), **5** (17 mg) was added and shielded from light for 48 h. The solution was then filtered through celite, and the celite column was rinsed 3 times with H_2O (5 mL). The filtrate was placed under rotary vacuum to afford **1**, a yellow solid (5.1 mg, 31 % yield). ^{1}H NMR (500 MHz, D_2O) δ (ppm) = 3.96-3.90 (m, 1H), 3.34-3.27 (t, 2H), 2.85-2.75 (q, 4H), 2.71-2.56 (m, 4H), 2.33-2.22 (t, 2H), 1.85 (t, 4H). ^{195}Pt NMR (500 MHz, d_7-DMF): δ –1975.

DNA Folding (Figure 3). The DNA hairpin (typically 5 nmol, 5'-TATGGTATTTTTATACCATA-3') was folded by rapid heating to 90 °C and slow cooling to 4 °C in a 10 mM Na_2HPO_4 (pH 7.0), 100 mM $NaNO_3$, and 100 mM $Mg(NO_3)_2$ solution to give a final volume of 13 μL.

Pt-DNA Hairpin Binding (Figure 3). 2μl of a 5 mM solution of **1** in DMF was added to the folded hairpin, the solution diluted with 3 μL of ddH_2O and incubated at 37 °C for 48 h.

The solution of **1**-bound DNA was purified with Sephadex G-25 Med. size exclusion resin (GE Healthcare) on laboratory- prepared spin columns (BioRad) to remove unbound Pt.

Platinum-DNA Hairpin Click Reaction (Fig 6.3). The **1**-bound DNA pellet was re-suspended in H_2O (18 μL), Na_2HPO_4 (pH 7.0, 3.7 μL, 100 mM), to which was added rhodamine alkyne (5 μL, 5 mM in H_2O), sodium ascorbate (5 μL, 10 mM), and finally CuSO4 (5 μL, 1 mM). The reaction was incubated for 30 min at RT. Upon completion of the reaction, the mixture was purified with Sephadex G- 25 Med. resin on laboratory-prepared spin columns to remove Cu and to quench the reaction. The eluent was dried to completion by SpeedVac and re-dissolved in H_2O (18 μL) and 70% v/v formamide (12 μL) for analysis by dPAGE (20%, 29:1).

*Platinum-Bovine Serum Albumin (BSA) Binding with **2** (Fig 6.4).*BSA (50 μM) was incubated with 250 μM **2** or **4** in 10 mM Na_2HPO_4/NaH_2PO_4 buffer (pH 7.0), 10 mM $NaNO_3$, and 100 μM $Mg(NO_3)_2$ at 37 °C for 6 or 24h. Pt-bound BSA was purified with Sephadex G-25 Medium size exclusion resin (GE Healthcare) on laboratory-prepared spin columns (Thermo Fisher) to remove unbound Pt. To perform the click reaction, 100 μM rhodamine B-alkyne fluorophore, 125 μM $CuSO_4$, 500 μM THPTA, and 2.5 mM sodium ascorbate was added to platinated BSA and allowed to react at 37 °C for 1 h. Free fluorophore was removed using Sephadex G-25 spincolumns. Purified protein was then analyzed by 10% SDS-PAGE.

Supplementary Figures

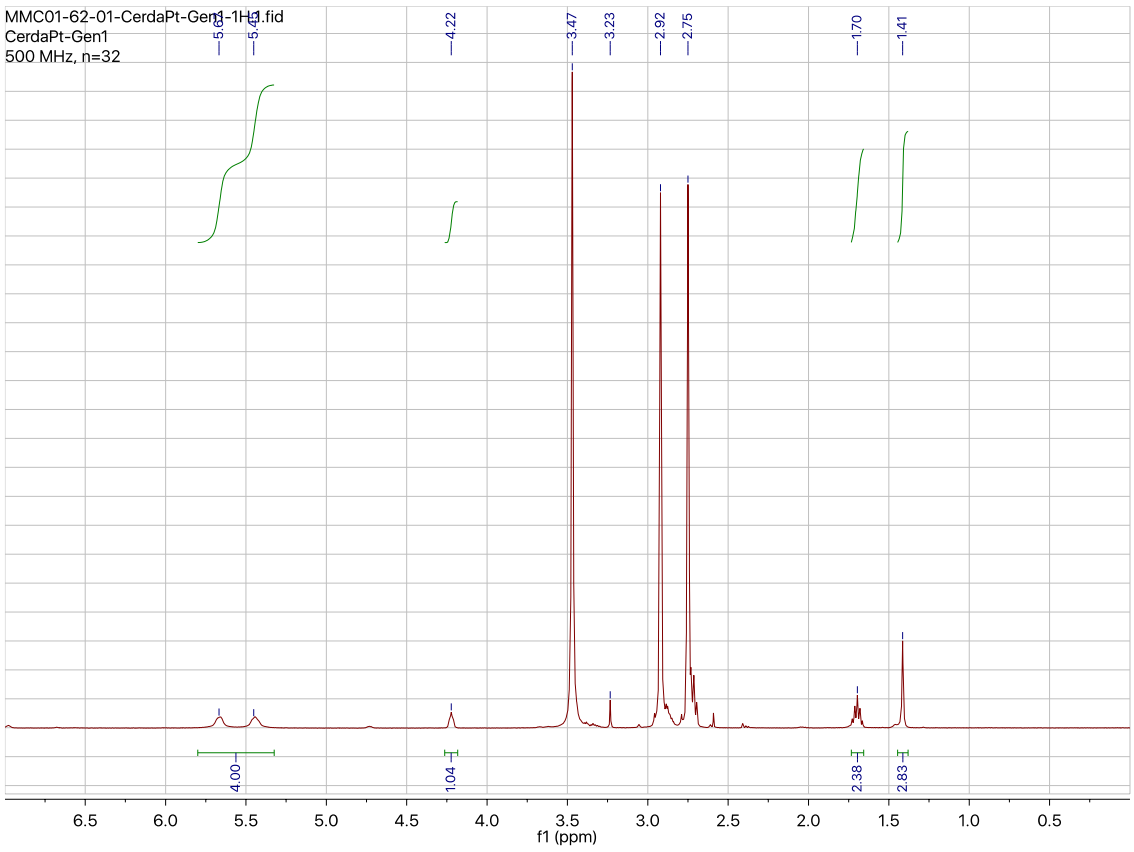

Figure E.1. ^{1}H spectrum for **1** in d_7-DMF.

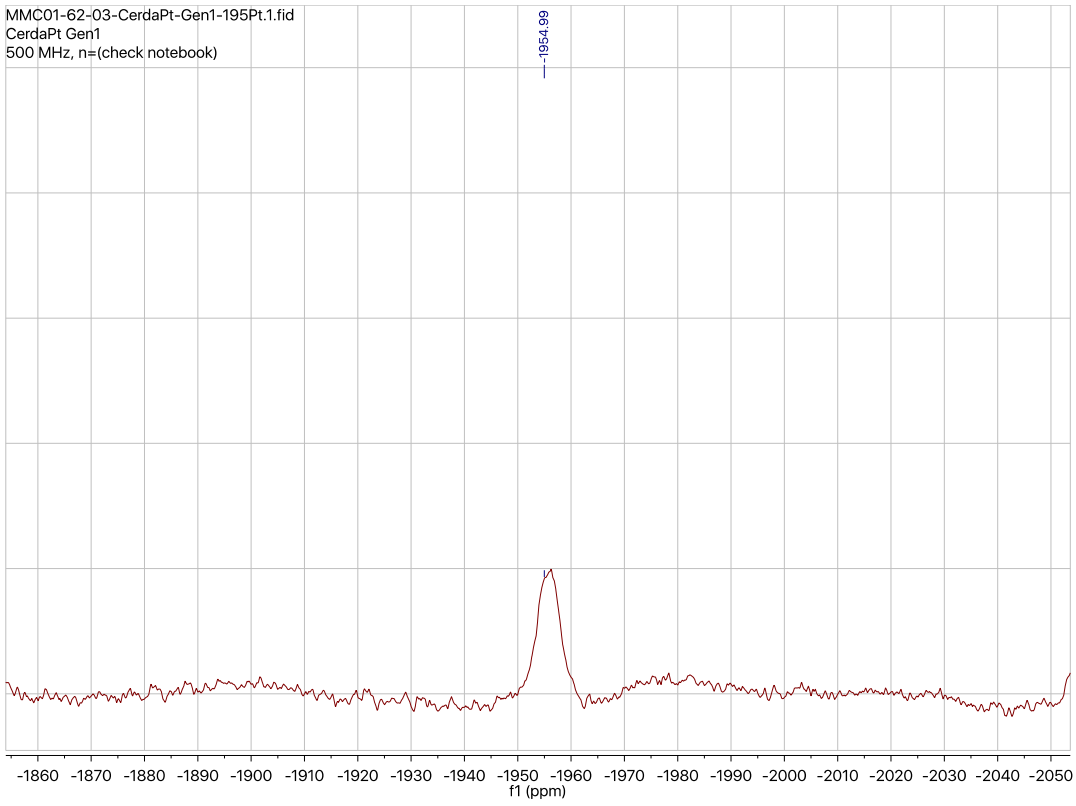

Figure E.2. ^{195}Pt spectra for **1** in d_7-DMF.

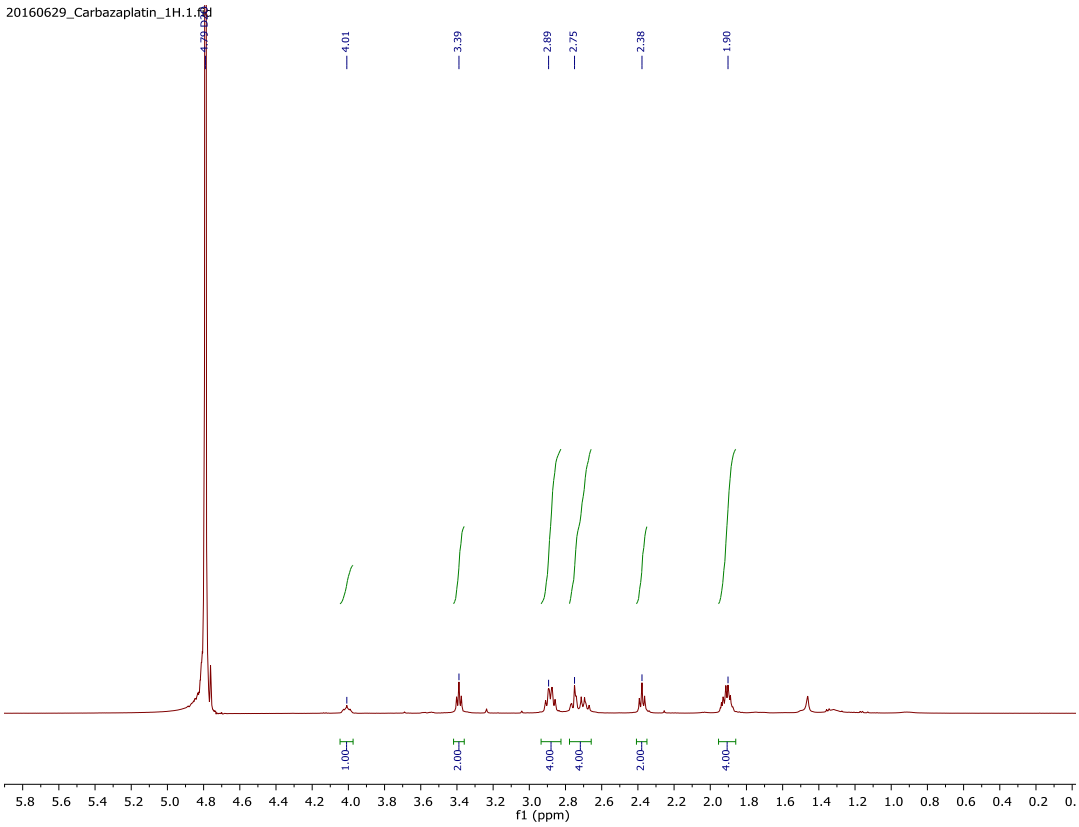

Figure E.3. ^{1}H NMR of **2** in D_2O.

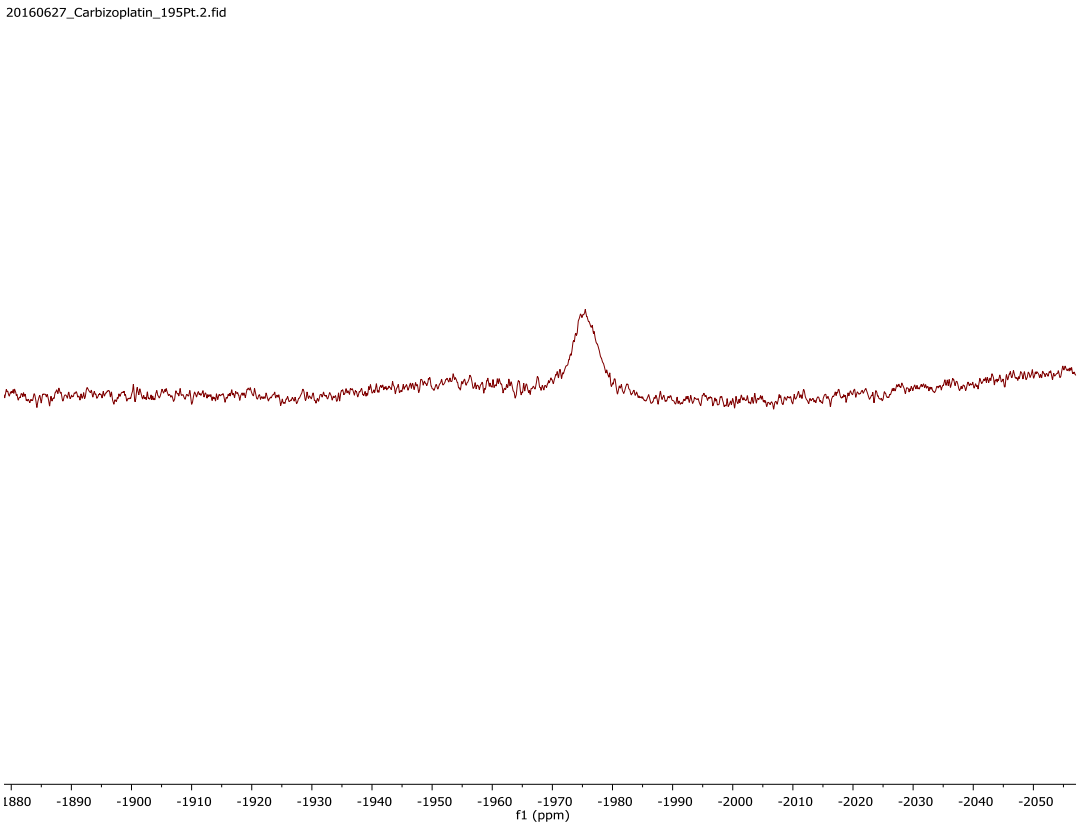

Figure E.4. ^{195}Pt NMR of **2** in D_2O.

REFERENCES CITED

Chapter I

1) Jones, E.G. Cisplatin: The Penicillin of Cancer. [cited 2016 March 14, 2016]; Available from: http://www.cisplatin.org.

2) Harper, B. W.; Krause-Heuer, A. M.; Grant, M. P.; Manohar, M.; Garbutcheon-Singh, K. B.; Aldrich-Wright, J. R.; *Chem. Eur. J.* **2010**, 16, 7064– 7077

3) Molenaar, C; Teuben, JM; Heetebrij, RJ; Tanke, HJ; Reedijk, J; *J Biol Inorg Chem*, **2010**, 5, 655–665

4) Safaei, R; Katano, K; Larson, BJ; Samimi, G; Holzer, AK; Naerdemann, W; Tomioka, M; Goodman, M; Howell, SB; *Clin Cancer Res*, **2005**, 11:756–767

5) Kuroda, NH; Hayami, Y; Ekimoto, OK; Takahashi, HK; *Chem. Pharm. Bull.*, **1989**, 37, 2406–2409

6) Benedetti, BT; Peterson, EJ; Kabolizadeh, P; Martínez, A; Kipping, R; Farrell, NP; *Mol Pharm*, **2011**, 8, 940–948

7) Jagodinsky, JC; Sulima, A; Joanna, YC; Poprawski, E; Blackman, BN; Lloyd, JR; Swenson, RE; Gottesman, MM; Hall, MD; *J. Bio. Inorg. Chem.*, **2015**, 20, 1081

8) Chen, Z; Zhang, S; Shen, L; Zhu, Z; Zhang, J; *NJC*, **2015**, 39, 1592-1596

9) Manikandamathavana, VM; Manikantan, ND; Kiran, S; Vaidyanathan, VG; Nair, BU; *Inorg. Chem.*, **2015**, 5, 24877-24885

10) Wu, S; Zhu, C; Zhang, C; Yu, Z; He, W; He, Y; Li, Y; Wang, J; Guo, Z; *Inorg. Chem.*, **2011**, 50, 11847-11849

11) Kolb, H C; Finn, M G; Sharpless, K B; *Angew. Chem. Ed*. **2001**, 40, 2004-2021

12) Ding, S; Qiao, X; Suryadi, J; Marrs, GS; Kucera, GL; Bierbach, U; *Angew. Chem. Int. Ed.*, **2013**, 52, 3350–3354

13) Qiao, X; Ding, S; Liu, F; Kucera, GL; Bierbach, U; *JBIC*, **2014**, 19, 415-426

Chapter II

1) (a) B. W. Harper, A. M. Krause-Heuer, M. P. Grant, M. Manohar, K. B. Garbutcheon-Singh, J. R. Aldrich-Wright, *Chem.-Eur. J.*, 2010, 16, 7064-7077; (b) P. J. Dyson, G. Sava, Dalton Trans., 2006, 1929-1933.

2) (a) G. Sava, G. Jaouen, E. A. Hillard, A. Bergamo, Dalton Trans., 2012, 41, 8226-8234; (b) A. Casini, J. Reedijk, Chem. Sci., 2012, 3, 3135-3144; (c) E. R. Guggenheim, D. Xu, C. X. Zhang, P. V. Chang, S. J. Lippard, Chem. Bio. Chem., 2009, 10, 141-157; (d) E. Wexselblatt, E. Yavin, D. Gibson, Inorg. Chim. Acta, 2012, 393, 75-83.

3) (a) E. G. Chapman, V. J. DeRose, J. Am. Chem. Soc., 2012, 134, 256-262; (b) E. G. Chapman, V. J. DeRose, J. Am. Chem. Soc., 2010, 132, 1946-1952; (c) A. A. Hostetter, E. G. Chapman, V. J. DeRose, J. Am. Chem. Soc., 2009, 131, 9250-9257.

4) J. D. White, M. F. Osborn, A. D. Moghaddam, L. E. Guzman, M. M. Haley, V. J. DeRose, J. Am. Chem. Soc., 2013, 135, 11680-11683.

5) (a) L. Kelland, Nat. Rev. Cancer, 2007, 7, 573-584; (b) F. I. Raynaud, F. E. Boxall, P. M. Goddard, M. Valenti, M. Jones, B. A. Murrer, M. Abrams, L. R. Kelland, Clin. Cancer Res., 1997, 3, 2063-2074; (c) Y. Chen, Z. Guo, S. Parsons, P. J. Sadler, Chem.-Eur. J., 1998, 4, 672-676; (d) Y. Chen, Y.; Z. Guo, J. A. Parkinson, P. J. Sadler, Dalton Trans., 1998, 3577-3586; (e) L. R. Kelland, S. Y. Sharp, C. F. O'Neill, F. I. Raynaud, P. J. Beale, I. R. Judson, J. Inorg. Biochem., 1999, 77, 111-115.

6) A. R. Battle, R. Choi, D. E. Hibbs, T. W. Hambley, Inorg. Chem., 2006, 45, 6317-6322.

7) (a) D. Wang, S. J. Lippard, Nat. Rev. Drug Discovery, 2005, 4, 307-320; (b) T. Boulikas, M. Vougiouka, Oncol. Rep., 2003, 10, 1663-1682; (c) E. R. Jamieson, S. J. Lippard, Chem. Rev., 1999, 99, 2467-2498.

8) (a) N. Stojanovic, D. Urankar, A. Brozovic, A. Ambriović-Ritsov, M. Osmak, J. Košmrlj, Acta Chim. Slov., 2013, 60, 368-374; (b) D. Urankar, J. Košmrlj, Inor. Chim. Acta, 2010, 363, 3817-3822.

9) (a) S. C. Dhara, Ind. J. Chem., 1970, 8, 193-134; (b) J. Zhang, L. Ma, H. Lu, Y. Wang, S. Li, S. Wang, G. Zhou, Eur. J. Med. Chem., 2012, 58, 281-286.

10) R. C. Todd, S. J. Lippard, J. Inorg. Biochem., 2010, 104, 9, 902-908.

11) (a) W. L. Ward, V. J. DeRose, RNA, 2012, 18, 16-23; (b) J. K. Frederiksen, J. A. Piccirilli, Methods in Enzymology, ed. D. Herschlag, Academic Press, 2009, vol. 468, ch. 14, pp. 289-309.

12) M. J. Bloemink, R. J. Heetebrij, K. Inagaki, Y. Kidani, J. Reedijk. Inorg. Chem., 1992, 31, 4656-4661.

13) A. Sugii, K. Nishimura, K. Harada, M. Nakayama, S. Masuda Chem. Pharm. Bull. 1991, 39, 408-410

14) N. H. Kuroda, Y. Hayami, O. K. Ekimoto, H. K. Takahashi, Chem. Pharm. Bull. 1989, 37, 9, 2406-2409

15) A. A. Hostetter , M. F. Osborn, V. J. DeRose, ACS Chem. Biol., 2012, 7, 1, 218-225

16) M. F. Osborn, J. D. White , M. M. Haley, V. J. DeRose, ACS Chem. Biol., 2014, 2014, 9 (10), 2404–2411

Chapter III

(1) Rozencweig, M.; Von Hoff, D. D.; Slavik, M.; Muggia, F. M. *Ann. Intern. Med*. **1977**, *112*, 100.

(2) Harper, B. W.; Krause-Heuer, A. M.; Grant, M. P.; Manohar, M.; Garbutcheon-Singh, K. B.; Aldrich-Wright, J. R. *Chem.–Eur. J*. **2010**, *16*, 7064.

(3) Dyson, P.J.; Sava, G. *Dalton Trans.* **2006**, 1929.

(4) Rosenberg, B.; Renshaw, E.; Van Camp, L.; Hartwick, J.; Drobnik, *J. Bacteriol*. **1967**, *93*, 716.

(5) Sava, G.; Jaouen, G.; Hillard, E. A.; Bergamo, A. *Dalton Trans.* **2012**, *41*, 8226.

(6) Casini, A.; Reedijk, J. *Chem. Sci.* **2012**, *3*, 3135.

(7) Guggenheim, E. R.; Xu, D.; Zhang, C. X.; Chang, P. V.; Lippard, S. J. *Chem. Bio. Chem.* **2009**, *10*, 141.

(8) Wexselblatt, E.; Yavin, E.; Gibson, D. *Inorg. Chim. Acta* **2012**, *393*, 75.

(9) Arnesano F.; Losacco, M.; Natile, G. *Eur. J. Inorg. Chem.* **2013**, 2701.

(10) Wang, D.; Lippard, S. J. *Nat. Rev.* **2005**, *4*, 307.

(11) Jamieson, E. R.; Lippard, S. *J. Chem. Rev.* **1999**, *99*, 2467.

(12) Todd, R. C.; Lippard, S. J. *Metallomics* **2009**, *1*, 280.

(13) (a) Caradonna, J. P.; Lippard, S. J.; Gait, M. J.; Singh M. *J. Am. Chem. Soc.* **1982**, *104*, 5793. (b) Fichtinger-Schepman, A. M. J; Van der Veer, J. L.; Den Hartog J. H. J; Lohman, P. H. M; Reedijk, J. *Biochemistry* **1985**, *24*, 707. (c) Eastman, A. *Biochemistry* **1986**, *25*, 3912. (d) Terheggen, P. M. A. B.; Floot, B. G. J.; Scherer, Begg, A.C.; Fichtinger-Schepman, A. M. J.; Engelse, L. *Cancer Res.* **1987**, *47*, 6719.

(14) (a) DeConti, R. C.; Toftness, B. R.; Lange, R. C.; Creasey, W. A. *Cancer Res*. **1973**, *33*, 1310. (b) Akaboshi, M.; Kawai, K.; Ujeno, Y.; Takada, S.; Miyahara, T. *Jpn. J. Cancer Res*. **1994**, *85*, 106. (c) Akaboshi, M.; Kawai, K.; Maki, H.; Akuta, K.; Ujeno, Y.; Miyahara, T. *Jpn. J. Cancer Res*. **1992**, *83*, 522.

(15) (a) Wisnovsky, S. P.; Wilson, J. J.; Radford, R. J.; Pereira, M. P.; Chan, M. R.; Laposa, R. R.; Lippard, S. J.; Kelley, S. O. *Chem. Biol.* **2013**, *20*, 1323. (b) Yu, F.; Megyesi, J.; Price, P. M. *Am. J. Physiol. Renal Physiol.* **2008**, *295*, F44-F52.

(16) *Inter alia*: (a) Gemba, M.; Nakatani, E.; Teramoto, M.; Nakano, S. *Toxicol. Lett.* **1987**, *38*, 291. (b) Samimi, G.; Katano, K.; Holzer, A. K.; Safaei, R.; Howell, S. B. *Mol. Pharmacol.* **2004**, *66*, 25. (c) Samimi, G.; Safaei, R.; Katano, K.; Holzer, A. K.; Rochdi, M.; Tomioka, M.; Goodman, M.; Howell, S. B. *Clin. Cancer Res.* **2004**, *10*, 4661. (d) Jansen, B. A. J.; Wielaard, P.; Kalayda, G. V.; Ferrari, M.; Molenaar, C.; Tanke, H. J.; Brouwer, J.; Reedijk, J. *J. Biol. Inorg. Chem*. **2004**, *9*, 403. (e) Molenaar, C.; Teuben, J.-M.; Heetebrij, R. J.; Tanke, H. J.; Reedijk, J. *J. Biol. Inorg. Chem*. **2000**, *5*, 655. (f) Kalayda, G. V.; Jansen, B. A. J.; Molenaar, C.; Wielaard, P.; Tanke, H. J.; Reedijk, J. *J. Biol. Inorg. Chem*. **2004**, *9*, 414. (g) Kalayda, G. V.; Jansen, B. A. J.; Wielaard, P.; Tanke, H. J.; Reedijk, J. *J. Biol. Inorg. Chem*. **2005**, *10*, 305. (h) Beretta, G. L.; Righetti, S. C.; Lombardi, L.; Zunino, F.; Perego, P. *Ultrastruc. Pathol*. **2002**, *26*, 331. (i) Meijer, C.; Van Luyn, M. J. A.; Nienhuis, E. F.; Blom, N.; Mulder, N. H.; De Vries, E. G. E. *Biochem. Pharmacol*. **2001**, *61*, 573. (j) Khan, M. U. A.; Sadler, P. J. *Chem.-Biol. Inter*. **1978**, *21*, 227. (k) Berry, J. P.; Galle, P.; Viron, A.; Kacerovská, H.; Macieira-Coelho, A. *Biomed. Pharmacother*. **1983**, *37*, 125. (l) Hall, M. D.; Hambley, T. W.; Beale, P.; Zhang, M.; Dillon, C. T.; Foran, G. J.; Stampfl, A. P.; Lai, B. *J. Inorg. Biochem*. **2003**, *96*, 141. (m) Hall, M. D.; Alderden, R. A.; Zhang, M.; Beale, P. J.; Cai, Z.; Lai, B.; Stampfl, A. P. J.; Hambley, T. W. *J. Struct. Biol*. **2006**, *155*, 38. (n) Safaei, R.; Katano, K.; Larson, B. J.; Samimi, G.; Holzer, A. K.; Naerdemann, W.; Tomioka, M.; Goodman, M.; Howell, S. B. *Clin. Cancer Res*. **2005**, *11*, 756.

(17) Molenaar, C.; Teuben, J.-M.; Heetebrij, R. J.; Tanke, H. J.; Reedijk, J. *J. Biol. Inorg. Chem*. **2000**, *5*, 655.

(18) Safaei, R.; Katano, K.; Larson, B. J.; Samimi, G.; Holzer, A. K.; Naerdemann, W.; Tomioka, M.; Goodman, M.; Howell, S. B. *Clin. Cancer Res*. **2005**, *11*, 756.

(19) White, J. D.; Haley, M. M.; DeRose, V. J. *submitted*.

(20) (a)Ding, S.; Qiao, X.; Suryadi,J.; Marrs, G. S.; Kucera, G. L.; Bierbach, U. *Angew. Chem., Int. Ed.* **2013**, *52*, 3350. (b) Qiao, X.; Ding, S.; Liu, F.; Kucera, G. L.; Bierbach, U. *J. Biol. Inorg. Chem*. **2014**, *19*, 415. (c) Wexselblatt, E.; Yavin, E.; Gibson, D. *Inorg. Chim. Acta* **2012**, *393*, 75. (d) Ghosh, B.; Jones, L. H. *Med. Chem. Commun.* **2014**, *5*, 247.

(21) Rijal, K.; Bao, X.; Chow, C. S. *Chem. Commun.* **2014**, *50*, 3918.

(22) (a) Kolb, H.C.; Finn, M. G.; Sharpless, K. B. *Angew. Chem., Int. Ed.* **2001**, *40*, 2004.

(23) White, J. D.; Osborn, M. F.; Moghaddam, A. D.; Guzman, L. E.; Haley, M. M.; DeRose, V. J. *J. Am. Chem. Soc*. **2013**, *135*, 11680.

(24) Osborn, M. F.; White, J. D.; Haley, M. M.; DeRose, V. J. *ACS Chem. Biol*. **2014**, *9*, 2404.

(25) Moghaddam, A. D.; White, J. D.; Cunningham, R. M.; Loes, A. N.; Haley, M. M.; DeRose, V. J. *Dalton Trans*. **2015**, *44*, 3536.

(26) White, J. D.; Guzman, L. E.; Zakharov, L. N.; Haley, M. M.; DeRose, V. J. *Angew. Chem., Int. Ed*. **2015**, *54*, 1032.

(27) Hostetter, A. A.; Osborn, M. F.; DeRose, V. J. *ACS Chem. Biol.* **2012**, *7*, 218.

(28) Ramalingam, K; Raju, N.; Nanjappan, P.; Nowotnik, D. P. *Tetrahedron* **1995**, 51, 2875.

(29) Still, B. M.; Kumar, Aldrich-Wright, J. R.; Price, W. S. *Chem. Soc. Rev.* **2007**, *36*, 665.

(30) X-Ray Data for **1**: $C_7H_{16}Cl_2N_6OPt$, M = 466.25, 0.07 x 0.04 x 0.03 mm, T = 173 K, triclinic, space group *P*-1, a = 7.330(2) Å, b = 7.583(2) Å, c = 11.831(3) Å, α = 85.465(5)°, β = 86.040(5)°, γ = 86.498(5)°, V = 653.1(3) Å^3, Z = 2, D_c = 2.371 Mg/m^3, μ(Mo)= 11.147 mm^{-1}, F(000) = 440, $2\theta_{max}$ = 50.0°, 7931 reflections, 2287 independent reflections [R_{int} = 0.0774], R1 = 0.0403, wR2 = 0.0644 and GOF = 1.011 for 2287 reflections (154 parameters) with I>2σ(I), R1 = 0.0627, wR2 = 0.0704 and GOF = 1.011 for all reflections, max/min residual electron density +1.423/-1.283 eÅ^3.

(31) Woollins, J. D.; Kelly, P. F. *Coord. Chem. Rev.* **1985**, *65*, 115.

(32) Odoko. M; Okabe, N. Acta Crystallogr. Sect. C: Cryst. Struct. Commun. **2006**, 62, m 136

(33) (a) Guo, L.; Thompson C. M.; Twamley B. *Acta Crystallogr. Sect. C: Cryst. Struct. Commun.* **2009**, *65*, 0179. (b) Yang, H.; Carter, R. G. *J. Org. Chem.* **2010**, *75*, 4929. (c) Brady, R. M.; Zhang, M.; Gable, R.; Norton, R. S.; Baell J. B. *Bioorg. Med. Chem. Lett.* **2013**, *23*, 4892. (d) Parsons, S.; Haxton, A.; Flitsch, S.; Wood, P. A., private communication to the Cambridge Crystallographic Data Centre, 2004, DOI:10.5517/cc88jrs

(34) (a) Braese, S.; Gil, C.; Knepper, K.; Zimmermann, V. *Angew. Chem., Int. Ed.* **2005**, *44*, 5188. (b) Chen, F-F.; Wang, F. *Molecules* **2009**, *14*, 2656.

(35) Baier, G.; Siebert, J. M.; Landfester, K.; Musyanovych, A. *Macromolecules* **2012**, *45*, 3419.

(36) Chapman, E. G.; DeRose, V. J. *J. Am. Chem. Soc.* **2012**, *134*, 256.

(37) Urankar, D.; Kosmrlj, J. *Inorg. Chim. Acta* **2010**, *363*, 3817.

(38) Uttamapinant, C.; Tangpeerachaikul, A.: Grecian, S.; Clarke, S.; Singh, U.; Slade, P.; Gee, K. R.; Ting, A. Y. *Angew. Chem., Int. Ed.* **2012**, *51*, 5852.

(39) (a) Liang, X. J.; Shen, D. W.; Chen, K. G.; Wincovitch, S. M.; Garfield, S. H.; Gottesman, M. M. *J. Cell. Physiol.* **2005**, *202*, 635. (b) Colombo, A; Fiorini, F.; Septiadi, D.; Dragonetti, C.; Nisic, F.; Valore, A.; Roberto, D.; Mauro,M.; DeCola,L. *Dalton Trans.*, **2015**, *44*, 8478. (c) Shen, C.; Harris, B. D. W.; Dawson, L. L.; Charles, K. A.; Hambley, T. W.; New. E. J. *Chem. Commun.*, **2015**, *51*, 6312. (d) Wu, S.; Zhu, C.; Zhang, C.; Yu, Z.; He, W.; He, Y.; Li, Y.; Wand, J.; Guo, Z. *Inorg. Chem.* **2011**, *50*, 11847.

(40) Belluco, U; Bertani, R.; Michelin, R. A.; Mozzon, M. *J. Organomet. Chem.* **2000**, *600*, 37.

Chapter IV

(1) Todd, R. C.; Lippard, S. J. *Metallomics* **1**, 280 (2009).

(2) Wang, D.; Lippard, S. J. *Nat. Rev. Drug Discovery* **4**, 307 (2005).

(3) Jamieson, E. R.; Lippard, S. J. *Chem. Rev*. **99**, 2467 (1999).

(4) Pabla, N.; Dong, Z. *Kidney Int*. **73**, 994 (2008).

(5) Langer, T.; Zehnhoff-Dinnesen, A.; Radtke, S.; Meitert, J.; Zolk, O. *Trends Pharmacol. Sci*. **34**, 458 (2013).

(6) McWhinney, S. R.; Goldberg, R. M.; McLeod, H. L. *Mol. Cancer Ther*. **8**, 10 (2009).

(7) Galluzzi, L.; Senovilla, L; Vitale, I; Michels, J; Martins, I; Kepp. O; Castedo, M; Kroemer, G; *Oncogene* **31**, 1869 (2012).

(8) Wexselblatt, E.; Gibson, D. *J. Inorg. Biochem*. **117**, 220 (2012).

(9) Wexselblatt, E.; Yavin, E.; Gibson, D. *Inorg. Chim. Acta* **293**, 75 (2012).

(10) Klein, A. V.; Hambley, T. W. *Chem. Rev*. **109**, 4911 (2009).

(11) White, J. D.; Osborn, M. F.; Moghaddam, A. D.; Guzman, L. E.; Haley, M. M.; DeRose, V. J.; *J. Am. Chem. Soc*. **135**, 11680 (2013).

(12) Osborn, M. F.; White, J. D.; Haley, M. M.; DeRose, V. J. *ACS Chem. Biol*. **9**, 2404 (2014).

(13) Moghaddam, A. D.; White, J. D.; Haley. M. M., DeRose, V. J. *Dalton Trans.*, 2015, 44, 3536-3539 (2015)

(14) White, J. D.; Guzman, L. E.; Zakharov, L. N.; Haley, M. M.; DeRose, V. J. *Angew. Chem. Int. Ed*. **54**, 1032 (2015).

(15) White, J. D.; Wirth, R; Moghaddam, A. D,; Ginzburg, A. L.; Zakharov, L. N.; Haley, M. M.; DeRose, V. J.; *J. Am. Chem. Soc.*, 137(48), 15169-15175 (2015)

(16) Qiao, D.X.; Suryadi, J;Marrs, G.S.; Kucera, L.G.; Bierbach, U; *Angew. Chem. Int. Ed.*, **52**, 3350–3354 (2013)

(17) Hostetter, A.A.; Osborn, M.F.; DeRose, V.J.; *ACS Chem. Biol*., **7**, 218–225 (2012)

(18) Seela, F; Sachin, I. A.; *J. Org. Chem.,* **75**, 284-95 (2010)

(19) Sirivolu, V. R.; Chittepu, P; Seela, F; *Chem. Bio. Chem.,* **9**, 2305-2316 (2008)

Chapter V

(1) Todd, R. C.; Lippard, S. J. *Metallomics* **1**, 280 (2009).

(2) Wang, D.; Lippard, S. J. *Nat. Rev. Drug Discovery* **4**, 307 (2005).

(3) Jamieson, E. R.; Lippard, S. J. *Chem. Rev*. **99**, 2467 (1999).

(4) White, J. D.; Osborn, M. F.; Moghaddam, A. D.; Guzman, L. E.; Haley, M. M.; DeRose, V. J.; *J. Am. Chem. Soc*. **135**, 11680 (2013).

(5) Moghaddam, A. D.; White, J. D.; Haley. M. M., DeRose, V. J. *Dalton Trans.*, 2015, 44, 3536-3539 (2015)

(6) White, J. D.; Guzman, L. E.; Zakharov, L. N.; Haley, M. M.; DeRose, V. J. *Angew. Chem. Int. Ed*. **54**, 1032 (2015).

(7) White, J. D.; Wirth, R; Moghaddam, A. D,; Ginzburg, A. L.; Zakharov, L. N.; Haley, M. M.; DeRose, V. J.; *J. Am. Chem. Soc.*, 137(48), 15169-15175 (2015)

(8) Cleator, S; Heller, W; Coombes, R.C.; *Oncology*, 8(3), 235-244 (2007)

(9) Noda, S; Yoshimura, S; Sawada, M, Nagnawa, T; Iwama, T; Nakashima, S; Sakai, N; *J. Neu. Onc.*, 52, 11 (2001)

(10) Krajčí, D; Mareš, V; Lisá, V; Španová, A; Vorlíček, J; *Eur. J. Cell Bio.*, 79, 365-376 (2000)

(11) Goto, S; Yoshida, K; Morikawa, T; Urata, Y; Suzuki, K; Kondo, T; *Cancer Research*, 55, 19, 4297-4301 (1995)

(12) Rocha, CR; Garcia, CM; Vieira, DB, Quinet, A; de Andrade-Lima, LC; Munford, V; Belizario, JE; Menck, CM; *Cell Death Disease*, 5, 1-10 (2015)

Chapter VI

(1) Wheate, NJ; Walker, S; Craig, GE; Oun, R; *Dalton Trans.*, **2010**, 39, 8113-8127

(2) Dilruba, S; Kalayda, G; *Cencer. Chemo. Pharm.*, **2016**, 77, 1103-1124

(3) White, J. D.; Osborn, M. F.; Moghaddam, A. D.; Guzman, L. E.; Haley, M. M.; DeRose, V. J.; J. Am. Chem. Soc. 135, 11680 (2013).

(4) Moghaddam, A. D.; White, J. D.; Haley. M. M., DeRose, V. J. Dalton Trans., 2015, 44, 3536-3539 (2015)

(5) White, J. D.; Guzman, L. E.; Zakharov, L. N.; Haley, M. M.; DeRose, V. J. Angew. Chem. Int. Ed. 54, 1032 (2015).

(6) White, J. D.; Wirth, R; Moghaddam, A. D,; Ginzburg, A. L.; Zakharov, L. N.; Haley, M. M.; DeRose, V. J.; J. Am. Chem. Soc., 137(48), 15169-15175 (2015)

(7) Bernhardta, G; Brunnerb, H; Gruberb, N; Lottnerb, C; Pushpanb, SK; Tsunoc, T; Zabelb, M; Inorg. Chem. Acta, 357, 15, 4452-4466 (2004)

(8) Harper, B. W.; Krause-Heuer, A. M.; Grant, M. P.; Manohar, M.; Garbutcheon-Singh, K. B.; Aldrich-Wright, J. R.; Chem. - Eur. J., 16, 7064– 7077 (2010)

(9) Hongo, A; Seki, S; Akiyama, K; Kudo, T; Int. J. Biochem., 26, 8, 1009-1016 (1994)

(10) Ramalingam, K.; Raju, N.; Nanjappan, P.; Nowotnik, D.P. Tetrahedron, 51, 2875 (1995)

(11) Yu, T.-B.; Bai, J.Z.; Guan, Z. Angew. Chem., Int. Ed., 48, 1097. (2009)

(12) Baier, G.; Siebert, J. M.; Landfester, K.; Musyanovych, A. Macromolecules 2012, 45, 3419.

(13) Bolletta, F.; Fabbri, D.; Lombardo, M.; Prodi, L.; Trombini, C.; Zaccheroni, N. Organometallics, 15, 2415. (1996)

(14) Price, J. H.; Williamson, A. N.; Schramm, R. F.; Wayland, B. B. Inorg. Chem., 11, 1280. (1972)

(15) Urankar, D.; Kosmrlj, J. Inorg. Chim. Acta, 363, 3817. (2010)

Appendix B

(1) Ramalingam, K.; Raju, N.; Nanjappan, P.; Nowotnik, D.P. *Tetrahedron* **1995,** *51*, 2875.

(2) Yu, T.-B.; Bai, J.Z.; Guan, Z. *Angew. Chem., Int. Ed.* **2009**, *48*, 1097.

(3) Baier, G.; Siebert, J. M.; Landfester, K.; Musyanovych, A. *Macromolecules* **2012**, *45*, 3419.

(4) Bolletta, F.; Fabbri, D.; Lombardo, M.; Prodi, L.; Trombini, C.; Zaccheroni, N. *Organometallics* **1996**, *15*, 2415.

(5) Price, J. H.; Williamson, A. N.; Schramm, R. F.; Wayland, B. B. *Inorg. Chem.* **1972**, *11*, 1280.

(6) Urankar, D.; Kosmrlj, J. *Inorg. Chim. Acta* **2010**, *363*, 3817.

(7) Peng, H.; Cheng, Y.; Dai, C.; King, A. L.; Predmore, B. L.; Lefer, D. J.; Wang, B. Angew. Chem. Int. Ed. 2011, 50, 9672.

(8) Legendre, F.; Kozelka, J.; Chottard, J. C. *Inorg. Chem.* **1998**, *37*, 3964.

(9) Sheldrick, G. M. *Bruker/Siemens Area Detector Absorption Correction Program*, Bruker AXS, Madison, WI, 1998.

(10) SHELXTL-6.10 "Program for Structure Solution, Refinement and Presentation" BRUKER AXS Inc., 5465 East Cheryl Parkway, Madison, WI 53711-5373 USA.

(11) Sheldrick, G. M. *Acta Cryst. A* **2008**, *64*, 112.

(12) Cookson, MR; Pentreath, VW; *Toxic. In Vitro*, **1996**, 257-264